# Variational description of Mott insulators

Thesis submitted for the degree of
*Doctor Philosophiæ*

**Candidate:**
Manuela Capello

**Supervisors:**
Prof. Sandro Sorella
Dr Federico Becca
Prof. Michele Fabrizio

October 2006

# Contents

# Introduction

Narrow-band materials, like transition-metal oxides, are generally characterized by a strong competition between the tendency of the electrons to delocalize on the whole crystal and the Coulomb repulsion among the charges, which drives the system towards localization. Indeed, when the latter contribution is predominant, it can dramatically change the properties of the system and turn a metal into a *Mott insulator* [1]. Besides the Mott-insulating character, most of the materials characterized by strong correlation show unusual properties, with high-temperature superconductivity being the most spectacular example [2–4]. The lack of a consistent microscopic description of these phenomena, which are still much debated both experimentally and theoretically, clearly implies that a better understanding of correlation effects is needed.

Since the early pioneering work on transition-metal oxides, the theoretical approach to Mott insulators has focused on the half-filled Hubbard model [5], the simplest model which takes into account electron correlation. Although very simple in its formulation, the Hubbard model is generally not solvable with the available analytical techniques, apart from the one-dimensional case [6]. Therefore, with the support of numerical calculations, several approximate schemes have been introduced.

Within the standard band-theory approach, widely used in electronic structure calculations, such as Hartree-Fock or Local Density methods, it is not possible to obtain a metal-insulator transition when the band is half-filled, unless some kind of magnetic order is imposed. As a consequence, these techniques, which turn the Mott transition into a conventional metal-band insulator transition, miss the essence of the Mott phenomenon, where a charge gap appears independently of spin order.

Very recently, Dynamical Mean Field Theory [7] offered an alternative route

to this problem, giving a description of the Mott metal-insulator transition without need for symmetry breaking. However, this scheme fully neglects spatial correlations and becomes exact only in the limit of infinite dimensionality. Since charge fluctuations are very strong in low-dimensional systems and can contribute to determine their physical properties, an alternative method which allows one to make predictions in the case of reduced dimensionality, by fully taking into account the role of charge fluctuations, would be very useful.

Another widely employed route to characterize the Mott insulating state is to consider effective spin models, that describe the low-energy physics of the Hubbard model in the limit of large Coulomb interaction [8]. These effective models allow one to work in a reduced Hilbert space, where the only degrees of freedom reside in the different arrangements of the spins. However, the total suppression of charge fluctuations, assumed in the strong-coupling limit, offers a rather unrealistic picture of correlated insulators, where charge fluctuations are surely present at small length scales.

In this thesis we consider the variational approach as a possible route to describe the Mott transition in the Hubbard model. Our goal is to find a realistic description of Mott insulators, which allows for charge fluctuations without breaking any symmetry and makes it possible to connect the strong-coupling insulating state to the weak-coupling region. Our approach is based on an approximate form for the ground-state wavefunction which contains the physically relevant terms for the correct description of the Mott insulating state, and, at the same time, is simple enough to allow a straightforward calculation of the physical quantities. We show that, with a good guess of the ground-state wavefunction, we obtain a transparent and physically intuitive way to understand the correlation-induced localization of electrons.

In the context of the $t - J$ and Heisenberg model, the general form for a correlated wavefunction corresponds to a fully-projected uncorrelated determinant, where the configurations having a finite number of double occupancies are completely neglected [9, 10]. At half-filling, with one electron per site, this wavefunction is obviously insulating, since no charge fluctuations can occur. Remarkably, in the case of frustrated systems, a fully-projected metallic Slater determinant (or a BCS mean-field wavefunction), without magnetic long-range order, turns out to be very close to the exact ground state.

On the other hand, in the Hubbard model, previous variational calculations showed that the variational description of an insulating state purely induced by correlation, which still allows for charge fluctuations, is a non-trivial problem. Indeed, the Gutzwiller on-site correlation factor [11], which at first sight could be considered as the natural extension of the full projector in the case of finite interaction, gives an insulating state only in the limit of infinite repulsion (apart from infinite dimension), while for finite Coulomb interaction it always corresponds to a correlated metallic state. The reason for its failure has been widely discussed in the past, and an intuitive argument has been found in the lack of correlation among the charge carriers, which correspond to the empty sites (holons) and doubly occupied sites (doublons) created by charge fluctuations at finite interactions [12]. Indeed, the holons possess an effective positive charge, since one electron is missing, and the doublons are negatively charged objects, having one more electron with respect to the average occupation number. If the system is perturbed with the insertion of an electric field, this implies that, in absence of correlation, holons and doublons can move freely in opposite directions, thus leading to a metallic behavior. However, subsequent variational attempts done by adding a short-range correlation term up to a distance $\xi$ among holons and doublons, turned out to be likewise unsuccessful [12, 13]. Naively, this happens because the configurations where holons and doublons are at distances larger than $\xi$ are not subject to any correlation term, hence they can move freely on the lattice and conduct. Following this insight, it turns out that, in order to describe a correlated insulator without breaking any symmetry, it is necessary to correlate particles over all length scales.

Let us consider a more general argument in view of the above considerations. According to a well accepted picture, for realistic Hamiltonians, the dynamical properties of a system reflect the long-distance behavior of the static correlation functions of its ground state. Within the variational approach, this implies that a good ansatz for an insulating state requires the correct description of the charge-density correlation function at large distances or, equivalently, the correct behavior of the charge-density structure factor at small momenta. For fermionic systems, the standard form for a correlated wavefunction is constituted by a correlation term acting on a Slater determinant, the latter being an uncorrelated metallic state at half filling and in absence of symmetry breaking. As a consequence, a variational wavefunction built with a short-range correlation factor cannot change the

metallic character of the determinant, unless one fully suppresses the charge fluctuations, since the large distance physics, which is relevant for the conducting properties of the system, remains untouched.

The above arguments suggest that a long-range correlation factor is needed in order to correctly describe the insulating state. In particular, since we are interested in the charge-charge correlations, a natural choice of the correlation factor contains a two-body charge-density term in its expression, which corresponds to the definition of the Jastrow correlation factor [14].

The Jastrow factor has been widely used in the context of liquid Helium, where it gives the correct behavior of the charge-density structure factor [15, 16]. In that case, since $^4He$ is a gapless system, the analytic form of the Jastrow parameters is successfully deduced from weak-coupling calculations, like the Random-Phase Approximation. However, to the purpose of describing an insulating state, a proper analytic form of the Jastrow parameters cannot be obtained by means of similar weak-coupling techniques. The lack of a functional form for the Jastrow term, together with the large number of variational parameters required for a long-range correlation factor, constitutes the main obstacle to the use of this wavefunction in presence of strong correlation.

In this thesis, this difficulty is successfully overcome with the help of the Stochastic minimization algorithm [17], which allows us to optimize many variational parameters independently, without assuming any functional form. Considering the half-filled Hubbard model, we find that the long-range correlations introduced by the Jastrow factor are the crucial ingredient to describe the Mott insulating state. Remarkably, the long-distance behavior of the optimized Jastrow parameters is deeply connected to the form of the charge-density structure factor, in analogy with the previous results on liquid Helium. This allows us to generalize the relations found at weak coupling and to obtain a simple understanding on the properties of the Jastrow wavefunction in different dimensions and for different behaviors of the Jastrow parameters. Indeed, we find that the long-range Jastrow factor not only is able to open a gap in the charge excitations, but also can induce anomalous properties, like a vanishing quasiparticle weight, both in metals and insulators, and can suppress the off-diagonal long-range order present in the uncorrelated determinant. Therefore, by exploring the "zoo of phases" that can be obtained with different forms of the Jastrow factor and different determinants, we

gain a notable insight into the properties induced by strong-correlation effects.

Though limited to zero temperature, this variational approach may represent a very important tool in the theory of strongly correlated systems. Remarkably, within our approach, the "Mott fingerprint" clearly emerges as a genuine ground-state property of strongly correlated systems.

# Overview

The thesis is organized as follows:

- In Chapter 1 we introduce the physics of Mott insulators, starting with Mott's original argument and considering several experimental examples where correlation effects lead to electron localization. Subsequently, we introduce the Hubbard model and the previous variational attempts employed to describe the Mott insulating state.

- In Chapter 2 we describe the Jastrow wavefunction and the analytic treatments which were used to gain insights into its properties. Moreover, we present the criteria that we adopt in order to detect the conducting properties of our variational state.

- In Chapter 3 we describe the Stochastic minimization algorithm which allows us to optimize several variational parameters independently.

- In Chapter 4 we show our variational results for the one-dimensional Hubbard model and for the $t - t'$ Hubbard model.

- In Chapter 5 we consider the Jastrow wavefunction in two dimensions and the possible occurrence of an unconventional metal-insulator transition within this kind of wavefunction.

- In Chapter 6 we consider the Bose-Hubbard model and compare the accuracy of our wavefunction with the exact results coming from diffusion Monte Carlo calculations.

# Chapter 1

# Mott insulators and the Hubbard model

Since its early applications, the independent-electron approach has led to a good understanding of the electronic properties of many different materials. This scheme allows one to distinguish in a straightforward way a metal from an insulator by simply looking at the filling of the electronic bands. Indeed, within this approach, the only effect of the electron interaction is to renormalize the various bands and the electrons can still be treated as non-interacting particles. Therefore, the metallic or insulating behavior is determined only by the existence of an energy gap between the highest occupied level and the lowest unoccupied one. As a consequence, within this picture, the fact of having an odd number of electrons per unit cell naturally implies a partially filled conduction band, and, therefore, a metallic behavior. Nevertheless, it is now well accepted that, when the electron interaction is sufficiently strong, the independent-electron picture fails and the system can be insulating even with an odd number of electrons per unit cell. A typical example comes from transition-metal compounds, where the electron-electron interaction is predominant and determines the localization of the charge carriers. These materials, whose insulating character is induced by electron correlation, are called *Mott insulators*.

Experimentally most of the materials that are classified as Mott insulators show antiferromagnetic ordering at low temperatures. This fact, together with the possibility to recover a consistent band-theory description of Mott insulators in

presence of antiferromagnetism, led to the assumption that a Mott insulating state at $T = 0$ is always accompanied by magnetic ordering. However, the essence of the Mott phenomenon surely resides in the presence of a strong Coulomb repulsion, and, even though it is often masked by magnetic ordering, its understanding requires to go beyond the standard band theory approach and to clarify the role played by strong correlation. From a theoretical point of view, this can be achieved through the definition of a microscopic Hamiltonian, which can capture the main physics of these systems: the Hubbard Hamiltonian. Within this model, the electrons move on a lattice within a tight-binding scheme and correlation is introduced through an on-site repulsive term. As a result of the competition among the kinetic and the interaction term, the Hubbard model shows a rich phase diagram where both the dimensionality and the different lattice geometries play an important role. Of course, one cannot expect that the Hubbard model explains in detail all the properties of strongly correlated materials. Nevertheless, this model contains the most relevant terms which allow one to understand qualitatively the role of correlation in these systems.

This chapter introduces the main ingredients of the physics of Mott insulators and the recent insight obtained through the experimental and theoretical approaches, focusing on the Hubbard model.

## 1.1 The Mott *Gedankenexperiment*

In his pioneering paper [1] Mott considered an ideal system of Hydrogen atoms arranged in a $d$-dimensional cubic lattice of lattice constant $a$. Each Hydrogen provides one electron, which can move on the lattice formed by the protons and is subject to the Coulomb repulsion due to the other electrons. The possibility for the electrons to move on different lattice sites depends on the overlap between the $s$-atomic orbitals, i.e. on the distance $a$ among the Hydrogen atoms forming the lattice.

The properties of the system are the result of two opposite tendencies. On one side the electrons tend to delocalize on the whole lattice, with a consequent kinetic energy gain. On the other hand the Coulomb repulsion among the electrons drives the system towards localization, since the presence of two electrons on the same lattice site, which occurs when they hop independently from site to site, implies

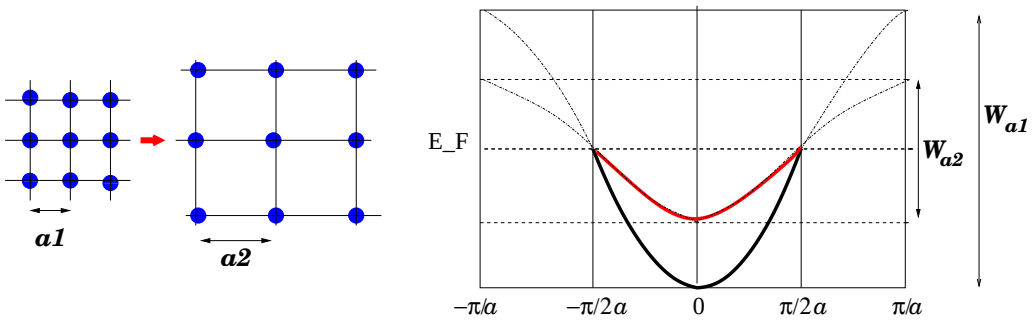


Figure 1.1: Schematic representation of the Mott *Gedankenexperiment*: a lattice of Hydrogen atoms with lattice constant $a1$ and $a2 > a1$ and related band-theory picture. $W_{a1}$ ($W_{a2}$) is the bandwidth associated to the lattice constant $a1$ ($a2$). By increasing the lattice constant, the bandwidth decreases, but the band is always half filled, i.e., the system is predicted to be metallic for any lattice constant $a$.

an energy cost $U$. The Mott's *Gedankenexperiment* follows what happens if the lattice constant $a$ is increased from its equilibrium value to larger interatomic separations. This corresponds to increase the ratio between the Coulomb repulsion and the kinetic energy. According to band theory, this systems would always be a metal since the tight-binding valence $s$-band, which becomes narrower when increasing $a$, is always half filled (see Figure 1.1). This metallic state is indeed realized for small lattice spacings. In the opposite limit, the independent-electron picture clearly fails, since for very large interatomic distances the system will be composed by a set of neutral atoms, which is no more conducting. This happens because at large distances the overlap between the atomic wavefunctions is small, giving a very small energy gain due to the hopping of charges among the lattice. Since the kinetic term is very small, the dominant contribution, which is responsible of the localization of the electrons, comes from the Coulomb repulsion $U$ of two electrons on the same lattice site. In this simple model, above a critical value of the lattice constant $a_c$, the system becomes an insulator which cannot be described by the band theory approach: the *Mott insulator*. Its insulating character does not result in the lack of available states at low energies, as it occurs in conventional band insulators. In a Mott insulator the repulsion among electrons is the most relevant term and determines their localization on the different atoms. The metal-insulator transition (MIT) just described is the prototype of a *Mott tran-*

*sition*. In his original paper, Mott considered for the repulsive term among the electrons a long-range Coulomb potential. The on-site repulsion $U$ is of course the most relevant term and is used here in order to have an intuitive and simple picture of the main contributions that drive the system towards a MIT. Indeed, in presence of a long-range repulsion, the previous arguments in view of a metal-insulator transition driven by electron correlation are still valid. The only notable difference concerns the type of transition involved. By using mean-field arguments, Mott predicts a discontinuous MIT for a three-dimensional system in presence of a long-range Coulomb repulsion, since a finite number of free charges is first required to screen the Coulomb potential and destroy the bound states among positive and negative charges forming the insulator. Therefore, when the system enters the conducting state, there is already a finite number of free carriers and the transition is first order. Instead, according to Mott, the presence of a short-range potential can be compatible with a continuous phase transition.

### 1.1.1 Mott insulators and quantum magnetism

In his *Gedankenexperiment*, Mott does not consider the spin degrees of freedom and their possible ordering. Indeed, in presence of strong Coulomb interaction,

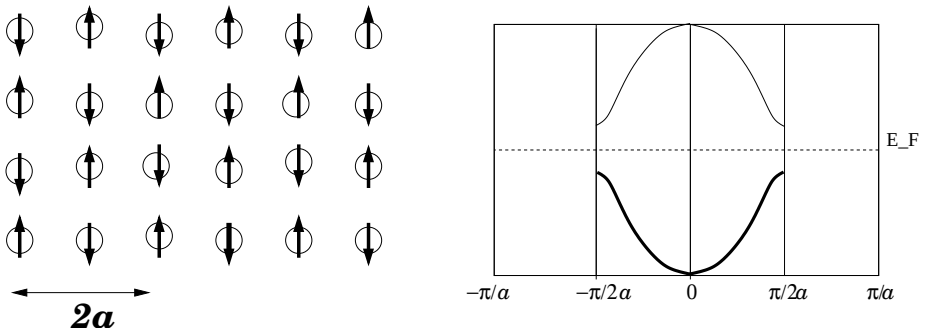


Figure 1.2: Schematic illustration of a system with antiferromagnetic order and Brillouin zone for an antiferromagnetic insulator: band theory allows one to recover an insulator with one electron per site.

the virtual hopping of electrons between neighboring sites favors an antiferromag-

netic arrangement of the spins. [1] Different kinds of spin order can be favoured for particular lattice geometries and, at temperatures lower than the magnetic energy scale, a thermodynamic phase transition towards an insulator with long-range magnetic order can occur. In general, an insulating state that breaks the translational symmetry can be recovered within the Slater picture. For example, in the case of antiferromagnetic ordering, since the doubling of the unitary cell corresponds to a reduction of the Brillouin zone by one half, the valence band turns out to be completely full at half filling (see Figure 1.2). In this case the correlation-induced electron localization is masked by antiferromagnetism, missing the essence of the Mott phenomenon, where a charge gap appears quite independently of spin order. The existence at $T = 0$ of an insulating state of purely "Mott type", that does not break any lattice symmetry, is a debated issue, both experimentally and theoretically. In one dimension magnetic ordering does not occur because, even at $T = 0$, quantum fluctuations dominate and contribute to disorder the system. Instead, in two dimensions the situation is more complicated and the result of the competition between the tendency towards an ordered phase and the disordering effect of quantum fluctuations cannot be predicted easily.

Theoretically, in order to understand the role of the spin degrees of freedom in the Mott insulating state, a wide class of spin models has been studied. In these models, which correspond to the limit of very strong correlation, where charge fluctuations are completely suppressed, each lattice site is occupied by one particle and the remaining degrees of freedom correspond to the different arrangements of the spins [18]. In several cases the spin rotational invariance is spontaneously broken and the ground state is magnetic; nevertheless $SU(2)$ invariant spin structures that do not break any symmetry are also possible. In this context, the most effective route that has been employed in order to describe a singlet state without antiferromagnetic long-range order is the so-called Resonating-Valence-Bond (RVB) state [8]. The RVB state consists of a linear superposition of valence bonds, i.e., configurations in which every lattice site is occupied by one particle and all the electrons are coupled to form singlets. The system resonates among the various valence-bond configurations, recalling the Pauling idea of resonance in the benzene molecule. Since the set of all possible singlet configurations forms a (over-

[1] A more rigorous proof of the antiferromagnetic nature of the exchange term will be given in Section 1.3.2.

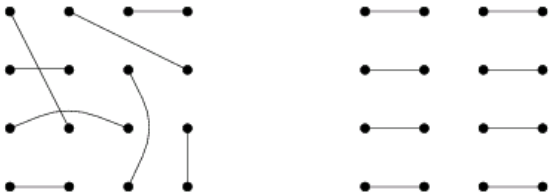


Figure 1.3: Schematic illustration of the RVB state. Sticks represent singlet bonds. (a) spin liquid (b) non-magnetic symmetry breaking RVB state.

complete) basis in the singlet sector, it naturally follows that also the magnetic state can be written in terms of this valence-bond basis, by varying the weights associated to the different configurations. In particular, if configurations characterized by long bond-lengths have large weights, the system can show magnetic long-range order [19]. On the other hand, the RVB picture is particularly useful for describing non-magnetic states, the simplest picture being given in terms of a RVB state with short-range bonds. Such bonds can be either homogeneously distributed over the lattice, with short-range singlet-singlet correlations (known as *spin-liquid*, see Figure 1.3 (a)) or they can be arranged in some special pattern which breaks some of the symmetries of the lattice (see Figure 1.3 (b)). There has been an large amount of theoretical effort in searching for two-dimensional spin-$1/2$ models which exhibit a spin-liquid ground state. The main indication of a possible existence of such states comes from frustrated systems, where the presence of competitive magnetic interactions or the lattice geometry can contribute to disorder the system. In this context, some indications of the existence of a two-dimensional spin-liquid state of the RVB type where found [20, 21]. The next step consists in moving from the spin system to the more realistic case of a finite electron-repulsion, where charge fluctuations are not completely suppressed. In this direction, a description of an insulating state which allows for charge fluctuations and can be connected to the RVB spin-liquid state is needed.

## 1.2 Experimental examples

The *Gedankenexperiment* of Section 1.1 explains in a very elementary way what is the main ingredient which characterizes Mott insulators: the presence of a sufficiently narrow band for valence electrons. In the following, we show different classes of materials where correlation plays a fundamental role. These systems are generally characterized by partially-filled valence bands, with a consequent failure of the band-theory approach in predicting their properties. Indeed, most of these materials are insulators with a large gap, while the independent-electron approach would predict a metallic behavior.

### 1.2.1 Transition-metal oxides

In transition-metal compounds [2], a transition-metal atom is surrounded by ligand atoms with a strong tendency towards negative valence (e.g., Oxygen). This different electron affinity between nearest-neighboring atoms determines the formation of strongly polarized bonds between the transition-metal atom and the ligands. In these materials, the valence electrons have a predominant $d$ character, that implies a very narrow overlap between the atomic states on nearest-neighbor atoms. More precisely, the overlap is often determined by indirect transfer of $d$-orbitals through the ligand $p$ orbitals of the atom located between the transition-metal atoms, contributing to create a narrow bandwidth. Moreover, the cage cre-

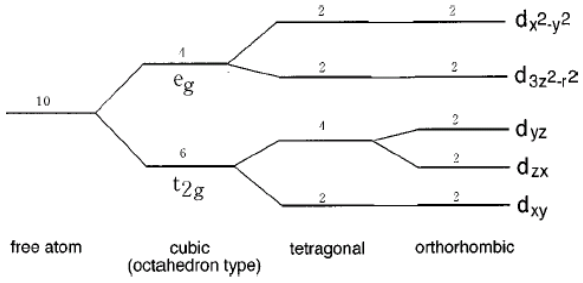


Figure 1.4: Crystal-field splitting of $3d$ orbitals for different symmetries. Numbers over each orbital indicate the degeneracy, including spin.

ated by the ligand atoms induces a crystal field splitting of the bonding orbitals,

which partially removes the degeneracy of the $d$ electrons (see Figure 1.4). The splitting of the $d$-orbitals, together with the different number of electrons in the valence band, causes distinct features for light transition elements compared to the heavy ones. In the case of light transition-metal compounds with a cubic structure and octahedral coordination (see Figure 1.5 (a)) like $Ti, V, Cr$, the $t_{2g}$ orbitals are partially occupied, whereas, for the heavier $Cu$ and $Ni$, the $t_{2g}$ band is fully occupied and low-energy excitations are related to the $e_g$ band. Simple geometric considerations can be drawn about the different overlap between the $p$ orbitals of Oxygen and the different $d$ orbitals. In the case of heavy transition atoms, the overlap between the $p_\sigma$ and the $e_g$ orbitals is much higher than in the light atom case, where the ligand $p_\pi$ orbitals form a weaker bond with the $t_{2g}$ ones (see Figure 1.5 (b)). This fact strongly influences the conducting properties of the different materials. Indeed, since the $t_{2g}$ orbitals point away from the $2p$ Oxygen

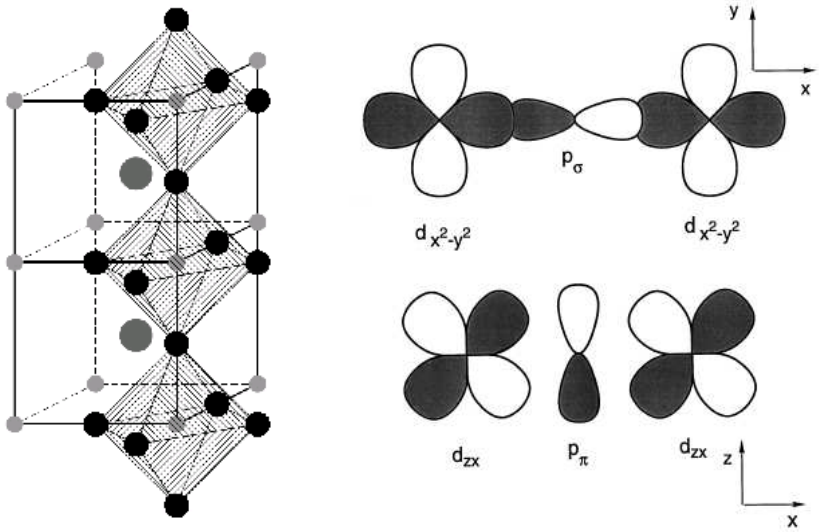


(a) (b)

Figure 1.5: (a) Typical cubic perovskyte structure of transition-metal compounds. Transition-metal atoms are the small grey spheres, at the center of Oxygen octahedra (dark spheres). (b) Different arrangements of $d$ (on top $e_g$ orbitals, at the bottom $t_{2g}$ orbitals) and $p$ orbitals in transition-metal oxides.

ones, in early transition compounds the hybridization with Oxygen is very weak,

leading to an insulating character of purely Mott type. Instead, for late-metal transition oxides, the Fermi level lies on the $e_g$ band, which strongly hybridizes with the $p$ band and induces a charge-transfer insulating behavior. These geometric considerations allow one to understand qualitatively the diagram of Figure 1.6. Another remarkable property of transition-metal oxides is the different screening

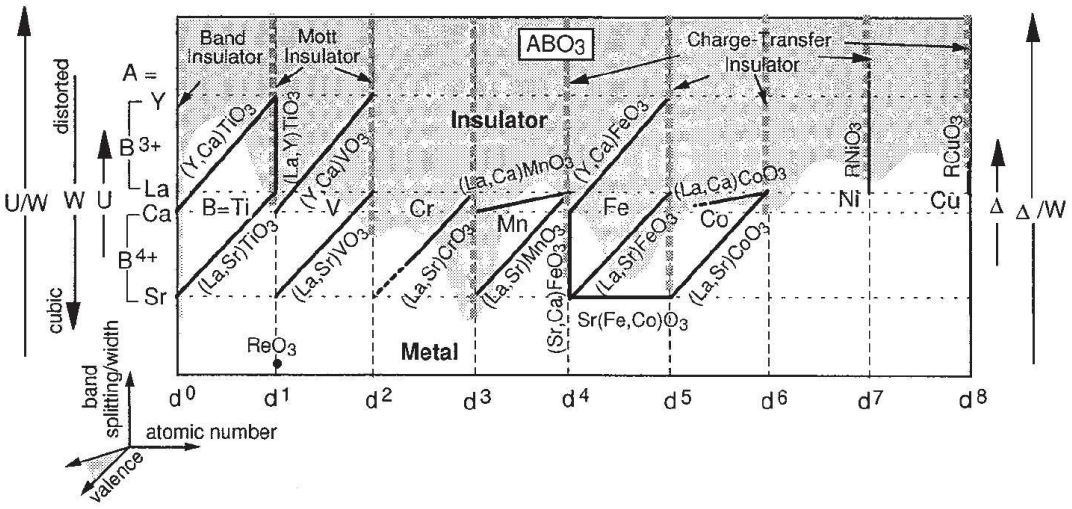


Figure 1.6: Schematic map of the transition-metal compounds with perovskyte structure $ABO_3$ [22]. The transition metal $B$ changes from left to right, increasing its atomic number. The positive ion $A^{n+}$ have a larger size going from bottom to top. Shaded areas denote the insulating compounds, unshaded regions correspond to metals. $W$ is the bandwidth, which increases from top to bottom (where all the compounds are metallic). On the left, for light transition-metal compounds, $U$ denotes the on-site repulsion, which increases from bottom to top. $\Delta$ is the charge-transfer energy, the smaller energy scale for charge excitations of heavy-transition metal compounds. Following the lines one substitutes $A^{n+}$ with another cation having different valence and/or size, and the system changes its properties.

generated by $4s$ and $4p$ electrons in the various compounds. Indeed, considering the early transition-metal oxides $CaO$ and $TiO$, the anti-bonding $4s$ band and the $3d$ bands are predicted to overlap strongly and cross the Fermi energy. Therefore, the screening is effective and determines the metallic behavior of $CaO$ and $TiO$, even in presence of a narrow bandwidth. On the other hand, from $V$ through $Cu$

the $4s$ bands are split-off the $3d$ bands, far away from the Fermi energy. Thus, the Coulomb interaction among electrons in this case becomes very important and these systems are indeed found to be *Mott insulators*.

The most celebrated transition-metal oxide that displays a Mott insulating state is Vanadium Sesquioxide ($V_2O_3$). This material crystallizes in a corundum structure, in which the $V^{3+}$ ions are arranged in $V-V$ pairs along the $c$ axis and form a honeycomb lattice in the $ab$ plane. Each $V$ ion has $3d^2$ electronic configuration and is surrounded by an octahedron of $O$ atoms. One electron per $V$ resides in a singlet bond among the $V-V$ pairs; the remaining electron per $V$ is accommodated in the doublet $e_g$ levels, and determines the electric and magnetic properties of this material. The pure stoichiometric $V_2O_3$ is an antiferromagnetic insulator

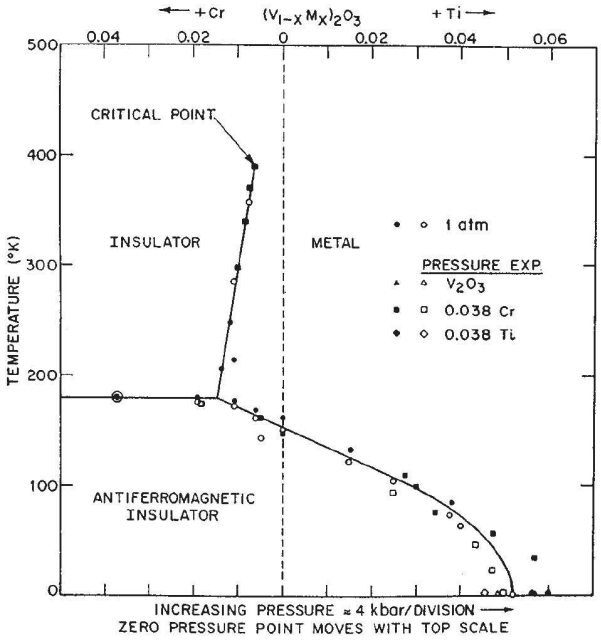


Figure 1.7: Generalized phase diagram of $V_2O_3$ as a function of doping with $Cr$ or $Ti$ (which corresponds to vary the pressure) and as a function of temperature [23].

below $T_{Neel} \sim 160K$ at ambient pressure. The antiferromagnetic-paramagnetic transition at the Néel temperature is at the same time a metal-insulator transition, of first order character: the resistivity drops abruptly [24, 25] after $T_{Neel}$. In

order to observe a metal-insulator transition induced by bandwidth control, it is possible to apply pressure which, by compressing the lattice, widens the bands. Indeed, one finds that $T_{Neel}$ decreases with increasing pressure, and the antiferromagnetic phase is completely suppressed at $P \sim 24$Kbar. The effect of applying a positive pressure can be equally recast by substituting some $V$ atoms with $Ti$ impurities, since the $Ti$ ions have a smaller size. On the other hand, it is possible to increase the interatomic distance by introducing impurities that are bigger than the $V$ ions. This is realized by substituting $Cr$ atoms to $V$. Considering the $(V_{1-x}Cr_x)_2O_3$ system, one recovers, above a certain temperature, a paramagnetic insulating state, which corresponds to the original definition of a Mott insulator. The resulting phase diagram [23] is reported in Figure 1.7.

### 1.2.2 Doping a Mott insulator: High-$T_c$ superconductors

The interest in the physics of Mott insulators had a huge growth after the discovery of High-temperature superconductors (HTSC) [26]. Indeed, all the HTSC are characterized by a universal phase diagram of the form depicted in Figure 1.8, where the Mott insulating state (usually accompanied by antiferromagnetism) appears to be one of the phases involved. It turns out that superconductivity emerges when doping this Mott insulator.

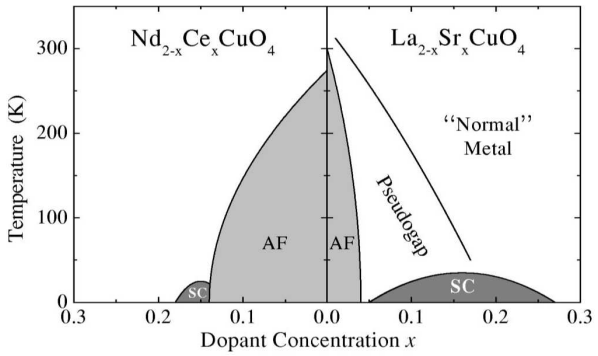


Figure 1.8: Schematic phase diagram for hole doped (right side) and electron doped (left side) High-temperature superconductors.

The main feature common to all the HTSC compounds is the presence of

$CuO_2$ layers sandwiched by block layers. In general, the crystallographic structure of these material is tetragonal, with one or more $CuO_2$ plane separated by layers of other atoms ($Ba$, $La$, $Y$), with a strong tendency towards positive valence. The most widely accepted picture assumes that superconductivity is related to processes occurring in the $CuO_2$ planes, while the other layers, called charge reservoir, simply provide the carriers. Therefore, most of the theoretical approaches consider a two-dimensional interacting system as the key issue to understand the main features of the HTSC compounds [3, 4].

One of the most celebrated examples of HTSC materials is $La_2CuO_4$. The lattice structure of this compound is that of a layered perovskyte, with a body-centered tetragonal structure. The $Cu$ atoms lie inside an elongated octahedra constituted by Oxygen atoms and are in the $3d^9$ configuration, resulting in a net spin $1/2$ and a hole, i.e., the system is half filled. The Fermi level lies in a band constructed mainly from the $d_{x^2-y^2}$ orbital, while the $p_\sigma$ orbital of Oxygens is relatively close. Therefore, since the $p_\sigma$ orbital lies between the Mott gap, the insulating character of $La_2CuO_4$ is mainly of charge-transfer type. The most interesting physics related to this compound of course emerges upon doping. For instance, by substituting $La$ with $Sr$ or $Ba$, extra holes are added into the $CuO$ planes, causing a quick collapse of antiferromagnetic order. With increasing the dopant concentration $x$, $La_{2-x}M_xCuO_4$ (with $M = Sr$ or $Ba$) undergoes a transition from an antiferromagnetic insulator to a paramagnetic metal, with a superconducting phase at low temperatures. The superconducting transition temperature has a maximum of $\sim 40K$ around $x_m \sim 0.15$, called the optimal doping. Above the superconducting transition temperature, the normal metallic phase shows unusual properties in the underdoped region $x < x_m$, which gradually become Fermi-liquid like when moving towards the overdoped region.

### 1.2.3 Layered Organic materials

Very recently, there has been a lot of experimental and theoretical interest into the novel physics of layered organic superconductors. These materials share many physical properties with the HTSC, but typically with much reduced critical temperature and with a possible spin-liquid phase at very low temperatures. Indeed, they are strongly correlated systems (having $2p_\pi$ orbitals partially occupied) with

quasi two-dimensional lattice structures, like cuprate superconductors. However, they differ from cuprates since their lattice is essentially triangular, and thus the effect of frustration may play an important role into their superconducting and magnetic properties.

In general, these materials are referred to as $k$-(ET)$_2X$ or $k$-(BEDT-TTF)$_2X$, where BEDT-TTF or ET denotes the bis(ethylenedithio)-tetrathiafulvalene, $X$ denotes an organic monovalent anion and $k$ defines the different arrangements of the molecules on each lattice site. The general structure is constituted by conducting ET layers, where couples of dimerized ET molecules are arranged into a triangular lattice (see Figure 1.9). In each dimer, two degenerate highest-occupied

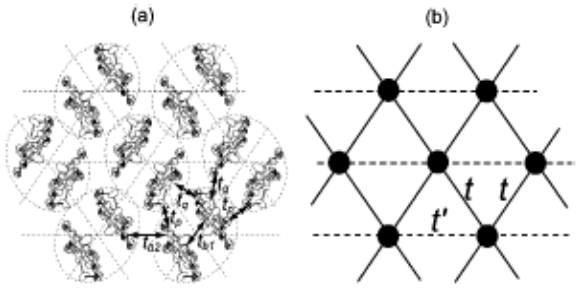


Figure 1.9: Crystal structure of an ET layer for $k$-(ET)$_2Cu_2(CN)_3$: couples of ET molecules dimerize and can be regarded as a dimer unit sitting on a site of a triangular lattice [27].

molecular orbitals (HOMO) belonging to each ET molecule are split into bonding and anti-bonding HOMO's, forming two bands that are separated in energy. Since one hole is introduced into the dimer by the ion $X$, the upper band, which is the anti-bonding HOMO band, is half filled. The replacement of anion $X$, equivalent to discrete pressure control, is quite effective to drive the Mott transition in these organic materials. In $k$-(ET)$_2Cu_2(CN)_3$ there is no sign of antiferromagnetic transition down to 32 $mK$ at ambient pressure, suggesting the possible existence of a quantum spin-liquid state [27, 28] (see the phase diagram in Figure 1.10). However, most of these organic compounds are antiferromagnetic at low temperature and are characterized by a Néel temperature much lower than the mean-field critical temperature. For example, in $k$-(ET)$_2Cu[N(CN)_2]Cl$ the antiferromag-

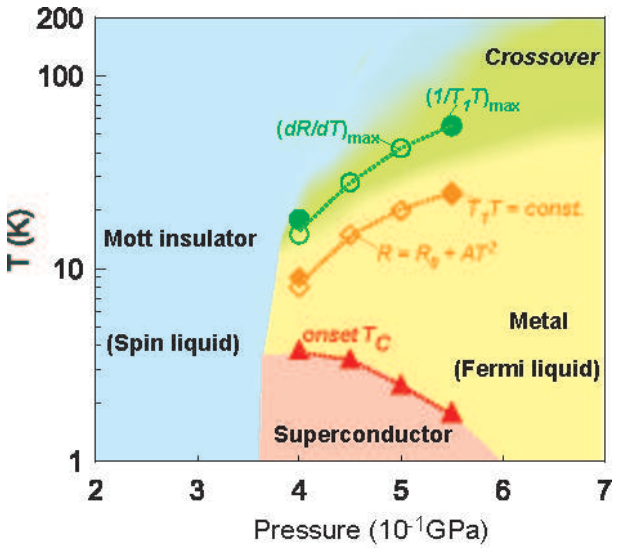


Figure 1.10: Phase diagram of $k$-(ET)$_2Cu_2(CN)_3$ [28].

netic transition occurs at $T_N = 27K$ at ambient pressure and the superconducting transition around $T_c = 13K$ under pressure [29].

### 1.2.4 Ultracold atoms

The recent advances in the physics of cold atoms generate an increasing interest among the community of theoretical condensed matter physicists, since they allow the experimental realization of several lattice models introduced in the last decades in order to understand the role of strong correlation in real materials. Among the most remarkable results obtained in the last years, there is the experimental work by Greiner *et al.* [30] on bosonic systems, which first observed a quantum phase transition from a superfluid to a Mott insulator in a gas of ultracold atoms. Most of the experiments of this type consider a gas of laser cooled $^{87}Rb$ atoms at low enough temperatures, such that a Bose-Einstein condensate is formed. The atoms are first put into a magnetic trapping potential, where the Bose-Einstein condensate (with up to $10^5$ atoms) is achieved. The condensate is a superfluid and exhibits long-range phase coherence. Next, a three-dimensional lattice potential is created, by using three optical standing wave lasers aligned orthogonal to each other. If the lattice potential is turned on smoothly, the system

remains in the superfluid phase as long as the atom-atom interaction are small compared to the tunnel coupling, which allows the hopping of the atoms among the lattice sites. As the lattice potential depth $V_0$ is increased, the tunnel coupling decreases and the system tends to localize. The reduction of fluctuations in the atom number on each site leads to increased fluctuations in the phase, until phase coherence is lost. In order to test experimentally the presence of phase coherence, the optical lattice is suddenly turned off. The atomic wavefunctions are then allowed to expand freely and interfere with each other. The interference pattern is then measured and absorption images are taken along orthogonal directions. If the system is superfluid, all atoms are delocalized over the entire lattice with equal relative phases, and a high-contrast interference pattern is expected. Greiner and coworkers found that the interference pattern changes markedly (see Figure 1.11) by increasing the potential depth. Initially the strength of higher-order interfer-

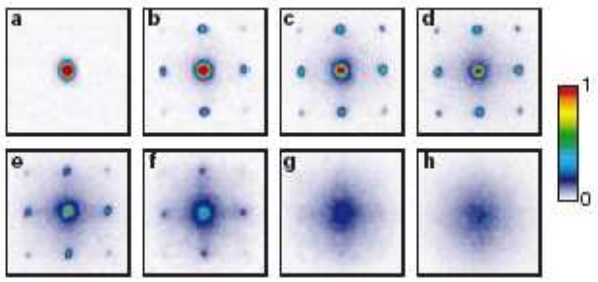


Figure 1.11: Absorption images of multiple matter wave interference patterns for different potential depths $V_0$. Values of $V_0$ increase from (a) to (h) [30].

ence maxima increases when increasing $V_0$, due to the tighter localization of the atomic wavefunction in each lattice site; then suddenly an incoherent background of atoms gains more and more strength, until the interference pattern is not visible any more. This is the most spectacular example of Mott transition, purely induced by correlation, that has been experimentally obtained.

## 1.3 The Hubbard model

The Hubbard model is the simplest example of a microscopic Hamiltonian that takes into account the electron interaction and its competition with the kinetic

energy. It was independently introduced by Hubbard [5], Gutzwiller [11] and Kanamori [31] in 1963 in order to understand magnetism in transition metals. Currently it is widely used in order to understand strongly-correlated systems of the kind described in the experimental Section 1.2.

### 1.3.1 Definitions and simple properties

The one-band Hubbard Hamiltonian is defined on a lattice of $L$ sites and can be written as:

$$H = -t \sum_{<i,j>,\sigma} (c^{\dagger}_{i\sigma} c_{j\sigma} + h.c.) + U \sum_{j} n_{j\uparrow} n_{j\downarrow} \ , \tag{1.1}$$

where $< i, j >$ denotes nearest-neighboring sites $i$ and $j$, $c^{\dagger}_{i\sigma}$ ($c_{i\sigma}$) creates (destroys) an electron with spin $\sigma$ on site $i$ and $n_{j\sigma} = c^{\dagger}_{j\sigma} c_{j\sigma}$ is the occupation number operator. The term *one-band* refers to the assumption that only one Wannier state per site is considered. This approximation is valid when the Fermi energy lies within a single conduction band, implying an irrelevant contribution of the other bands. Since only one atomic level per atom is considered, each lattice site can appear in four different quantum states:

$|0\rangle_j$ empty site (*holon*)
$|\uparrow\rangle_j = c^{\dagger}_{j\uparrow}|0\rangle$ site $j$ occupied by an $\uparrow$ electron
$|\downarrow\rangle_j = c^{\dagger}_{j\downarrow}|0\rangle$ site $j$ occupied by a $\downarrow$ electron
$|\uparrow\downarrow\rangle_j = c^{\dagger}_{j\uparrow} c^{\dagger}_{j\downarrow}|0\rangle$ site $j$ doubly occupied (*doublon*).

The first term in Eq.(1.1) expresses the kinetic part $\mathcal{K}$, which *delocalizes* the $N$ electrons among the lattice. The hopping parameter $t$ controls the bandwidth of the system and depends on the overlap between neighboring orbitals:

$$t_{i,j} = \int dr \ \phi^{*}_{i}(r) \left( \frac{\nabla^2}{2m} + V_{ion} \right) \phi_j(r) \ , \tag{1.2}$$

where $\phi_j(r)$ is a Wannier orbital centered on site $j$ and $V_{ion}$ is the potential created by the positive ions forming the lattice. In translationally invariant systems, $t_{ij}$ depends only upon the distance among the sites $i$ and $j$ and in (1.1) we have considered only a nearest-neighbor hopping $t$. The kinetic term $\mathcal{K}$ can be diagonalized in a single-particle basis of Bloch states:

$$\mathcal{K} = \sum_{k,\sigma} \epsilon_k c^{\dagger}_{k\sigma} c_{k\sigma} \qquad \epsilon_k = -2t \sum_{j=1}^{d} \cos(k_j) \ , \tag{1.3}$$

where $c^{\dagger}_{k,\sigma} = \frac{1}{\sqrt{L}} \sum_j e^{ikj} c^{\dagger}_{j\sigma}$ and a simple $d$-dimensional cubic lattice has been considered.

The *Hubbard U* comes from the Coulomb repulsion of two electrons sharing the same orbital:

$$U = \int dr_1 \, dr_2 \, |\phi_j(r_1)|^2 \frac{e^2}{|r_1 - r_2|} |\phi_j(r_2)|^2 \quad . \tag{1.4}$$

This term is only an approximation of the true Coulomb interaction, since it completely neglects the long-range components which are present in realistic systems. Nevertheless, in spite of its simplicity, the Hubbard model is far from being trivial and the exact solution is known only in the one-dimensional case [6]. Its phase diagram, depends on the electron density $n = N/L$ and the ratio $U/t$. Moreover, different lattice geometries and the addition of longer-range hopping terms could influence the resulting phase diagram.

The form of the Hubbard Hamiltonian given in Eq.(1.1) immediately suggests that its phase space comes out from two competing tendencies: from one side the hopping term tends to delocalize the electrons in the crystal and from the other side the interaction term encourages electrons to occupy different sites, otherwise the system must pay an energy cost $U$ per each doubly occupied site. Whenever the electron density is *away from half filling*, i.e., $n \neq 1$, the number of holes or doubly occupied sites is always different from zero and charge fluctuations are possible without a further energy cost. In this case, the ground state of the system is predicted to be *metallic* for any value of $U/t$, unless for special charge-density wave instabilities at incommensurate wavevectors, that could happen for small dopings and weak correlations [32]. Moreover, the possible occurrence of *superconductivity* in the Hubbard model for $n \neq 1$ has been widely investigated and there are now important evidences that superconductivity emerges at finite doping [33]. Instead, at *half filling* ($n = 1$), there are no extra holes (or double occupancies) and each site is (in average) singly occupied. The two tendencies of delocalizing and localizing the system are strictly dependent on the value of $U/t$, according to the two limiting cases:

- for $U/t = 0$ (*band limit*) the system is a non-interacting metal;
- for $t/U = 0$ (*atomic limit*) the system is an insulator with no charge fluctuations.

The presence of two different phases, for the two limiting values of $U/t$, suggests the existence of a phase transition which is purely due to the increasing of correlation: the *Mott metal-insulator transition*.

As anticipated in Section 1.1.1, the Mott transition is often accompanied by magnetic ordering. In the following, we discuss the possible occurrence of antiferromagnetic order for the Hubbard model on the square lattice, both at weak and strong coupling. For the latter case, we show the canonical transformation that allows one to derive an effective spin Hamiltonian which describes the low-energy physics of the Hubbard model at strong coupling and acts on the Hilbert space with no double occupancies. This is important in view of obtaining an insulating state that still contains charge fluctuations and can be connected to the ground state of the corresponding spin model at strong coupling.

### 1.3.2 Large-$U$ limit: $t - J$ and Heisenberg model

The $t - J$ Hamiltonian was pioneered by Anderson [8] and rederived by Zhang and Rice [34], starting from the two-band Hubbard model, in order to describe the low-energy properties of the $CuO_2$ planes of HTSC. If the system is at half filling, the same problem reduces to an effective spin Hamiltonian, the *Heisenberg Hamiltonian*. The general procedure for their derivation consists in looking for a Schrieffer-Wolff canonical transformation [35], which allows one to achieve a separation between low-energy and high-energy subspaces. In the Hubbard model at large $U/t$, these subspaces are characterized by a different number of double occupancies $n_d$. The operator that mixes these different sectors of the Hilbert space corresponds to the kinetic part (1.3), which can be rewritten as:

$$\mathcal{K} = H_t^+ + H_t^- + H_t^0 \ ,$$

where $H_t^+$ ($H_t^-$) increases (decreases) the number of doubly occupied sites by one and $H_t^0$ corresponds to the hopping processes which do not change the number of double occupancies. The effective Hamiltonian is obtained through the rotation:

$$H_{eff} = e^{iS} H e^{-iS} = H + i[S, H] + \frac{i^2}{2}[S, [S, H]] + \dots \ , \tag{1.5}$$

where the generator $S$ is chosen such that $H_{eff}$ does not contain the operators $H_t^+$ and $H_t^-$. In order to eliminate the terms which are first order in $t$, the generator $S$

reads:

$$S = -\frac{i}{U}(H_t^+ - H_t^-), \tag{1.6}$$

and we obtain the effective $t - J$ *model* to order $t^2/U$:

$$\begin{aligned} H_{t-J} &= -t \sum_{<i,j>,\sigma} [(1 - n_{i-\sigma}) c_{i\sigma}^\dagger c_{j\sigma} (1 - n_{j-\sigma}) + \ h.c.] + \\ &\quad + J \sum_{<i,j>} \left( S_i \cdot S_j - \frac{n_i n_j}{4} \right) + \text{three sites term}, \end{aligned} \tag{1.7}$$

where $S_i = \frac{1}{2} \sum_{\sigma\sigma'} c_{i\sigma}^\dagger \tau_{\sigma\sigma'} c_{i\sigma'}$ is the spin operator for site $i$ ($\tau_{\sigma\sigma'}$ being the Pauli matrices) and $J = \frac{4t^2}{U}$ is a magnetic coupling that favors an antiferromagnetic alignment of spins. The first term of Eq. (1.7) describes hopping constrained on the space with no doubly occupied sites. The nature of the antiferromagnetic coupling $J$ in the superexchange term is due to the possibility of a virtual hopping of antiparallel neighboring spins, which creates an intermediate doubly occupied site with an energy gain $-t^2/U$. Finally, the canonical transformation generates a three-sites term, which is proportional to the hole doping and usually neglected for simplicity. At half filling, the first term in Eq. (1.7) is zero, because every site is already occupied by one electron, and one obtains a pure-spin model:

$$H_{Heis} = J \sum_{<i,j>} S_i \cdot S_j, \tag{1.8}$$

which is the *antiferromagnetic Heisenberg model*. This Hamiltonian describes the low-energy properties of the Hubbard model at half filling for very large $U/t$. The corresponding ground state is smoothly connected to the insulating phase found for large $U/t$ in the Hubbard model. In principle, in order to recover a realistic insulating state which still has charge fluctuations, one could perform the canonical transformation in the opposite direction, reintroducing a finite number of double occupancies on top of the Heisenberg spin state. Practically, as discussed above, the canonical transformation cannot be performed exactly, since the operator $S$ contains a very complicated many-body operator. Therefore, one must find another route in order to connect the two limits. The variational approach constitutes a valid alternative tool to accomplish this task: instead of applying the canonical transformation, one must find an alternative ansatz that allows one to recover an insulating state with a finite number of double occupancies, whose number decreases asymptotically to zero when the interaction strength is increased. From

the above arguments, it turns out that a good variational state, which properly describes the Mott insulating state in the Hubbard model, must contain the correct low-energy properties of the Heisenberg Hamiltonian, and, by increasing the interaction, must connect smoothly to the ground state defined for the Heisenberg spin model.

### 1.3.3 Instability towards antiferromagnetic ordering

The possibility of having an antiferromagnetically ordered ground state for the Heisenberg Hamiltonian has been widely investigated in the last years. In one dimension, quantum fluctuations destroy the antiferromagnetic order and the system remains critical with power-law spin correlations [36]. Instead, in two dimensions, accurate numerical results [37–39] indicate that, for a square lattice, quantum fluctuations are not able to destroy the antiferromagnetic long-range order at $T = 0$.

In the following, we show that also at weak coupling, for particular lattice geometries, the Hubbard model has a tendency towards antiferromagnetic order [40]. Standard calculation done using Random-Phase Approximation gives the following expression for the spin susceptibility:

$$\chi(Q) \sim \frac{\chi^0(Q)}{1 - U\chi^0(Q)}, \tag{1.9}$$

where the bare susceptibility $\chi^0(Q)$ is given by:

$$\chi^0(Q) = \frac{1}{L}\sum_k \frac{f_k - f_{k+Q}}{\epsilon_{k+Q} - \epsilon_k}, \tag{1.10}$$

with $f_k$ being the Fermi occupation number and $\epsilon_k$ the energy levels associated to the unperturbed ground state corresponding to $U = 0$. The magnetic instability occurs when the denominator in Eq.(1.9) vanishes, i.e., for $U\chi^0(Q) = 1$. This condition is known as the Stoner criterion. Considering the instability towards a Néel phase for a two-dimensional system, the vector $Q$ has components $Q = (\pi, \pi)$. Given this vector, one can easily predict the behavior of the spin susceptibility if the *perfect nesting* condition $\epsilon_{k+Q} = \epsilon_k$ holds. This is indeed the case at the Fermi vector $k_F$ for an hypercubic lattice at half filling, with a consequent divergence of $\chi^0(Q)$ in Eq.(1.10). Since $\chi^0(Q)$ diverges, the Stoner

criterion signals a tendency towards antiferromagnetic ordering for any non-zero $U$.

Therefore, both at weak and strong coupling, the Hubbard model on the hypercubic lattice shows an instability towards antiferromagnetism. The metal-insulator transition occurs at an infinitesimally small $U$, as a transition between an uncorrelated metal and an antiferromagnetic insulator. However, the possibility of a metal-insulator transition of purely Mott-type is realistic for frustrated systems, where the different geometry (e.g., triangular lattice) or the addition of a further hopping term for next-nearest neighbors break the perfect nesting condition at weak coupling and discourages a symmetry-breaking state at strong coupling.

## 1.4 Early Variational approaches for the Mott transition

Even though at half filling the Hubbard model on the square lattice shows an insulating phase with antiferromagnetic ordering for all finite values of $U/t$, several studies have been made by imposing the restriction of a paramagnetic solution, in order to understand the nature and the possible occurrence of the insulating state. This is important since the perfect nesting condition can be overcome with the addition of a frustrating hopping term in the system, and a disordered insulating phase might occur at finite $U/t$. This paramagnetic insulating phase cannot be described with a single Slater determinant and with the available tools coming from the independent-electron picture. In this sense, it constitutes a new state of matter, whose properties could be very different from those of standard insulators.

The variational approach offers a simple route to describe this problem, since a good guess of the form of the wavefunction allows one to derive the properties of the corresponding phases in a straightforward way. The key point is to find a proper variational ansatz for an insulating state that breaks no symmetry but still allows for charge fluctuations. For fermionic systems, the trial wavefunction generally contains a determinantal part that ensures the correct antisymmetry when particles are interchanged. In absence of symmetry breaking, being the system half filled, this determinant is metallic. Therefore, in order to describe a metal-insulator transition induced by the electron repulsion, one must find a proper way

of inserting correlation among particles, since this is the missing ingredient of the independent-electron scheme. The correlation term must be able to determine the localization of the electrons, which otherwise are free to conduct. A widely accepted tool for describing a Mott insulating state is to consider the limit of strong coupling, where *total projection*, i.e., the complete suppression of double occupancies, is imposed on top of the Slater determinant. At half filling, this system is a trivial and unrealistic insulator, where charges are completely frozen. A valid description of the Mott transition requires an insulating state where charge fluctuations are gradually increased when reducing the repulsion $U$, until the system becomes delocalized, hence metallic.

In the following we report the early variational attempts done in this direction.

### 1.4.1 General form of correlated wavefunctions

The general form of a correlated wavefunction is given by:

$$|\Psi_{\mathcal{P}}\{v_i, \Delta_i\}\rangle = \mathcal{P}(\{v_i\})|D(\{\Delta_i\})\rangle \tag{1.11}$$

where $\mathcal{P}\{v_i\}$ is the *correlation factor* (or *projector*) and $|D(\{\Delta_i\})\rangle$ is a mean-field Slater determinant. The correlation factor $\mathcal{P}$ is commonly expressed as the exponential of a two-body operator, whose explicit form will be specified in the following. It depends on a set of variational parameters, which we denote with $\{v_i\}$. At this level, it is important to stress that the projector inserts correlation into the wavefunction, whose remaining part corresponds to the mean-field Slater determinant $|D\rangle$. Notice that the term *projector* is often used in the context of spin models, where $\mathcal{P}$ totally projects out the configurations with a finite number of double occupancies. In that case $\mathcal{P}$ is denoted as *full projector*. On the other hand, in many cases, the projector simply gives different weights to the configurations coming from the independent-electron picture. In this latter case, which is of interest in the description of the Hubbard model for any finite $U/t$, $\mathcal{P}$ corresponds to a *partial projector*.

The Slater determinant generally corresponds to the ground state of a mean-field Hamiltonian. In the simplest case, it is the uncorrelated Fermi sea:

$$|FS\rangle = \prod_{\epsilon_k \leq \epsilon_F} c^\dagger_{k\uparrow} c^\dagger_{k\downarrow} |0\rangle, \tag{1.12}$$

which is the ground state of the free tight-binding Hamiltonian with energy dispersion $\epsilon_k$:

$$H_{FS} = \sum_{k\sigma} \epsilon_k c^\dagger_{k\sigma} c_{k\sigma}, \tag{1.13}$$

where $\epsilon_k = -2t \sum_{j=1}^{d} \cos(k_j)$ and $\epsilon_F$ is the Fermi energy. Nevertheless, also the determinant can be parametrized, for example it can be the ground state of the BCS Hamiltonian:

$$H_{BCS} = \sum_{k,\sigma} \epsilon_k c^\dagger_{k\sigma} c_{k\sigma} + \sum_{i,j} \Delta_{ij} (c_{i\uparrow} c_{j\downarrow} + c^\dagger_{j\downarrow} c^\dagger_{i\uparrow}), \tag{1.14}$$

where $\{\Delta_{ij}\}$ depend on the distance $|i-j|$ and are chosen in order to minimize the expectation value of the energy. The BCS ground state is a singlet state that corresponds, in the case of total projection, to the RVB state according to the definition of Section 1.1.1. Another possible Slater determinant comes from the mean-field antiferromagnetic (AF) Hamiltonian:

$$H_{AF} = \sum_{k,\sigma} \epsilon_k c^\dagger_{k,\sigma} c_{k,\sigma} + \Delta_{AF} \sum_i (-1)^{r_i} (n_{i\uparrow} - n_{i\downarrow}), \tag{1.15}$$

with the variational antiferromagnetic parameter $\Delta_{AF}$. In this case, the corresponding Slater determinant breaks the translational symmetry.

In the following, we describe the most widely used variational wavefunctions which have been studied in order to approach the correlated metallic phase and the Mott insulating phase in the Hubbard model.

### 1.4.2 The Gutzwiller wavefunction

In the Hubbard Hamiltonian, the expectation value of the energy contains a repulsive term for two electrons of opposite spins located on the same lattice site. This energy loss cannot be avoided within an uncorrelated wavefunction, since in a paramagnetic state the configurations of electrons with opposite spin are independent. The starting point for a good guess of a correlated wavefunction is to notice that the Hubbard $U$ affects the number of double occupancies $n_d$, inducing their reduction. Following this route, Gutzwiller [11] considered a correlated

wavefunction $|\Psi_g\rangle$, where configurations having a different number of double occupancies $n_d$ have different weights:

$$|\Psi_g\rangle = \exp\left[-g\sum_i n_{i\uparrow}n_{i\downarrow}\right]\,|FS\rangle, \tag{1.16}$$

where $g$ is the Gutzwiller variational parameter, the operator $n_{i\uparrow}n_{i\downarrow}$ counts the number of double occupancies on each site $i$ and $|FS\rangle$ is the Fermi sea (1.12). The Gutzwiller wavefunction (GWF) for $g = 0$ corresponds to the simple $|FS\rangle$, and, therefore, it is exact for $U/t = 0$. On the other hand, for $g = \infty$, the wavefunction (1.16) contains no double occupancies, and corresponds to the atomic limit obtained for $U/t = \infty$. In this limit the Gutzwiller wavefunction is usually written as:

$$|\Psi_{g=\infty}\rangle = \prod_i (1 - n_{i\uparrow}n_{i\downarrow})\,|FS\rangle \tag{1.17}$$

and corresponds to the *fully-projected Gutzwiller wavefunction*. At half filling, this wavefunction is insulating by definition, since no charge fluctuations can occur when the number of electrons $N$ equals the number of sites $L$.

For finite $U/t$, the probability of finding configurations with large $n_d$ decreases with increasing $g$. Since the two end points given by the uncorrelated metal and the atomic limit are properly described by this wavefunction and the minimum variational energy might occur for $g = \infty$ even at finite $U/t$, one expects to find a metal-insulator transition between the above mentioned limits.

Despite its simplicity, the Gutzwiller wavefunction is difficult to handle analytically, since the correlation term acts on the configuration space, while the determinant is easily expressed in momentum space. The evaluation of the kinetic energy leads to the calculation of a different Slater determinant for any configuration of the electrons in the lattice, each being weighted with the Gutzwiller correlation factor $\exp(-gn_d)$. The *Gutzwiller approximation* (GA) consists in neglecting the different weights introduced by the determinants, and counts the terms that are associated to an equal number of double occupancies $n_d$ with the only use of combinatorics. This approximation, which neglects the spatial correlation of the spins given by the Slater determinants, might be a poor approximation that cannot be controlled in a systematic way. Nevertheless, in the past it was used to get insight into the property of the Hubbard model at half filling. Brinkman and

Rice, in their famous paper [41], by using the Gutzwiller approximation, found that the Hubbard model undergoes a metal-insulator transition at a finite $U/t$. They obtained:

$$n_d^{GA} = \frac{1}{4}\left(1 - \frac{U}{U_c}\right), \tag{1.18}$$

with the minimum variational energy per site given by:

$$E_g^{GA} = \epsilon_0 \left(1 - \frac{U}{U_c}\right)^2, \tag{1.19}$$

where $\epsilon_0$ is the uncorrelated energy per site and $U_c = 8\epsilon_0$. Therefore, for $U = U_c$, the number of doubly occupied sites vanishes and the system becomes insulating. The insulator is described by zero doubly-occupied sites, i.e., $n_d = 0$, and, therefore, charge fluctuations are totally suppressed, implying zero-energy gain ($E_g^{GA} = 0$ in the insulator). However, subsequent numerical studies done on the Gutzwiller wavefunction, by using Quantum Monte Carlo (free of the approximations introduced in the GA approach) [12, 42] and exact analytic treatments of the GWF (in one dimension) [43], clarified that the Gutzwiller correlation factor is not sufficient to create an insulator in any finite dimension. At half filling, the minimized GWF on the Hubbard model is always metallic, apart from the atomic limit that occurs only at $U/t = \infty$ and $g = \infty$. For any finite $U$, the $g$ parameter is finite, leading to a finite number of double occupancies, and the system turns out to be metallic. This is due to the fact that, once a holon-doublon pair is formed, these objects are free to move without paying any further energy cost, and, therefore, they can participate to the conduction events. More specifically, in the lattice occupied in average by one electron per site, holes are positively charged objects, while the doublons are negatively charged. When an electric field is applied to the system, they are consequently free to move in opposite directions, and the system shows a metallic behavior.

### 1.4.3 Short-range holon-doublon correlation term

The failure of the GWF in describing the insulating state at finite $U$ was attributed to the lack of correlation among empty and doubly occupied sites in Eq.(1.16) [12]. The next steps, in order to construct an insulating variational wavefunction,

were done by adding to the Gutzwiller factor a term which promotes configurations where holons and doublons are nearest neighbors:

$$|\Psi_{g,HD}>=\exp\left[-g\sum_i n_{i\uparrow}n_{i\downarrow}\right]\exp\left[f\sum_{<l,m>}h_l d_m\right]\,|FS\rangle, \tag{1.20}$$

where $h_l=(1-n_{l\uparrow})(1-n_{l\downarrow})$ counts the number of holons on site $l$, $d_m=n_{m\uparrow}n_{m\downarrow}$ counts the number of doublons on the neighboring site $m$, and $f$ is the holon-doublon variational parameter. An analytic treatment of the wavefunction of Eq.(1.20) for the Hubbard model, done using the analogous of the GA for this wavefunction [44], shows that the holon-doublon factor allows one to recover the correct large-$U$ behavior of the energy $E\sim -t^2/U$. Nevertheless, this wavefunction is also metallic for any finite $U/t$. The metallic behavior of wavefunction (1.20) comes out when looking at the momentum distribution, which has a step-function component for any finite $U/t$, signaling that the system has Fermi-liquid character [44]. Subsequent numerical studies confirmed that the short-range holon-doublon projector fails in describing an insulating state [13]. This can be explained by considering that, once a holon-doublon pair reaches a distance larger than one lattice site (notice that this is possible unless $f=\infty$), then these two objects can move further apart, without paying any energy cost.

Another short-range correlation factor that contains a many-body operator has been studied in [45], and has the form:

$$|\Psi_{g,MB}\rangle=\exp\left[-g\sum_i n_{i\uparrow}n_{i\downarrow}\right]\exp\left[-g_{MB}\eta_{MB}\right]|FS\rangle, \tag{1.21}$$

where $g_{MB}$ is the many-body variational parameter and the many-body operator:

$$\eta_{MB}=\sum_i\left[h_i\prod_\delta(1-d_{i+\delta})+d_i\prod_\delta(1-h_{i+\delta})\right]$$

($\delta$ being the vector connecting nearest neighbors) counts the number of isolated holons and doublons. This operator is capable to reduce the weight of the configurations with isolated holons and doublons. Nevertheless, even this correlation factor cannot give a good representation of the Mott insulating state. An intuitive picture is that it does not take into account situations in which one holon is surrounded by several doublons (or viceversa), constituting again a charged negative (positive) object, free to move under the action of an electric field.

## 1.5 DMFT approach to the Mott transition

Among the various approaches to the Mott transition, the Dynamical Mean Field Theory (DMFT) is one of the most widely used in the last years [7]. Indeed, within DMFT, it is possible to obtain a metal-insulator transition purely induced by correlation, without any symmetry breaking. Moreover, very recently this scheme has been addressed to study realistic systems [46], offering an alternative tool for post-Hartree Fock calculations.

The DMFT technique inherits the idea coming from standard mean-field theories, which approximate a lattice problem with many degrees of freedom by a single-site effective problem. The underlying physical idea is that the dynamics at a given site can be thought of as the interaction of this site with an external bath constituted by all the other sites. All interactions with the degrees of freedom of the bath are contained into an effective field, called the Weiss field. Unlike the classical case, in which the Weiss field is a number, the quantum case requires a time dependent function, that captures the ability of one electron to enter or leave the atom on a certain time scale.

Considering the Hubbard Hamiltonian, a possible mapping of the original Hubbard model into a single-site effective problem corresponds to the Anderson impurity model [47]. This model describes a single site embedded in a bath of non-interacting fermions, that can hop from the bath to the site and viceversa. The original Hubbard term resides only on the single site, and discourages the hopping of the electrons from the bath, if another electron is already present. The parameters associated to Anderson impurity model are obtained in a self-consistent way such that the Green's function of the effective model coincides with the local Green's function of the Hubbard model. Within DMFT, the spatial fluctuations are frozen, but local dynamical quantum fluctuations are fully taken into account. This reflects into the fact that the calculated self energy does not have any $k$ dependence. This approximation scheme has been shown to be exact in the limit of infinite dimension [7].

A qualitative picture of the Mott transition obtained within DMFT for the Hubbard model is shown in Figure 1.12, where the density of states is plotted for different values of $U/t$. The density of states of the strongly correlated metal displays a three-peak structure, made by a quasiparticle band close to the Fermi

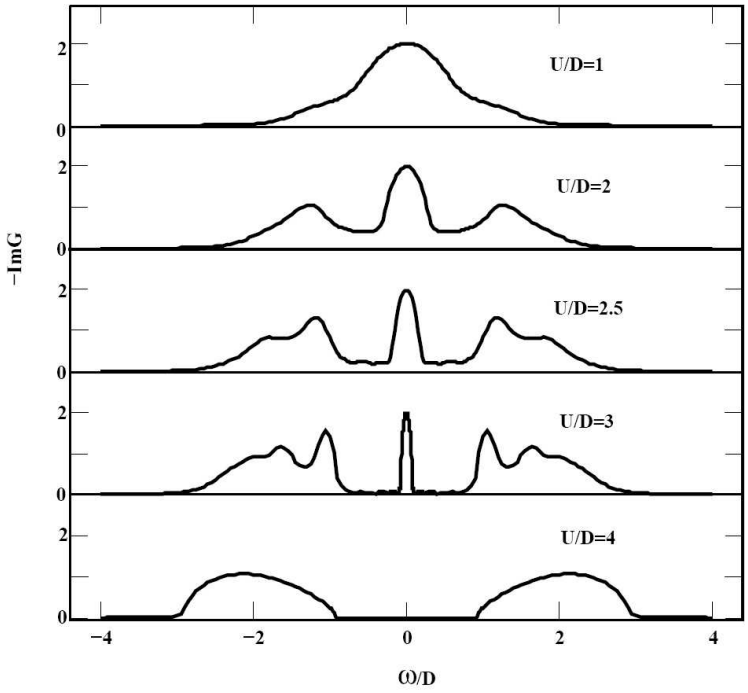


Figure 1.12: Local spectral function for the half-filled Hubbard model and different values of the interaction $U/D$, where $D$ is half the bandwidth [48].

energy, surrounded by a lower and an upper Hubbard band. The quasiparticle peak corresponds to the low-energy coherent excitations described within Fermi-liquid theory. Its width is reduced when approaching the insulator, since part of the spectral weight is transfered to the Hubbard bands. These latters describe the atomic-like transitions corresponding to the addition or the removal of one electron on an atomic site, which broaden into bands in the solid. At $T = 0$, the mean-field solution that corresponds to the paramagnetic metal disappears at a critical coupling $U_{c2}$. At this point, the quasiparticle weight $Z$ vanishes (i.e, $Z \sim 1 - U/U_{c2}$), giving a scenario very similar to the Brinkman-Rice transition. On the other hand, a mean-field insulating solution is found for $U > U_{c1}$, with the Mott gap $\Delta$ opening up at $U_{c1}$. Since $U_{c2} > U_{c1}$, there is a region of coexistence of the two solutions and, when the quasiparticle peak disappears, the gap $\Delta$ has already a finite value. The disappearance of the quasiparticle peak in correspondence of a finite value of the charge gap has been widely discussed within the DMFT approach. In order to

understand whether this is an artifact of the technique, several improvements have been worked out, like the possibility to consider a cluster of sites embedded in the bath instead of the single-site problem. Indeed, the absence of spatial correlations and the fact that DMFT does not take into account the role played by the dimensionality constitute the main drawback of this technique. The cluster DMFT [49] could give remarkable improvements in this direction.

# Chapter 2

# The Jastrow wavefunction and the criteria for an insulating state

In the previous chapter, by considering the early variational attempts for the description of a Mott insulating state, we have seen that a short-range correlation term of the Gutzwiller type, even in presence of a holon-doublon short-range term, always gives a metallic state, unless charge fluctuations are completely frozen. However, in any realistic insulator, the presence of a gap in the charge excitations does not forbid the possibility to have charge fluctuations. Of course, the charge fluctuations of an insulator must be radically different from those of a metal, since their behavior at small energies reflects the presence of a charge gap. Therefore, a proper wavefunction (WF) for the realistic description of an insulating state must give the correct behavior for the charge fluctuations at low energy.

In a fermionic system, a well-established approach to describe a correlated state that does not break any symmetry is to take a metallic Slater determinant and change its amplitudes by means of a correlation factor. Therefore, in order to adjust the form of the charge fluctuations, i.e., give the correct Mott-insulating character, the correlation term plays the main role. A valid indication of a correlation factor that can accomplish this task comes from the literature on liquid Helium. In this context, several numerical results on the continuum, sustained by analytical calculations, have shown that the Jastrow WF gives the correct low-energy properties of the system [15, 16]. In particular, it turns out that the Jastrow factor is capable of giving the correct behavior of the static structure factor, the observable

which gives direct insight into the density fluctuations. Notice that liquid Helium ($^4He$) is a correlated bosonic system, which generally exhibits Bose-Einstein condensation and whose zero-temperature structure factor is dominated by the zero point motion of gapless phonon modes. Therefore, the physics involved in this system appears quite far from that of a Mott insulator. However, the capability of the Jastrow factor to give the correct static structure factor suggests that, if we are interested in the correct description of charge fluctuations, the Jastrow term constitutes the fundamental ingredient for a good variational ansatz of an insulating state. Of course, for a proper variational description of insulators, we expect a form of the Jastrow remarkably different from the one of a gapless system like Helium.

In this chapter we review the analytical and numerical progresses that have been made in the past, in order to understand the properties and the range of applications of the Jastrow WF. This insight will be useful to understand the role of the Jastrow factor in strongly correlated fermionic systems on a lattice and its ability to describe the Mott insulating state.

Next, we introduce the criteria that will be used in the numerical calculations in order to test the insulating character of the optimized Jastrow WF in the Hubbard model.

## 2.1 The Jastrow factor

The Jastrow factor, introduced for continuum systems [14], takes into account correlation effects through a two-body term of the form:

$$\mathcal{P}_J = \exp\left[\frac{1}{2}\sum_{i,j} v(r_{ij}) n_i n_j\right] \quad , \tag{2.1}$$

where $v(r_{ij}) = v(|r_i - r_j|)$ are variational parameters, which for isotropic systems depend only on the relative distance among the particles and $n_i$ is the particle density at position $r_i$. It is useful to consider also the Fourier-transformed Jastrow factor:

$$\mathcal{P}_J = \exp\left[\frac{1}{2}\sum_{q} v_q n_q n_{-q}\right] \quad , \tag{2.2}$$

where $v_q = \sum_r v(r)\mathrm{e}^{iqr}$ and $n_q = \frac{1}{\sqrt{L}}\sum_r n_r \mathrm{e}^{iqr}$ are the Fourier transformed Jastrow parameters and particle density, respectively. The exponential form (2.1), which can be written in terms of a pair-product state, guarantees the size consistency of the WF. For bosons the form (2.1) already ensures the correct symmetry. Instead, for fermionic systems, the Jastrow factor is applied to a Slater determinant $|D\rangle$, in order to recover the correct antisymmetric form:

$$|\Psi_J\rangle = \mathcal{P}_J|D\rangle \ .$$

The Jastrow WF has been widely studied on continuum systems, with the employment of a large variety of analytic and numerical techniques. In a series of papers, Sutherland showed that the Jastrow WF corresponds to the exact ground-state of a family of one-dimensional Hamiltonians defined on the continuum. In Ref. [50] Sutherland considers a system of particles defined on a ring of circumference $L$, interacting with a potential $V(x_{ij}) = g\frac{\pi^2}{L^2}\left[\sin\left(\frac{\pi x_{ij}}{L}\right)\right]^{-2}$, with $g$ fixing its strength. The corresponding ground-state wavefunction is

$$\Psi(\{x_j\}) = \prod_{i>j}\left|\sin\frac{\pi(x_i - x_j)}{L}\right|^{\lambda}$$

where $\lambda$ depends on the potential strength $g$ as $2\lambda(\lambda-1) = g$. The case $\lambda = 1$ corresponds to free fermions. The lattice version of the Sutherland's problem was found for a spin system by Shastry and Haldane [51, 52], who considered a spin 1/2 chain with a long-range $1/r^2$ antiferromagnetic exchange. Following previous results of Metzener and Vollhardt on the exact spin properties of the fully-projected Gutzwiller WF, they find that $|\Psi_{g=\infty}\rangle$, defined in Eq.(1.17), corresponds to the exact ground state of this model.

However, the most interesting analytic and numerical results concerning the properties of the Jastrow WF come from its wide applications in Helium physics. In this field, starting from the very early approach of McMillan [15], who used a parametrization of the Jastrow term coming from the solution of the corresponding two-body problem, the form of the Jastrow factor has been subsequently fine-tuned [16, 53–55] in order to reproduce accurately the properties of the $^4$He liquid state. It turned out that, even if the ground-state energy is well approximated by using a short-range correlation term, the addition of a structure in the parameters $v(r_{ij})$ at large distances is fundamental, in order to reproduce correctly the pair-distribution function and structure factor of the liquid. Since many results related

to the properties of the Jastrow WF for liquid Helium are widely used in this thesis, we will analyze them in detail in the following sections.

Furthermore, among the applications of the Jastrow WF, a successful and recent case corresponds to the fractional quantum Hall effect. Indeed, the Laughlin WF [56], which describes a two-dimensional electron gas subject to a magnetic field perpendicular to the layer, can be easily written in terms of one and two-body Jastrow factors:

$$\Psi_L(\{z_i\}) = \exp\left[\frac{1}{\nu}\sum_{i\neq j}\ln(z_i - z_j)\right]\exp\left[\sum_l |z_l|^2\right] \quad , \tag{2.3}$$

where $z_j = x_j + iy_j$ indicates the dimensionless complex coordinate of the $j$-th particle and $\nu$ is the filling fraction ($\nu$ must be an odd fraction in order to have the correct antisymmetry). In this system, correlation effects are very important since, in that geometry, the magnetic field strongly reduces the kinetic energy of the electrons. The two-body Jastrow factor is able to capture this physics and WF (2.3) turns out to be extremely close to the exact ground state [57].

Finally, in the last years the Jastrow WF has been also widely applied in quantum chemistry calculations [58], where it allows one to include correlation effects on top of the Hartree-Fock or Local Density approximation. Also in this case, a simple analytic form of the Jastrow parameters is generally used [59]:

$$v(r_{ij}) = \frac{a_{\sigma_i\sigma_j} r_{ij}}{1 + b_{\sigma_i\sigma_j} r_{ij}} \quad , \tag{2.4}$$

where $a_{\sigma_i\sigma_j}, b_{\sigma_i\sigma_j}$ are spin-dependent parameters. At short distance, the value of $a_{\sigma_i\sigma_j}$ is fixed by imposing the cusp condition, which cancels the divergence of the potential energy as $r_{ij} \to 0$. Instead, the long-wavelength behavior of the Jastrow parameters, in analogy with what is done for liquid Helium, is usually deduced from Random-Phase Approximation (RPA).

On the other hand, considering the application of the Jastrow WF on lattice models, one does not find the same counterpart. The fact that the Jastrow factor involves many variational parameters, whose number grows with the lattice size, constitutes the main drawback for the application of this WF. For this reason, in many calculations, the functional form of the Jastrow parameters is kept fixed and the number of independent parameters is reduced. This implies an easy-to-handle

WF, which on the other hand is biased by the choice of the functional form and looses the variational flexibility of Eq.(2.1).

However, there are examples where a good guess for the functional form of the Jastrow parameters gives accurate results also for lattice models. Indeed, a long-range Jastrow WF with a logarithmic form $v_{ij} = \ln(r_i - r_j)$ turns out to be the correct ansatz which induces Luttinger-liquid-type correlations in the one dimensional $t - J$ model [60].

Moreover, the use of the spin-Jastrow factor on the Heisenberg model gave strong indications that a WF of this type is very accurate for quantum-spin systems [61]. The spin-Jastrow factor has the following form:

$$\mathcal{P}_J^{S_z} = \exp\left[-\frac{1}{2}\sum_{i,j} v_{ij}^z S_i^z S_j^z\right] \quad , \tag{2.5}$$

where $S_j^z$ is the $z$-component of the spin associated to the particle on site $j$. In this case, the long-range form of $v_{ij}^z$, deduced from analytic calculations, allows one to reproduce the correct spin-correlation functions in quantum-spin models [62, 63].

Nevertheless, in the case of the Hubbard model at half filling, the role of the density Jastrow factor has been generally considered irrelevant for the description of its physical properties and its use was believed to influence only the accuracy in energy. Therefore, most of the studies did not employ this tool, and considered the on-site Gutzwiller projection as the standard starting point [13, 64].

## 2.2 Gaussian approximation for the structure factor

In a pioneering paper [16] Reatto and Chester realized that, in order to correctly reproduce the structure of liquid Helium, a long-range component of the Jastrow factor is required. In order to understand the relation among the Jastrow and the structure factor, they derived an approximate formula, as shown below.

They construct the approximate ground-state of an interacting bosonic system in terms of a short-range wavefunction, that we denote with $|\Psi^0\rangle$, and a Jastrow factor. The key point of their derivation resides in the Gaussian approximation for the probability density associated to $|\Psi^0\rangle$, which corresponds to write it in terms of a cumulant expansion, and truncate to second order (see Appendix A).

The calculation of the structure factor $N^0(k)$ for $|\Psi^0\rangle$, within the Gaussian approximation, corresponds to the following quantity:

$$N^0(k) = \frac{\langle\Psi^0|n_{-k}n_k|\Psi^0\rangle}{\langle\Psi^0|\Psi^0\rangle} \simeq \frac{\int[\{d\rho_q\}]e^{-\sum_q C(q)\rho_q\rho_{-q}}\rho_k\rho_{-k}}{\int[\{d\rho_q\}]e^{\sum_q C(q)\rho_q\rho_{-q}}} = \frac{1}{2C(k)},$$

where $\int[\{d\rho_q\}]...$ is a functional integral defined for the set of continuous functions $\{\rho_q\}$. [1] From the above relation, one finds the cumulant $C(q) = 1/2N^0(q)$. Now consider the structure factor $N(q)$ for a correlated wavefunction $|\Psi_J\rangle = \mathcal{P}_J|\Psi^0\rangle = e^{-\frac{1}{2}\sum_q v(q)\rho_q\rho_{-q}}|\Psi^0\rangle$, constituted by a Jastrow term acting on $|\Psi^0\rangle$:

$$N(k) = \frac{\langle\Psi^0|\mathcal{P}_J\, n_{-k}n_k\, \mathcal{P}_J|\Psi^0\rangle}{\langle\Psi^0|\mathcal{P}_J^2|\Psi^0\rangle} \simeq \frac{\int[\{d\rho_q\}]e^{-\sum_q 1/2N^0(q)\rho_q\rho_{-q}}e^{-\sum_{q'} v(q')\rho_{q'}\rho_{-q'}}\rho_k\rho_{-k}}{\int[\{d\rho_q\}]e^{\sum_q 1/2N^0(q)\rho_q\rho_{-q}}e^{-\sum_{q'} v(q')\rho_{q'}\rho_{-q'}}} \tag{2.6}$$

a simple Gaussian integration allows one to get [16]:

$$N(q) = \frac{N^0(q)}{1 + 2v(q)N^0(q)} \quad . \tag{2.7}$$

This relation, which has a standard RPA form, gives the structure factor of an interacting system described by $|\Psi_J\rangle$, from the form of the Jastrow and the structure factor of the $|\Psi^0\rangle$. The Gaussian approximation for $|\Psi^0\rangle$, which assumes that its charge fluctuations are essentially Gaussian and all the higher-order moments can be neglected, is surely valid for an uncorrelated system, and, in case of short-range correlations, still holds at large distances, i.e., at small $q$. Whenever $2v(q)N^0(q) \gg 1$, one obtains from Eq.(2.7) that $N(q) \sim \frac{1}{v(q)}$, i.e., the small-$q$ behavior of the structure factor, which is generally associated to the low-energy collective excitations, reflects the small-$q$ behavior of the Jastrow factor. Notice that this result can be easily extended to the case of a fermionic system, by considering $|\Psi^0\rangle$ as the uncorrelated Slater determinant. In the case of $|\Psi^0\rangle = |FS\rangle$, the bare structure factor $N^0(q) \sim |q|$, while for a BCS Slater determinant one has $N^0(q) \sim const.$ In the latter case the presence of a Jastrow factor is necessary, in order to obtain the correct behavior of $N(q)$. Moreover, the same relation can be obtained for the spin, by substituting the spin Jastrow parameters $v^z(q)$ and the spin structure factor in Eq.(2.7).

[1] Notice that $\rho_q$ is in general a complex function and its complex conjugate is $\rho_{-q}$.

## 2.3 Jastrow WF on the continuum: Gaskell approach

Given the Jastrow WF in Eq.(2.1), the minimization of the energy as a function of $\{v(r_{ij})\}$ is a complicated problem, that depends on a large number of parameters and in general cannot be solved exactly. Considering a fermionic system on the continuum, Gaskell [65] addressed this problem by using RPA.

Consider the following Hamiltonian, which describes a system of $N$-interacting particles:

$$H = -\frac{\hbar^2}{2m}\sum_i \nabla_i^2 + \frac{1}{2}\sum_{i\neq j} V(r_{ij}) = -\frac{\hbar^2}{2m}\sum_i \nabla_i^2 + \frac{1}{2}\sum_q V(q)\rho_{-q}\rho_q, \quad (2.8)$$

where $V(r_{ij})$ is a generic pairwise interaction, $V(q)$ is its Fourier transform and $\rho_q = \frac{1}{\sqrt{L}}\sum_j \mathrm{e}^{iqr_j}$.

One simple possibility to optimize the variational WF is to minimize the expectation value of the energy:

$$E_T = \frac{\langle \Psi_J|H|\Psi_J\rangle}{\langle \Psi_J|\Psi_J\rangle} \ , \quad (2.9)$$

where $|\Psi_J\rangle = \mathcal{P}_J|FS\rangle$ is the variational WF, constituted by the Jastrow factor (2.1) and the Slater determinant corresponding to the uncorrelated Fermi sea. The use of the Feenberg identity and the fact that the uncorrelated determinant is an exact eigenstate of the kinetic operator, with eigenvalue $\mathcal{K}_0$, allow one to write the kinetic energy as:

$$\begin{aligned} \mathcal{K} &= -\frac{\hbar^2}{2m}\sum_i \frac{\langle FS|\mathcal{P}_J\nabla_i^2\mathcal{P}_J|FS\rangle}{\langle FS|\mathcal{P}_J^2|FS\rangle} = \quad (2.10)\\ &= \mathcal{K}_0 + \frac{\hbar^2}{2m}\sum_i \frac{\langle FS|\sum_{j\neq i}\nabla_i v(r_{ij})\cdot\sum_{l\neq i}\nabla_i v(r_{il})|FS\rangle}{\langle FS|\mathcal{P}_J^2|FS\rangle}. \end{aligned}$$

Fourier transforming the $v(r_{ij})$ parameters and using the Gaussian approximation for the density (RPA) one obtains:

$$\mathcal{K} = \mathcal{K}_0 - \frac{\hbar^2}{2m}\sum_q q^2 v^2(q) N(q) \ , \quad (2.11)$$

where $N(q) = \langle \Psi_J|\rho_{-q}\rho_q|\Psi_J\rangle$ is the structure factor for the interacting system and $v(q)$ are the Fourier transformed Jastrow parameters. The potential energy

can be easily calculated in terms of $N(q)$ as:

$$\mathcal{V} = \frac{1}{2}\sum_q [N(q) - 1]V(q) \quad . \tag{2.12}$$

By making use of expression (2.7) for the structure factor $N(q)$ of the interacting system, one obtains an expression for the kinetic and potential energy as a function of the Jastrow parameters $v(q)$ and the structure factor $N^0(q)$ of the non-interacting system. The minimization of the energy with respect to the $v(q)$ parameters gives:

$$2v(q) = -\frac{1}{N^0(q)} + \sqrt{\frac{1}{[N^0(q)]^2} + \frac{4mV(q)}{\hbar^2 q^2}}, \tag{2.13}$$

which relates the form of the Jastrow to the non-interacting structure factor $N^0(q)$ and to the potential $V(q)$. Unfortunately, this formula cannot be easily generalized for a wavefunction that is not an eigenstate of the kinetic operator (e.g., the BCS state). Moreover, the Feenberg identity, which remarkably simplifies the kinetic term, cannot be applied for the corresponding problem defined on a lattice. Finally, notice that this formula, in presence of a short-range interaction of the Hubbard type $V(q) = U$, since $N_q^0 \sim |q|$ at small $q$ for free electrons, leads to $v(q) \sim 1/q$, and, therefore, following (2.7), to $N(q) \sim |q|$. This result will be compared with the form of the minimized Jastrow parameters on the Hubbard model in the following chapter, where it turns out that, for the insulating phase on a lattice, the Gaskell approach does not give the correct behavior for $v(q)$.

## 2.4 The generalized uncertainty principle

The generalized uncertainty principle, combined with the variational approach, allows one to evaluate the possible occurrence of long-range order, just by looking at the form of the corresponding WF. This principle was originally introduced to detect the possible occurrence of a Bose-Einstein condensate in bosonic systems, but it can be easily generalized for fermions and different types of order.

The fundamental restrictions on quantum fluctuations are generally provided by the Heisenberg uncertainty principle, which holds for hermitian operators. This

principle has been generalized for non-hermitian operators $A$ and $B$ by Pitaevskii and Stringari in [66]:

$$\langle\{A^\dagger, A\}\rangle\langle\{B^\dagger, B\}\rangle \geq |\langle[A^\dagger, B]\rangle|^2 \tag{2.14}$$

where $\langle ...\rangle$ indicates the expectation value over a normalized state $|\Psi\rangle$ and $[A, B] = AB - BA$, $\{A, B\} = AB + BA$. Pitaevskii and Stringari used the above relation in order to evaluate the presence of condensate in a system of interacting bosons. Considering $A = c_q^\dagger$ and $B = n_q = \sum_k c_{k+q}^\dagger c_k$, i.e., the Fourier transformed particle creation operator and density, respectively, they obtain:

$$\mathtt{n}_q \geq \frac{\mathtt{n}_0}{4N(q)} - \frac{1}{2} \tag{2.15}$$

where $\mathtt{n}_q = \langle c_q^\dagger c_q\rangle$ is the momentum distribution, $N(q) = \langle n_{-q} n_q\rangle$ is the static structure factor and $\mathtt{n}_0$ is the condensate fraction, $0 \leq \mathtt{n}_0 \leq 1$. Consider now the normalization condition:

$$\frac{1}{V}\sum_{q\neq 0} \mathtt{n}_q = \int_{0^+}^{\infty} dq \left(\frac{q}{2\pi}\right)^{d-1} \mathtt{n}_q = 1 - \mathtt{n}_0$$

where $V$ is the volume and $d$ the dimensionality. The above inequality, together with the normalization condition, ensures that, in one and two dimensions, no condensate exists if $N(q) \sim q^2$. Indeed if $N(q) \sim q^2$ for $q \to 0$, then Eq. (2.15) implies that at long wavelengths the momentum distribution diverges as $\mathtt{n}_q \sim \frac{1}{q^2}$ and the normalization condition is violated for $d = 1, 2$. The only possibility is that, in presence of $N(q) \sim q^2$, there is no condensate, i.e., $\mathtt{n}_0 = 0$. In this way the divergence of $\mathtt{n}_q$ in Eq.(2.15) is avoided and the normalization condition holds.

Within the variational approach, Eq.(2.14) can be used in combination with the Reatto-Chester formula given in (2.7), which sets $N(q) \sim \frac{1}{v(q)}$, and shows explicitly the relation between the form of the Jastrow factor and the possibility of having Bose-Einstein condensation. It turns out that, with $v(q) \sim \frac{1}{q^2}$, no condensate exists both in one and two dimensions. Instead, a less singular Jastrow of the form $v(q) \sim \frac{1}{|q|}$ guarantees the absence of a condensate only in $1d$. Moreover, by considering different operators $A$ and $B$ and different forms of the Jastrow factor and determinant, one can investigate the possible occurrence of ordering also in the fermionic case. The results for BCS and antiferromagnetic (AF) order are shown in Table 2.1. For the BCS off-diagonal long-range order, one uses the

| Dimension | $v_q$ | $N_q$ | $\|D\rangle$ | $\|\Psi_J\rangle$ |
|---|---|---|---|---|
| 1d | $1/q$ | $\|q\|$ | BCS | no-BCS |
| 2d | $1/q$ | $\|q\|$ | BCS | BCS |
| 1d | $1/q^2$ | $q^2$ | BCS | no-BCS |
| 2d | $1/q^2$ | $q^2$ | BCS | no-BCS |

| Dimension | $v_q^z$ | $S_q$ | $\|D\rangle$ | $\|\Psi_J^{S_z}\rangle$ |
|---|---|---|---|---|
| 1d | $1/q$ | $\|q\|$ | AF | no-AF |
| 2d | $1/q$ | $\|q\|$ | AF | AF |
| 1d | $1/q^2$ | $q^2$ | AF | no-AF |
| 2d | $1/q^2$ | $q^2$ | AF | no-AF |

Table 2.1: Various types of order in $|\Psi_J\rangle$ and $|\Psi_J^{S_z}\rangle$ according to the generalized uncertainty principle (2.14) combined with the Reatto-Chester relation (2.7). The first column indicates the dimensionality. In the second column $v_q$ ($v_q^z$) shows the leading behavior for small-$q$ of the density (spin) Jastrow parameters. The third column $N_q$ ($S_q$) shows the small-$q$ behavior of the corresponding charge (spin) structure factor obtained with the Reatto-Chester relation. The last two columns give the type of order associated to the uncorrelated Slater determinant $|D\rangle$ used to construct the variational WF and the resulting order in the Jastrow WF $|\Psi_J\rangle$ ($|\Psi_J^{S_z}\rangle$) respectively.

operators $A = n_q$ and $B = \Delta_q^\dagger = \sum_j e^{iq\cdot j} c_{j\uparrow}^\dagger c_{j+\delta\downarrow}$ with $\delta$ being the vector corresponding either to zero or to a nearest-neighbor lattice displacement. For AF order, one uses $A = S_q^z$ and $B = \Omega_q^\dagger = \sum_j (-1)^j e^{iq\cdot j} c_{j\uparrow}^\dagger c_{j\downarrow}$. It turns out that the dimensionality plays a fundamental role in determining the occurrence of ordered phases for $|\Psi_J\rangle$. In particular, a Jastrow of the form $v(q) \sim \frac{1}{|q|}$ is able to destroy the long-range order only in $1d$, while $v(q) \sim \frac{1}{q^2}$ can kill the long-range order both in $1d$ and $2d$. The two leading behaviors of the Jastrow factor that are considered reflect the two realistic possibilities for the structure factor, namely $N_q \sim |q|$ or $N_q \sim q^2$. These relations will be verified numerically in the next chapters.

## 2.5 Criteria for detecting an insulating ground state

Within the band-theory approach, a straightforward way to distinguish between metals and insulators is to look at the position of the Fermi level: either the Fermi level crosses one (or more) band, i.e., the system is metallic, or it is located within a band gap, and therefore the system is insulating. This picture explains the insulating/metallic behavior by only looking at the one-particle spectrum of the system. In the variational approach, one can only handle the trial ground state and not the full spectrum of the Hamiltonian. Therefore, another criterion to detect the conducting properties of a system is needed. In a milestone paper Kohn [67] discussed this problem, emphasizing that the qualitative difference in the conducting properties of a system *reflects a different organization of the electrons in the ground state*. Indeed, for realistic Hamiltonians, apart from pathological cases, it is well accepted that the long-distance behavior of correlation functions reflects the presence or absence of a gap in the low-energy excitations.

Following these ideas, in order to detect the insulating or metallic properties of the WF, we calculate of the expectation value of proper operators on the ground state. One possible route consists in using the $f$-sum rule, that gives an upper bound for the gap associated to the low-energy excitations by looking at the small-$q$ behavior of the charge density structure factor. Another possibility comes from the calculation of the Berry phase, which allows us to evaluate the degree of localization of the ground state. Finally, for fermionic systems, one can also evaluate the insulating or metallic character of a state by looking at the momentum distribution and at the presence of Friedel oscillations.

In the following we describe these observables and their different behavior for both metallic and insulating states.

### 2.5.1 The $f$-sum rule

In a series of seminal papers [68, 69], Feynman considers the low-energy excitations of liquid Helium and derives an important relation among the form of the structure factor of the system and the presence of a gap. He uses the following *ansatz* for the excited-state WF:

$$|\Psi_q\rangle = n_q|\Psi_0\rangle, \tag{2.16}$$

where $n_q$ is the Fourier-transformed particle density and $|\Psi_0\rangle$ is the normalized ground-state WF. Notice that Eq. (2.16) describes collective excitations at different wavevectors $q$, that correspond to phonons for liquid Helium and to plasmons for a system of electrons.

Now consider the variational estimator for the excitation energy:

$$\Delta(q) = \frac{\langle\Psi_q|(H-E_0)|\Psi_q\rangle}{\langle\Psi_q|\Psi_q\rangle} = \frac{\langle\Psi_0|n_{-q}[H,n_q]|\Psi_0\rangle}{N(q)},$$

where $N(q)$ is the static structure factor for the ground state $N(q) = \langle\Psi_0|n_{-q}n_q|\Psi_0\rangle$. The interaction term, which generally depends only on the density, commutes with $n_q$, while the kinetic term does not and gives:

$$\langle\Psi_0|n_{-q}[H,n_q]|\Psi_0\rangle \sim q^2,$$

from the two previous equations one recovers the $f$-sum rule:

$$\Delta(q) \simeq \frac{q^2}{N(q)} \quad . \tag{2.17}$$

Since the form of $|\Psi_q\rangle$ is only an approximation of the true excited state, Eq.(2.17) gives an upper bound for the excitation energy. Then, it follows that, whenever the structure factor is quadratic in $q$, $\Delta(q)$ is different from zero, i.e., the system is gapped (or more precisely the gap has a non-zero upper bound). On the other hand, if $N(q) \sim |q|$ the system is surely metallic, since the upper bound for the energy associated to the lowest excitations is zero. In his famous paper, Feynman specifies that the $f$-sum rule gives a true upper bound for the gap when the only low-energy excitations correspond to the collective modes given by the ansatz (2.16). This assumption is known as the *single mode approximation*, and has been applied also for fermions in [70, 71].

Within the variational approach, the use of a long-range Jastrow factor ensures that the $f$-sum rule holds also variationally. Indeed, consider the condition which holds at the variational minimum:

$$\frac{\partial E_T}{\partial v_q} = 0 \qquad \forall q, \tag{2.18}$$

where as usual $E_T = \frac{\langle\Psi_J|H|\Psi_J\rangle}{\langle\Psi_J|\Psi_J\rangle}$ and $|\Psi_J\rangle$ is the Jastrow WF. Standard derivation of $E_T$ with respect to the parameters $v_q$ allows one to obtain the $f$-sum rule of

Eq. (2.17), where $\Delta(q)$ now corresponds to the *variational* charge gap, namely to the difference among the variational energy of $|\Psi_J\rangle$ and the energy of the excited state $n_q|\Psi_J\rangle$.

### 2.5.2 The Berry phase

This method, introduced in [72], is good for studying the conducting properties of one-dimensional periodic systems. It basically consists in measuring the degree of *localization* of the WF. This is a non-trivial property since the use of periodic boundary conditions makes the evaluation of the localization of a WF very hard to formulate. Indeed, the expectation value of the position operator $\hat{x}$ has no meaning inside a set of periodic WFs and it is necessary to introduce a new position operator. In [72] it is shown that a well defined position operator can be written in the following form, which recalls the definition of the Berry geometrical phase:

$$\langle x\rangle = \frac{L}{2\pi}\Im m\left(\ln\langle\Psi|e^{i\frac{2\pi}{L}\sum_{j=1}^{L} jn_j}|\Psi\rangle\right), \tag{2.19}$$

where $\Im m$ denotes the imaginary part and $|\Psi\rangle$ is a normalized periodic WF. With this definition, the position operator is periodic, and the expectation value $\langle x\rangle$ is defined modulo $L$. In order to evaluate the degree of localization for a periodic system, one must calculate the related quantity:

$$z_L = \langle\Psi|e^{i\frac{2\pi}{L}\sum_{j=1}^{L} jn_j}|\Psi\rangle, \tag{2.20}$$

where as usual $n_j$ counts the number of electrons on site $j$.

In [72] it is shown that $z_L$, in the thermodynamic limit, assumes the value:

$I)$ $z_L \to 1$ if the system is localized, hence *insulating*;

$II)$ $z_L \to 0$ if the system is delocalized, hence *metallic*.

An intuitive argument, which suggests the two limiting values of $z_L$, comes from the usual band theory picture, by considering an uncorrelated WF $|\Psi\rangle$ under the action of a magnetic field. In one dimension, the periodic system has a ring geometry. Consider a magnetic flux through the center of the ring, and the associated vector potential $A = \frac{2\pi}{L}$. The corresponding WF can be written as:

$$|\Psi_A\rangle = e^{i\frac{2\pi}{L}\sum_{j=1}^{L} jn_j}|\Psi\rangle \tag{2.21}$$

i.e., the magnetic field shifts the occupied $k$ vectors of $|\Psi\rangle$, giving $k_A = k + 2\pi/L$. The quantity $z_L$ defined in Eq.(2.20) corresponds to the overlap between $|\Psi_A\rangle$ and $|\Psi\rangle$. If the system is metallic, there are other levels available and in general the set of occupied states $\{k_A\}$ of $|\Psi_A\rangle$ will be different from that of the unperturbed $|\Psi\rangle$. Therefore, the two WFs $|\Psi_A\rangle$ and $|\Psi\rangle$ will be different and generally orthogonal, leading to a zero overlap, implying $z_L \to 0$ in the thermodynamic limit. On the other hand, in the insulator, the shift in $k$ vectors gives again the same set for both $|\Psi_A\rangle$ and $|\Psi\rangle$, because there are no other levels available within the first Brillouin zone, leading to $z_L \to 1$ in the thermodynamic limit.

### 2.5.3 The quasiparticle weight and the momentum distribution

Consider a system of $N$ particles described by a ground-state WF $|\Psi_0^N\rangle$ and ground-state energy $E_0^N$. In the Lehmann representation the corresponding Green's function can be written as:

$$G(k,\omega) = \sum_m \left( \frac{Z_m^+(k)}{\omega - E_0^N - E_m^{N+1} + i\delta} + \frac{Z_m^-(k)}{\omega - E_0^N - E_m^{N-1} - i\delta} \right), \quad (2.22)$$

where the sum is over all the possible $(N \pm 1)$-particle states with momentum $k$ and energy $E_m^{N\pm1}$ that are connected by a *one particle excitation* to the ground state $|\Psi_0^N\rangle$, and $Z_m^\pm(k)$ is given by:

$$Z_m^\pm(k) = |\langle \Psi_m^{N\pm1}(k) | c_k^\pm | \Psi_0^N \rangle|^2, \quad (2.23)$$

where $c_k^+ = c_{k\sigma}^\dagger$ ($c_k^- = c_{k\sigma}$) creates (annihilates) an electron with momentum $k$ and spin $\sigma$ in the $N$ particle initial state $|\Psi_0^N\rangle$.

For free fermions $Z_m^\pm(k) = \delta_{m,m_0}$, since the excited state $|\Psi_m^{N\pm1}(k)\rangle$ exactly corresponds to $c_k^\pm|\Psi_0^N\rangle$ and each $k$ univocally defines the excitation (labeled with $m_0$). This reflects in a sudden drop from 1 to 0 in the momentum distribution $\mathtt{n}_k$ around the Fermi momentum $k_F$. When Landau-Fermi liquid theory holds, the low-energy excitations are coherent and $Z_k$, the *quasiparticle weight*, represents the amplitude associated to the quasiparticle excitations close to the Fermi surface, with momentum $k$. Similarly, one finds that the quasiparticle weight of a Fermi liquid corresponds to the step discontinuity of the momentum distribution near $k_F$, which is reduced to $Z_k < 1$ when interaction is turned on. Notice that the

calculation of the overlap (2.23) requires the knowledge of the $N \pm 1$ particle eigenstate. In general, one introduces an ansatz for this excited state, that for projected WFs of the form $|\Psi_{\mathcal{P}}\rangle = \mathcal{P}|D\rangle$ reads:

$$|\Psi^{N\pm1}(k)\rangle = \mathcal{P}c_k^{\pm}|D\rangle = \mathcal{P}c_k^{\pm}\mathcal{P}^{-1}\mathcal{P}|D\rangle = \tilde{c}_k^{\pm}|\Psi_{\mathcal{P}}\rangle, \tag{2.24}$$

where, if the projector $\mathcal{P}$ admits an inverse, $\tilde{c}_k^{\pm}$ can be interpreted as a dressed quasiparticle with momentum $k$ [73]. The behavior of the quasiparticle weight strongly depends on the accuracy of the ansatz for $|\Psi^{N\pm1}(k)\rangle$, as we will see in the following chapters.

If $Z_k = 0$ there are no quasiparticles defined, and Landau-Fermi liquid theory breaks down: the excitations cannot be represented by quasiparticles and the Green's function contains only the incoherent part. In the case of insulators, the quasiparticle weigth $Z_k$ can be finite, but this does not imply a step discontinuity in the momentum distribution, which turns out to be a smooth function of $k$ due to the finite gap in (2.22). It is a debated issue if, for correlated antiferromagnetic insulators, the quasiparticle weight vanishes or remains finite as it happens in standard band insulators [74–76]. The absence of a jump in the momentum distribution is a necessary (but not sufficient [2]) condition in order to have an insulator that does not break any symmetry.

### 2.5.4 Friedel oscillations

The Friedel oscillations [77] are periodic modulations in the density profile that arise as a direct consequence of the presence of a Fermi surface. Consider for simplicity free electrons in a one-dimensional chain of length $L$. For each $k$ the WF associated to each electron can be written as a superposition of an incoming and a reflected plane wave:

$$\Psi_k(x) = \frac{1}{\sqrt{L}}(\mathrm{e}^{ikx} - \mathrm{e}^{-ikx}) = \frac{2i}{\sqrt{L}}\sin(kx).$$

The corresponding charge density is:

$$\langle n(x)\rangle = 2\sum_k f_k|\Psi_k(x)|^2 = \frac{4}{\pi}\int_0^{k_F} dk\,\sin^2(kx) = \bar{n} - \frac{\sin(2k_F x)}{\pi x}, \tag{2.25}$$

[2] One can also have a metal with no Fermi surface like in Luttinger liquids

where $f_k$ is the Fermi distribution function and $\bar{n}$ is the density of the homogeneous electron gas. From the above derivation, it turns out that the presence of a Fermi surface at $k_F$ determines the oscillatory character of the charge. In general, for each $d$-dimensional weakly-interacting fermionic system, which is characterized by a discontinuity in the momentum distribution $\mathtt{n}_k$ around $k_F$, one recovers the same behavior, with the oscillations that decay as $r^{-d}$ with the distance.

Therefore, since the discontinuous character of $\mathtt{n}_k$ at $k_F$ signals a metallic phase, the presence of Friedel oscillations constitute another criterium in order to distinguish a metallic from an insulating state. Notice that the modulation of the charge given by (2.25) corresponds to a singularity at $2k_F$ in the corresponding structure factor. Therefore, just by looking at the behavior of the charge structure factor at $2k_F$, one has information about the metallic character of the corresponding state.

# Chapter 3

# The Variational Quantum Monte Carlo method

Monte Carlo methods allow one to evaluate, by means of a stochastic sampling, integrals over a multidimensional space. This is very useful for quantum many-body problems, where in general the calculation of expectation values cannot be handled analytically, since the wavefunction of the system cannot be factorized into one-particle states.

The core of all Monte Carlo methods is the Metropolis algorithm [78] which generates a Markov chain, i.e., a random walk in configuration space. The configurations sampled during the random walk are distributed, after a certain number of steps required to reach equilibrium, according to a given stationary probability distribution.

The Variational Quantum Monte Carlo approach consists in the direct application of the Metropolis algorithm to sample the probability distribution given by the modulus squared of a given trial wavefunction.

Since the topic of Monte Carlo methods is covered by many textbooks we will not describe its general principles in this Thesis. In the following, we will focus on the direct implementation of the Monte Carlo statistical method in our quantum variational problem, showing the tricks which allow us to obtain an efficient algorithm for the description of remarkably large systems. Moreover, we will describe in detail the Stochastic Reconfiguration algorithm which allows us to minimize the variational energy in presence of a large number of parameters.

## 3.1 The Metropolis algorithm for quantum problems

We have seen in Section 1.4 that the general form of a correlated wavefunction is constituted by a correlation term acting, in the fermionic case, on a Slater determinant, i.e., $|\Psi\rangle = \mathcal{P}|D\rangle$. In the following we show how the statistical evaluation of integrals containing the square modulus of this wavefunction is efficiently implemented.

The first step in the Variational Monte Carlo algorithm consists in choosing the initial coordinates $\{x_i\}_0$ for the $N$ particles on the lattice, either randomly (with the condition that $|\Psi(x)|^2 \neq 0$) or taking them from a previous Monte Carlo simulation. Then a a new trial configuration $\{x_i^T\}_0$ is chosen by moving one of the particles from its old position to another site. The Markov chain is then constructed following the Metropolis algorithm, as shown below. For any move from the $n$-th configuration of the Markov chain $\{x_i\}_n$ to the new trial configuration $\{x_i^T\}_n$, the latter is accepted, i.e., $\{x_i\}_{n+1} = \{x_i^T\}_n$ with a probability equal to:

$$P = \min\left[1, \mathcal{R}\right] \qquad \text{with } \mathcal{R} = \left| \frac{\Psi(\{x_i^T\}_n)}{\Psi(\{x_i\}_n)} \right|^2 , \tag{3.1}$$

where $\Psi(\{x_i\}_n)$ is the wavefunction of the system associated to the configuration $\{x_i\}_n$. This is done in practice by extracting a positive random number $0 < \eta \leq 1$; if $\mathcal{R} \geq \eta$ then $\{x_i\}_{n+1} = \{x_i^T\}_n$, otherwise the proposed move is rejected and $\{x_i\}_{n+1} = \{x_i\}_n$. The calculation of the ratio $\mathcal{R}$ would require, for fermions, the evaluation of two Slater determinants, which scale as $N^3$. The fact that the two configurations are related among each other by the displacement of one particle, allows us to perform a more efficient calculation, which for fermions corresponds to $O(N^2)$ operations. Also the ratio among the correlation terms can be performed in an efficient way, taking into account that only one particle changes its position. For bosons, where only the correlation term is present, this allows us to obtain an algorithm that scales as $O(N)$ instead of $O(N^2)$. These procedures are explained in Appendix B.

After a certain number of steps, known as thermalization time, the configurations $\{x_i\}_n$ generated at each step $n$ in the Markov chain are independent from the initial condition $\{x_i\}_0$ and are distributed according to the probability:

$$p_{\{x_i\}} = \frac{|\Psi(\{x_i\})|^2}{\sum_{\{x_i\}} |\Psi(\{x_i\})|^2}.$$

Notice that this algorithm does not require to know the normalization of the wavefunction, since it always deals with its ratios over different configurations. This is a big advantage of Monte Carlo methods, since many times the normalization constant is not known.

Finally, the expectation value $\langle F \rangle$ of any operator $F$ reduces to average over the values assumed by $F$ along the Markov chain:

$$\bar{F} = \frac{1}{M} \sum_{n=1}^{M} F(\{x_i\}_n), \tag{3.2}$$

where $F(\{x_i\}_n)$ is the observable $F$ calculated for the configuration $\{x_i\}_n$. Indeed the central limit theorem ensures that:

$$\lim_{M \to \infty} \bar{F} = \langle F \rangle,$$

where $\langle F \rangle$ is the true expectation value of $F$ calculated from the probability $p_x$. The statistical error related to the fact that we are sampling a finite set of configurations can be deduced from the variance:

$$\sigma^2(\bar{F}) = (\bar{F} - \langle F \rangle)^2.$$

One can show that the statistical error scales as the square root of the inverse length $M$ of the Markov chain, namely:

$$\sigma^2(\bar{F}) \simeq \frac{\tau}{M} \sigma^2(F),$$

where $\sigma^2(F) = \langle (F^2 - \langle F \rangle^2) \rangle$ and $\tau$ is the autocorrelation time, i.e., the number of steps of the Markov chain which separate two statistically independent configurations. Therefore, for large enough samplings, the average quantities calculated with the Metropolis algorithm give reliable estimates of the true expectation values of the system. In order calculate expectation values among uncorrelated samplings, the *bin technique* is usually employed. This corresponds to average first among $M_{bin}$ configurations, according to (3.2):

$$\bar{F}^{bin} = \frac{1}{M_{bin}} \sum_{n=1}^{M_{bin}} F(\{x_i\}_n) \tag{3.3}$$

In this way the quantities $\bar{F}^{bin}$ are less correlated than the original $F(\{x_i\}_n)$. Then, the calculation of the expectation value follows:

$$\bar{F} = \frac{1}{N_{bin}} \sum_{n=1}^{N_{bin}} \bar{F}_n^{bin}, \tag{3.4}$$

where $N_{bin} = M/M_{bin}$. In this way we get $\tau \simeq 1$, hence $\bar{F} = \langle F \rangle$ and the variance can be evaluated in the standard way as:

$$\sigma^2(F) = \frac{1}{(N_{bin}-1)} \sum_{n=1}^{N_{bin}} (\bar{F}_n^{bin} - \langle F \rangle)^2 \tag{3.5}$$

## 3.2 The minimization algorithm

Consider the variational wavefunction $|\Psi_T(\alpha)\rangle$, where $\alpha = \{\alpha_k\}$ generally corresponds to the set of variational parameters for both the correlation factor and the Slater determinant introduced in Section 1.4. The expectation value of the variational energy can be written as:

$$E_T(\alpha) = \frac{\langle \Psi_T(\alpha)|H|\Psi_T(\alpha)\rangle}{\langle \Psi_T(\alpha)|\Psi_T(\alpha)\rangle} = \frac{\sum_x |\langle x|\Psi_T(\alpha)\rangle|^2 e_L(x)}{\sum_x |\langle x|\Psi_T(\alpha)\rangle|^2} \geq E_0, \tag{3.6}$$

where $E_0$ is the ground-state energy and the completeness relation $\sum_x |x\rangle\langle x|$ over all possible configurations $|x\rangle$ has been inserted. [1] The quantity $e_L(x)$ is called *local energy* and is given by:

$$e_L(x) = \frac{\langle x|H|\Psi_T(\alpha)\rangle}{\langle x|\Psi_T(\alpha)\rangle}. \tag{3.7}$$

Eq.(3.6) shows that the expectation value of the energy corresponds the mean value of the the local energy $e_L(x)$ calculated among all possible configurations $|x\rangle$, each weighted according to the square modulus of the normalized wavefunction. As shown in the previous section, this can be done stochastically by means of a sum over the Markov chain in configuration space:

$$E_T(\alpha) = \frac{1}{M} \sum_{n=1}^{M} e_L(x_n).$$

[1] For simplicity we indicate with $|x\rangle$ the configuration $\{x_i\}$ for $N$ particles.

Let us now explain how to vary the parameters $\alpha = \{\alpha_k\}$ in order to minimize the variational energy, following the Stochastic Reconfiguration algorithm introduced in [17]. To this purpose consider the starting trial wavefunction $|\Psi_T(\alpha^0)\rangle$, where $\alpha^0 = \{\alpha_k^0\}$ is the set of $p$ initial variational parameters (where $k = 1, \dots p$). [2] In linear approximation the new wavefunction, obtained after a small change of the parameters, can be written as:

$$\begin{aligned} |\Psi_T(\alpha')\rangle &\simeq |\Psi_T(\alpha^0)\rangle + \sum_{k=1}^{p} \delta\alpha_k \frac{\partial |\Psi_T(\alpha^0)\rangle}{\partial \alpha_k} = \\ &= \left[1 + \sum_{k=1}^{p} \delta\alpha_k O_k\right] |\Psi_T(\alpha^0)\rangle, \end{aligned} \tag{3.8}$$

where the operators $O_k$ are defined for any configuration $|x\rangle$ as the logarithmic derivative of the wavefunction with respect to the parameters $\alpha_k$:

$$O_k(x) = \frac{\partial \ln \Psi_T^\alpha(x)}{\partial \alpha_k} \tag{3.9}$$

and $\Psi_T^\alpha(x) = \langle x|\Psi_T(\alpha)\rangle$. Putting $O_0 = 1,\ \delta\alpha_0 = 1$ we can write:

$$|\Psi_T(\alpha')\rangle = \sum_{k=0}^{p} \delta\alpha_k O_k |\Psi_T(\alpha^0)\rangle. \tag{3.10}$$

In general $\delta\alpha_0 \neq 1$, due to the normalization of $|\Psi_T(\alpha')\rangle$, and one can redefine $\delta\tilde{\alpha}_k = \frac{\delta\alpha_k}{\delta\alpha_0}$ for each variational parameter $\alpha_k$. In order to find $|\Psi_T(\alpha')\rangle$ such that it approaches the ground state, one possibility resides in projection methods. A standard procedure of projection methods corresponds to filter out the exact ground-state wavefunction by iteratively applying the Hamiltonian operator to the trial ground state. Therefore, we can apply the *power method* to the starting wavefunction:

$$|\bar{\Psi}_T(\alpha^0)\rangle = (\Lambda - H)|\Psi_T(\alpha^0)\rangle, \tag{3.11}$$

where $\Lambda > \frac{E_{max}+E_0}{2}$ is a positive constant, which ensures convergence to the ground state, $E_0$ being the ground-state energy and $E_{max}$ the largest eigenvalue of the Hamiltonian. The next step, in order to ensure that $|\Psi_T(\alpha')\rangle$ has a lower energy with respect to $|\Psi_T(\alpha^0)\rangle$, corresponds to equate Eqs. (3.10) and (3.11) in the subspace spanned by the vectors $\{O_k|\Psi_T(\alpha^0)\rangle\}$.

[2] In the following let us assume for simplicity that $|\Psi_T(\alpha^0)\rangle$ is normalized.

Combining the r.h.s. of Eqs. (3.10) and (3.11) and projecting them on the $k'$-th component we get:

$$\langle\Psi_T(\alpha^0)|O_{k'}(\Lambda - H)|\Psi_T(\alpha^0)\rangle = \sum_{k=0}^{p} \delta\alpha_k \langle\Psi_T(\alpha^0)|O_{k'}O_k|\Psi_T(\alpha^0)\rangle. \quad (3.12)$$

In this way the quantities $\delta\alpha_k$ correspond to the variations of the wavefunction parameters that lower the variational energy. They can be calculated by solving the linear system of equations of the type given in (3.12). It is a system of $(p+1)$ equations, which can be written as:

$$f_{k'} = \sum_{k=0}^{p} \delta\alpha_k S_{kk'}, \quad (3.13)$$

where $f_k$ are the *generalized forces*:

$$f_{k'} = \langle\Psi_T(\alpha^0)|O_{k'}(\Lambda - H)|\Psi_T(\alpha^0)\rangle \quad (3.14)$$

and $S_{kk'}$ is the $(p+1)\times(p+1)$ positive definite matrix given by:

$$S_{kk'} = \langle\Psi_T(\alpha^0)|O_{k'}O_k|\Psi_T(\alpha^0)\rangle. \quad (3.15)$$

The system can be reduced to $p$ equations since $\delta\alpha_0$ is related to the normalization of the wavefunction. Indeed, considering Eq.(3.12) for $k' = 0$, since we have put $O_0 = 1$ in (3.10), the value of $\delta\alpha_0$ reduces to:

$$\delta\alpha_0 = \Lambda - E_T(\alpha_0) - \sum_{k=1}^{p} \delta\alpha_k S_{k0}. \quad (3.16)$$

Substituting (3.16) in (3.12) we obtain the reduced system of equations:

$$\bar{f}_k = \sum_{k'=1}^{p} \delta\alpha_{k'} \bar{S}_{kk'}, \quad (3.17)$$

where:

$$\bar{f}_k = \langle\Psi_T(\alpha^0)|O_k|\Psi_T(\alpha^0)\rangle\langle\Psi_T(\alpha^0)|H|\Psi_T(\alpha^0)\rangle - \langle\Psi_T(\alpha^0)|O_kH|\Psi_T(\alpha^0)\rangle \quad (3.18)$$

and

$$\bar{S}_{kk'} = S_{kk'} - S_{k0}S_{k'0}. \quad (3.19)$$

Notice that the forces $\bar{f}_k$ correspond to $\bar{f}_k = \frac{\partial E_T(\alpha)}{\partial \alpha_k}$. Since at equilibrium one has $\bar{f}_k = 0$, implying $\delta\alpha_k = 0$, this corresponds to satisfy the Euler equations for the variational minimum: [3]

$$\frac{\partial E_T(\alpha)}{\partial \alpha_k} = 0.$$

Moreover, from the definition (3.18), the fact that $\bar{f}_k = 0$ implies that the variational wavefunction fulfills the same property of an exact eigenstate, namely:

$$\langle O_k H \rangle = \langle O_k \rangle \langle H \rangle, \tag{3.20}$$

which suggests a good accuracy of the variational state also with respect to the expectation values of the operators $O_k$.

Let us remark that the Stochastic Reconfiguration method is very close to the Steepest Descent method. The main difference, which allows us to obtain a more stable algorithm, is that the Stochastic Reconfiguration method takes also into account the variation of the wavefunction. Indeed it is straightforward to show, by using the linear approximation (3.10), that Eq. (3.17) is equivalent to the Euler equation with the addition of a constraint related to the norm of the wavefunction, namely:

$$\frac{\partial \left[ E_T(\alpha^0) - \lambda \left( \langle \Psi_T(\alpha^0) | \Psi_T(\alpha') \rangle - 1 \right) \right]}{\partial \alpha_k^0} = 0, \tag{3.21}$$

where $\lambda$ is a Lagrange multiplier that ensures that the norm of the two wavefunctions does not differ of a large quantity. The fact that we can change the parameters of a large amount, without changing notably the wavefunction, allows us to reach the minimum in a stable way, with fewer iterations.

Indeed, in the Stochastic reconfiguration algorithm, the variations $\delta\alpha_k$ are related not only to the forces, but also to the inverse covariance matrix $\bar{S}^{-1}$, namely, by writing Eq. (3.17) in vectorial notations:

$$\delta\alpha = \bar{S}^{-1} \bar{f}.$$

The diagonal elements of the reduced covariance matrix (3.19) give direct information about the fluctuations of the parameters $O_k$. The fact that each component of the force is multiplied by the inverse of the fluctuations allows us to move

[3] This is strictly valid in the case in which the Hamiltonian does not depend on the variational parameters, which is our case.

mainly along the directions where the variance of the corresponding operator $O_k$ is small, i.e., where the signal-noise ratio is small. This avoids undesired instabilities due to the fluctuations of the stochastic system. Moreover, the presence of non-zero off-diagonal elements $\bar{S}_{ij}$ allows us to move each parameter by taking into account all the other directions at the same time. Therefore, we reach the variational minimum being driven not only by the high-energy contributions, but also by the parameters which contribute at low energy.

The equations (3.17) are solved stochastically with the Monte Carlo algorithm. In practice, we perform $M_{SR}$ Metropolis steps in order to calculate the expectation values of (3.18) and (3.19) and have small enough fluctuations. Then the linear system (3.17) is solved in order to find the variations $\delta\alpha_k$. Finally, once the variations $\{\delta\alpha_k\}$ are calculated, the variational parameters $\{\alpha_k\}$ are modified according to:

$$\alpha'_k = \alpha^0_k + \Sigma\,\delta\alpha_k,$$

where $\Sigma$ is a number that can be tuned in order to control the change of the parameters. Generally one starts with a large $\Sigma$ in order to reach the minimum in few iterations, and consequently $\Sigma$ is decreased in order to reduce the fluctuations of the converged parameter. The new wavefunction $|\Psi(\alpha')\rangle$ is then considered as the starting state $|\Psi(\alpha^0)\rangle$ and the method is reiterated, until convergence is achieved.

Indeed, the stochastic nature of the system (3.17) implies that the forces $\bar{f}_k$ are always determined with some statistical noise $\eta_k$, and by iterating the minimization procedure several times, even when the variational minimum is reached, the parameters will fluctuate around their mean values. Therefore, once convergence is reached, one must average over a certain number of iterations in order to find the optimal parameters that are close to the energy minimum. Indeed, in the case of a quadratic energy landscape, the averaged parameters correspond to the minimum energy. However, in many cases it is possible to have non-harmonic contributions, and the larger are the fluctuations, the larger is the bias that is introduced. Indeed, one can describe the evolution of the variational parameters during the minimization iterations by means of a standard Langevin dynamics. The statistical fluctuations are similar to the thermal noise of the Langevin equation:

$$\partial_t \alpha_k = f_k + \eta_k, \tag{3.22}$$

where the thermal noise is defined as:

$$\langle \eta_k(t)\eta_{k'}(t')\rangle = 2T_{noise}\delta(t-t')\delta_{k,k'}. \tag{3.23}$$

By increasing the number of sampled configurations $T_{noise}$ diminishes, since the fluctuations are reduced, namely $T_{noise} \propto M_{SR}^{-1}$. Therefore, there is an optimal value of $M_{SR}$, which guarantees a fast convergence and avoids the parameters to be biased within the statistical accuracy of the sampling. Moreover, we find that the optimal $M_{SR}$ also depends on the type of operators $O_k$ included in the minimization, hence on the type of variational parameters to be minimized. For example, when considering the Hubbard model, if $O_k = \sum_j h_j d_{j+k}$, namely $O_k$ is the holon-doublon operator associated to the distance $k$, one must sample enough configurations in order to have $\langle O_k \rangle \neq 0$, which, for large distances $k$, is strictly dependent on the value of the interaction, since the number of holons and doublons decreases with $U/t$. Therefore, by increasing $U/t$, one is forced to increase $M_{SR}$.

# Chapter 4

# Mott transition in the one-dimensional Hubbard model

In Chapter 1 we have seen that the Hubbard model on the hypercubic lattice orders antiferromagnetically for any finite $U$, thus masking the correlation-induced Mott transition. In one dimension instead, since quantum fluctuations are very strong, no symmetry breaking occurs. Therefore, the one-dimensional Hubbard model, whose exact solution is known by Bethe Ansatz [6], constitutes a good playground where to check the accuracy of possible variational wavefunctions describing an insulating state that does not break any symmetry.

Although analytical techniques, especially bosonization [79], give important insights into the low-energy properties of one-dimensional systems, they do not provide a simple representation of the ground-state wavefunction (WF). In particular, in the Hubbard model, the ground-state WF is very involved within the Bethe ansatz formalism and only in the strong-coupling limit it is possible to obtain significant simplifications because of the explicit factorization of the WF into a charge and a spin part [80]. Therefore, a good variational ansatz that enables one to obtain the physical properties of the system in a straightforward way could be very helpful.

In this chapter we show that a *long-range Jastrow factor* is able to describe correctly the Mott insulating state. We compare the properties of the minimized Jastrow WF with those found for the short-range Gutzwiller and many-body correlation factors described in Section 1.4, and show that, contrarily to the latters,

the Jastrow factor allows us to recover an insulating state with the correct charge fluctuations, without breaking any symmetry. In the simple one-dimensional Hubbard model at half filling, we find, in agreement with Bethe ansatz [6], that a metal-insulator transition occurs as soon as one turns on the interaction, and the system is insulating for any non-zero $U/t$.

Moreover, in order to study the feasibility of the Jastrow WF to describe the Mott transition, in the second part of this chapter we consider the Hubbard model with the addition of a next-nearest neighbor hopping term: the $t - t'$ Hubbard model. This model has a richer phase diagram, which indeed shows a metal-insulator transition at a finite value of $U/t$. We show that, with the long-range Jastrow WF and a proper choice of the determinant, we are able to characterize all the phases involved, namely the ordinary Mott insulator with power-law spin correlations at small $t'/t$, the spin-gapped metal above a critical $t'/t$ and small $U$, and a dimerized Mott insulator at large repulsion. For the metal-insulator transition, we find a critical $U/t$ in agreement with other approaches, signaling that the Jastrow WF offers a valid and accurate tool for the variational description of the Mott transition.

Finally, a metal-insulator transition can be driven not only by increasing correlation, but also by varying the band filling. We consider this filling-controlled metal-insulator transition in the last part of this chapter, where we show that the addition of holes in the half-filled Hubbard model at finite $U/t$ turns the Mott-insulating state into a correlated metal. We show that the Jastrow WF can accurately describe the metal-insulator transition induced by band filling and gives the correct power-law behavior of the correlation functions in the metallic phase, with the exponents predicted from Luttinger-liquid theory.

## 4.1 Results for the one-dimensional Hubbard model at half filling

Let us recall the one-dimensional Hubbard Hamiltonian, using the same notations of Section 1.3:

$$H = -t \sum_{i,\sigma} (c^{\dagger}_{i\sigma} c_{i+1,\sigma} + h.c.) + U \sum_{i} n_{i\uparrow} n_{i\downarrow} \quad . \tag{4.1}$$

Here we consider a chain of $L$ sites, with periodic boundary conditions and $N$ electrons, with $N = N_{\uparrow} + N_{\downarrow}$, being $N_{\uparrow}$ ($N_{\downarrow}$) the total number of spin up (down) electrons and $N_{\uparrow} = N_{\downarrow}$. Since we are interested in the properties of the Hubbard Hamiltonian at half filling, we take $N = L$ electrons. Moreover, in order to have a closed shell in the uncorrelated Fermi sea determinant that is used to construct the variational WF, we consider different lattices of $L = 4n + 2$ sites, with $n$ a positive integer.

In the following, we consider different variational WFs to describe the Mott insulating phase for the Hubbard Hamiltonian defined above. In order to show the advantage of our approach and check the validity of our criteria for distinguishing a metallic from an insulating state, we begin with the early variational attempts for the description of Mott insulators.

Following the same notations of Section 1.4, we compare the *Gutzwiller wavefunction*:

$$|\Psi_g\rangle = \exp\left[-g \sum_{i} n_{i\uparrow} n_{i\downarrow}\right] \; |FS\rangle \tag{4.2}$$

and the *Gutzwiller plus short-range holon-doublon wavefunction*:

$$|\Psi_{g,HD}\rangle = \exp\left[-g \sum_{i} n_{i\uparrow} n_{i\downarrow}\right] \exp\left[f \sum_{<l,m>} h_l d_m\right] \; |FS\rangle \quad , \tag{4.3}$$

with the properties of two wavefunctions that have a long-range component in the correlation term. The presence of a long-range correlation factor constitutes the main novelty of our approach. Our argument is that, in order to bind holons and doublons over all distances such that they cannot move freely, a long-range correlation term is needed. To this purpose we consider the *Gutzwiller plus long-*

*range holon-doublon wavefunction*:

$$|\Psi_{g,nHD}\rangle = \exp\left[-g\sum_i n_{i\uparrow}n_{i\downarrow}\right]\exp\left[\sum_{l,m} f_{lm}h_l d_m\right]\ |FS\rangle\ , \qquad (4.4)$$

where $f_{lm} = f_{|l-m|}$ are translationally invariant variational parameters associated to all independent distances. This holon-doublon term allows in principle to correlate holons and doublons at all length scales. Finally, we consider the *long-range density Jastrow wavefunction* introduced in Eq. (2.1), which for a fermionic systems on a lattice has the form:

$$|\Psi_J\rangle = \exp\left[\frac{1}{2}\sum_{ij} v_{ij}n_i n_j\right]\ |FS\rangle\ . \qquad (4.5)$$

In the following, we minimize the energy for the WFs of Eqs. (4.2-4.5) for different values of $U/t$, and compare the conducting properties of the variational ground states corresponding to the different ansatz.

### 4.1.1 Conduction properties of the variational wavefunctions

In order to detect the conduction properties of the different WFs described above, we consider the Berry phase $z_L$ and the charge-density structure factor $N_q$, following the criteria described in Section 2.5.2 and 2.5.1, respectively.

Let us first consider the simple Gutzwiller WF, with and without the short-range holon-doublon term. In both cases, the Berry phase vanishes in the thermodynamic limit, signaling that the system is delocalized, hence metallic. The same insight comes from the behavior of the charge-density structure factor $N_q$, see Figure 4.1 and 4.2. By increasing $U/t$, the charge fluctuations decrease as expected, but the structure factor is always characterized by a linear behavior for small $q$, i.e., $N_q \sim |q|$, as it happens for the non-interacting structure factor $N_q^0$ of free fermions. This shows that the short-range terms of Eqs.(4.2) and (4.3) cannot change the charge-density correlation functions at low energy, and the structure factor keeps the same metallic behavior inherited from the Slater determinant $|FS\rangle$. The effect of the Gutzwiller and short-range holon-doublon terms is just to renormalize the charge-fluctuations of free electrons at small distances, giving a correlated metallic state characteristic of Fermi liquids. In these WFs, the values of the optimized parameters $g$ and $f$ remain finite for any finite value of $U/t$,

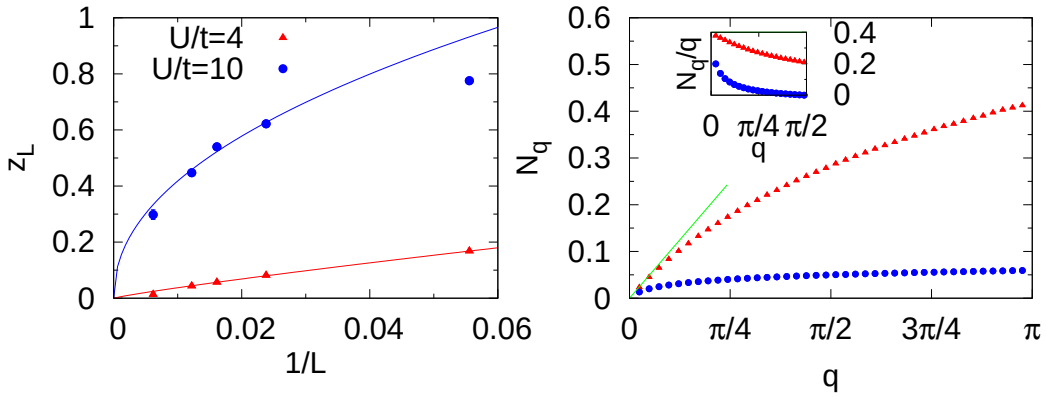


Figure 4.1: Gutzwiller WF. Left panel: Berry phase calculated for $U/t = 4$ and $U/t = 10$ as a function of $1/L$. Lines are two parameters fits. Right panel: corresponding charge density structure factor $N_q$ for 82 sites. The dashed line denotes the behavior of $N_q^0$, the charge structure factor for free fermions. Inset: $N_q/q$ taken at the same $U/t$.

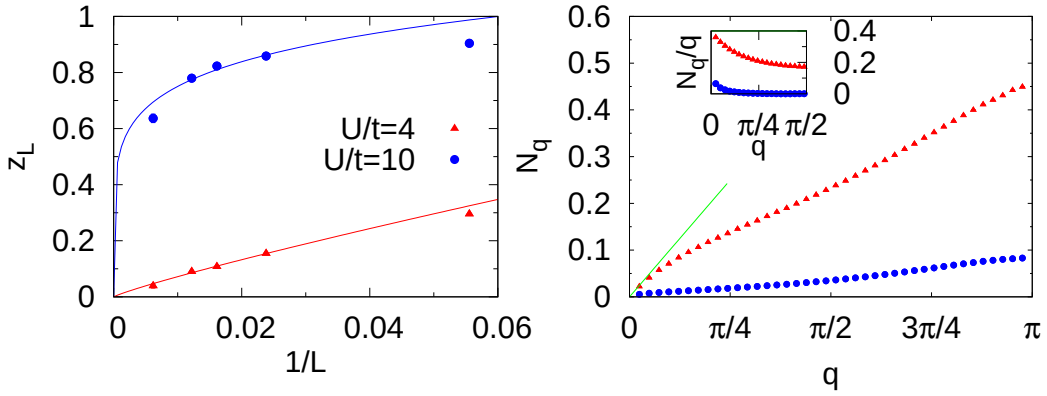


Figure 4.2: Gutzwiller + short-range holon-doublon WF. The same as in Figure 4.1 for the WF defined in Eq. (4.3).

even in the thermodynamic limit, implying that holons and doublons are always present. Since the WFs of Eq. (4.2) and (4.3) lack the long-range correlations that could bind these charged objects, we naturally obtain a metallic state for any value of the Coulomb strength $U/t$.

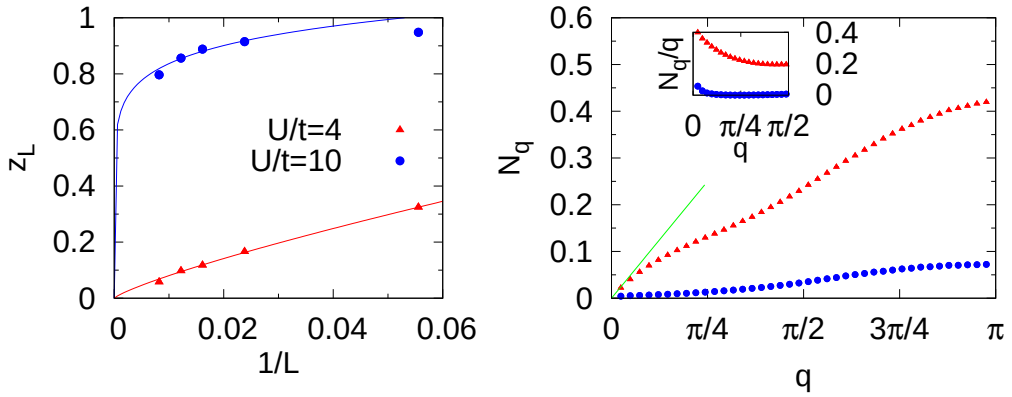


Figure 4.3: Gutzwiller+ long-range holon-doublon WF. The same as in Figure 4.1 for the WF defined in Eq. (4.4).

Quite surprisingly, the addition of a long-range holon-doublon correlation factor does not change the qualitative behavior of $z_L$ and $N_q$, signaling that also WF (4.4) is metallic for all $U/t$, as shown in Figure 4.3. Indeed, the simple argument of correlating the empty and doubly-occupied sites over all distances is not sufficient to give an insulating state: at the variational minimum there is no sign of this long-range correlation. This is clear from the behavior of the holon-doublon parameters, which are positive at short distances (without any size dependence), promoting configurations where holons and doublons are close to each other, and they become negative for large distances (see Figure 4.4). Even for $U/t = 16$ the long-range part drops abruptly to very small values (see inset). Indeed, a strong attraction among holons and doublons for all distances would determine an accumulation of charges in one region of the lattice and a consequent kinetic-energy loss. In order to avoid these energetically-unfavored configurations, at the variational minimum the holon-doublon parameters $f_r$ remain small at large distances. We will see in the following that a good wavefunction, capable of correlating holons and doublons at all distances, must contain *also* a repulsive term among holon-holon and doublon-doublon, which avoids the charge accumulation and guarantees the correct correlation among charges.

Indeed, considering the long-range Jastrow WF (4.5), in Figure 4.5 we show that it is characterized by $z_L \to 1$ in the thermodynamic limit, signaling that

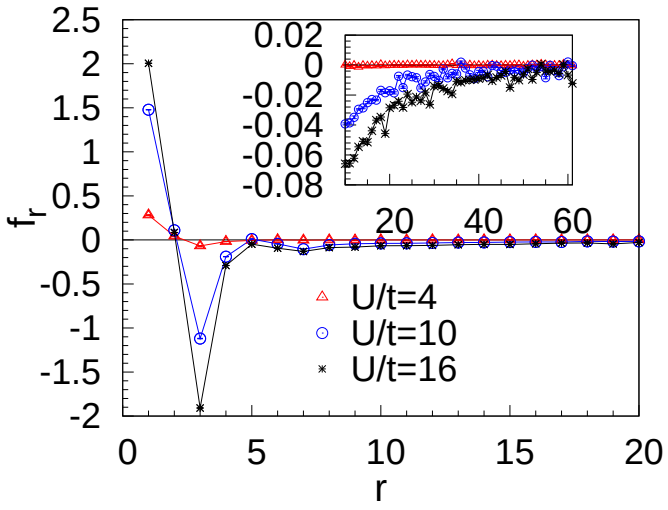


Figure 4.4: Holon-doublon parameters vs. distance for the Gutzwiller plus long-range holon-doublon WF (4.4). A chain of 122 sites is considered for $U/t = 4, 10, 16$. Inset: Long-range behavior of the holon-doublon variational parameters for the same $U/t$.

the system is *localized*. Moreover, the small-$q$ behavior for the charge-density

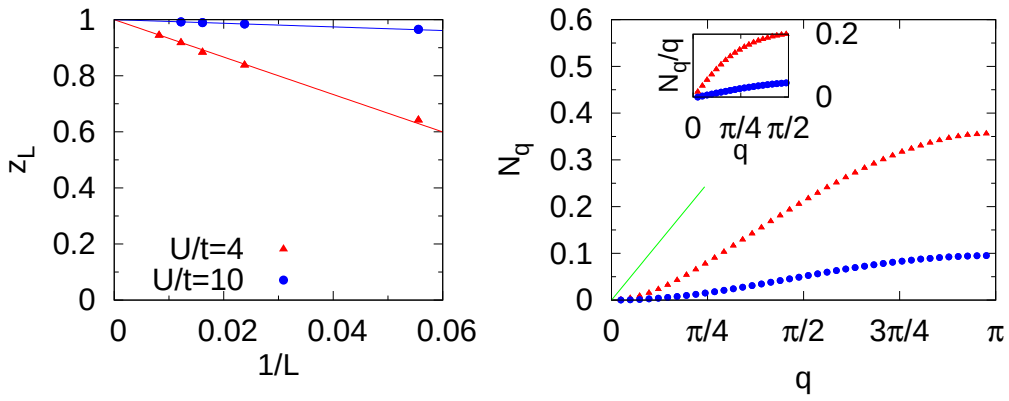


Figure 4.5: Long-range Jastrow WF. The same as in Figure 4.1 for the WF defined in Eq. (4.5).

structure factor is $N_q \sim q^2$, which, according to the $f$-sum rule, indicates a finite

upper bound for the charge gap. Remarkably, the behavior of $N_q$ strongly differs from the structure factor of the non-interacting Fermi sea, especially at small-$q$. Indeed, the inset of Figure 4.5 clearly shows that $N_q/q$ vanishes at small $q$, contrarily to what happens for the other variational WFs described above. Both criteria therefore indicate that *the system is an insulator*, where charge fluctuations are still possible but strongly suppressed at large distances.

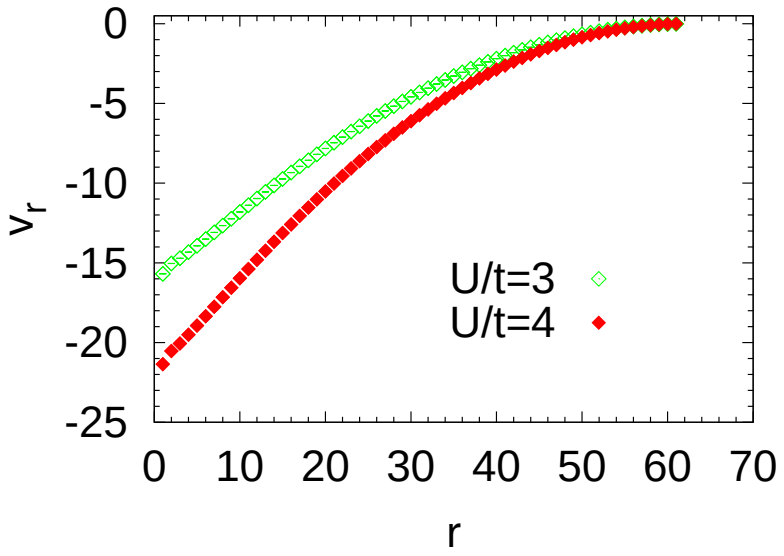


Figure 4.6: Jastrow parameters for all independent distances for a chain $L = 122$ sites.

The importance of the long-range component in the correlation factor is clear from Figure 4.6, where we show the behavior of the Jastrow parameters as a function of the distance. It turns out that $v_r$ is a smooth function of the distance, and the strength of the Jastrow parameters increases when increasing $U/t$. Notice that the relative strength of the long-range part is very pronounced, even for very large $r$, a characteristic feature of strongly-correlated insulators, where particles are correlated over all distances. Of course, the short-range component contributes to the main part of the variational energy, while the long-range terms give only low-energy corrections. However, the long-range Jastrow tail becomes more and more relevant when approaching the strong-coupling regime and allows us to recover the correct charge-correlation functions for the insulator. In view of the previ-

ous discussion concerning the Gutzwiller plus long-range holon-doublon WF, it is useful to write the density-density operator in the Jastrow factor in terms of holon and doublon operators:

$$(n_i - 1)(n_j - 1) = h_i h_j + d_i d_j - h_i d_j - d_i h_j, \tag{4.6}$$

where $h_i$ is the holon (H) creation operator and $d_i$ is the corresponding creation operator for doublons (D). It turns out that $v_{i,j} < 0$ (see Figure 4.6) implies H-H (D-D) repulsion and H-D attraction. The latter embodies the binding of H and D, while the repulsion prevents accumulation of H-D pairs. That is just the desired type of correlations missing in the previously analyzed WFs. A noteworthy fact is that also the Gutzwiller WF with a long-range holon-doublon correlation factor given in (4.4) misses one of the fundamental ingredients to recover an insulating state, i.e., the H-H and D-D repulsive term. The correct insulating behavior is recovered only when both the attractive and repulsive terms are present for all possible distances.

### 4.1.2 Properties of the insulating Jastrow wavefunction

In order to characterize the properties of the Jastrow WF (4.5), which shows the correct insulating behavior at half filling, in Figure 4.7 we compare its variational energy with the one found for the Gutzwiller WF. It is well known that, for the Heisenberg model, the fully projected Gutzwiller wavefunction $|\Psi_{g=\infty}\rangle$ is very accurate [81, 82]. Instead, considering the half-filled Hubbard model, it turns out that, in the limit of large $U/t$, the Gutzwiller WF (4.2) gives a rather poor variational description, missing completely the superexchange energy generated by the virtual hopping processes. This happens because, by increasing $U/t$, the Gutzwiller parameter $g$ increases, and the hopping processes, which create double occupancies, become less probable, with a consequent kinetic-energy loss.

In Section 1.3.2 we have seen that the strong-coupling limit of the Hubbard Hamiltonian can be obtained by means of a canonical transformation $\mathrm{e}^{iS}$. Following this procedure, the expectation value of the energy for the Heisenberg Hamiltonian with respect to the fully-projected Gutzwiller state reads:

$$E_V^{Heis} = \frac{\langle \Psi_{g=\infty} | H_{Heis} | \Psi_{g=\infty} \rangle}{\langle \Psi_{g=\infty} | \Psi_{g=\infty} \rangle} = \frac{\langle \Psi_{g=\infty} | \mathrm{e}^{-iS} H_{Hub} \mathrm{e}^{iS} | \Psi_{g=\infty} \rangle}{\langle \Psi_{g=\infty} | \Psi_{g=\infty} \rangle} \sim -\frac{4t^2}{U} \ . \tag{4.7}$$

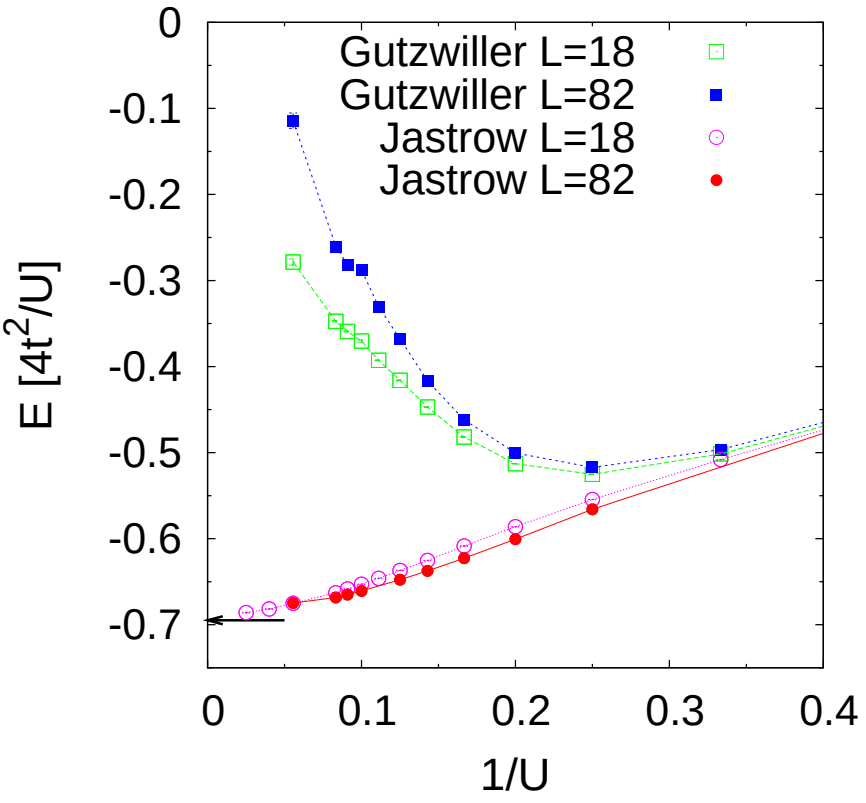


Figure 4.7: Energy per site in units of $4t^2/U$ for the simple Gutzwiller WF ($L = 18$, empty squares, and $L = 82$, full squares) and for the WF with long-range density-density Jastrow ($L = 18$, empty circles, and $L = 82$, full circles). The arrow indicates the energy per site for the fully-projected Fermi sea in the Heisenberg model.

Accordingly, in order to have an accurate description of the Hubbard model, the natural extension of $|\Psi_{g=\infty}\rangle$ to finite $U$ would be $\mathrm{e}^{iS}|\Psi_{g=\infty}\rangle$. However, the canonical transformation cannot be handled easily, since the generator $S$ of the transformation is non-diagonal. This constitutes the technical difficulty which does not allow one to connect easily the (variational) states of the Heisenberg model to the Hubbard model at finite $U/t$. The lack of accuracy of the Gutzwiller WF indicates that the partial Gutzwiller projector does not correspond to the canonical transformation. Instead, by considering the accuracy of the Jastrow WF for

large $U/t$, it turns out that the long-range Jastrow factor enables us to connect the fully-projected insulator valid in the strong-coupling limit to an insulating state at finite $U/t$. The variational energy of $|\Psi_J\rangle$ approaches the one calculated for the fully-projected Gutzwiller state $|\Psi_{g=\infty}\rangle$ for the one-dimensional Heisenberg model. Therefore, since the Jastrow factor gives the correct superexchange energy for large $U/t$, it gives approximately the same effect of the canonical transformation on the fully-projected Fermi sea.

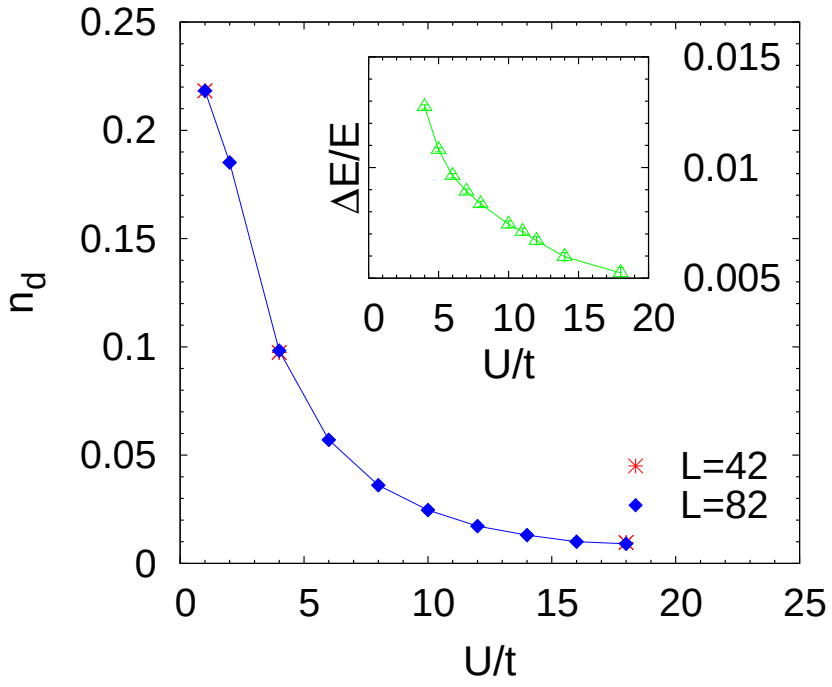


Figure 4.8: Jastrow WF: Average number of doublons per site $n_d$ vs. $U/t$ for a chain of 42 and 82 sites. Inset: Energy accuracy as a function of $U/t$ for the Jastrow WF for a chain of 82 sites. The accuracy is obtained by $\frac{E_T - E_0}{E_0}$, with $E_0$ being the exact energy and $E_T$ the variational energy.

We find that the insulating state recovered with the Jastrow WF is always characterized by a finite number of double occupancies, giving a more realistic picture of the Mott insulator, where charge fluctuations always occur (see Figure 4.8). The variational picture of the Mott insulating state in this case is clearly different from the Brinkman-Rice scenario described in Section 1.4.2, where double occu-

pancies are completely suppressed. Remarkably, the presence of a finite number of holons and doublons implies a finite kinetic-energy gain even for very large $U/t$ and allows us to obtain the correct low-energy behavior described above. Finally, in the inset of Figure 4.8, we show the accuracy of the Jastrow WF, by comparing the variational energy with the exact ground-state energy calculated with the Bethe-ansatz solution. Notice that the Jastrow WF becomes more accurate upon increasing $U/t$.

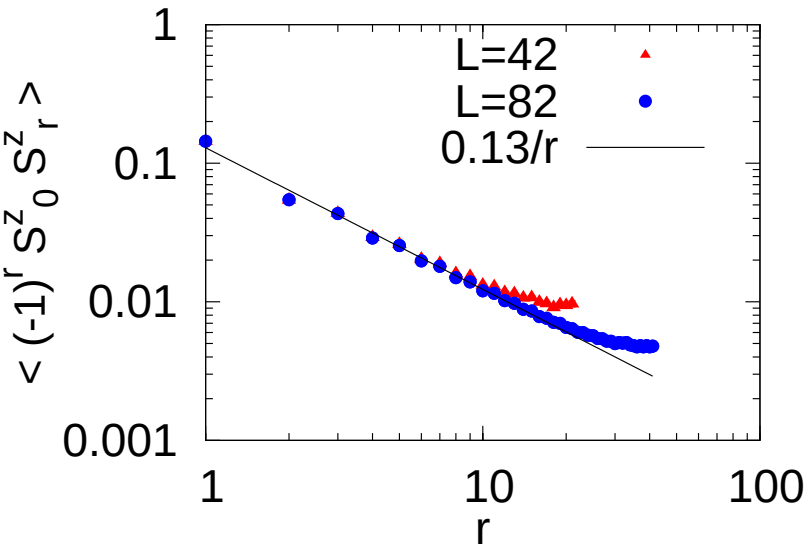


Figure 4.9: Jastrow WF: Staggered spin correlation function for $U/t = 18$ plotted in logarithmic scale for 42 and 82 sites.

Moreover, considering the large-$U$ limit, the Jastrow factor allows us to recover the correct spin properties: as shown in Figure 4.9 the staggered spin-spin correlation function has the correct power-law behavior characteristic of the model. This is remarkable, since, without the long-range Jastrow, the spin-spin correlation function of $|FS\rangle$ decays much faster, namely $\langle(-1)^r S_0^z S_r^z\rangle \sim |r|^{-2}$, and the density Jastrow factor does not act directly on spins, but on charges. Indeed, it should be noticed that also the fully projected Gutzwiller WF $|\Psi_{g=\infty}\rangle$ has the correct long-distance spin behavior [81, 82].

In order to have a better understanding of the properties of our WF, let us consider the Fourier-transformed Jastrow parameters $v_q$. In Figure 4.10, it turns

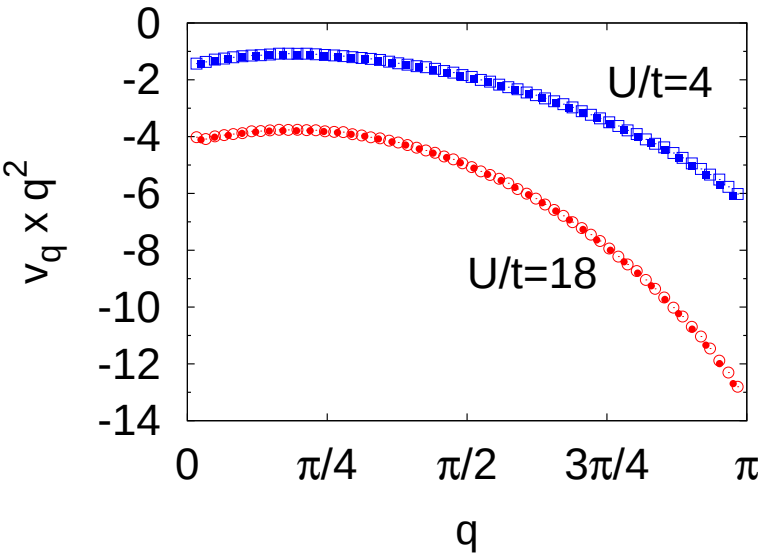


Figure 4.10: Fourier transformed Jastrow parameters multiplied by $q^2$ for $82$ sites (full symbols) and $122$ sites (empty symbols), for $U/t = 4, 18$.

out that the leading behavior of the Jastrow parameters at small $q$ is $v_q \sim 1/q^2$, with a coefficient fixing its strength that increases with $U/t$. Recalling the Reatto-Chester relation (2.7), obtained for continuum systems within the Gaussian approximation:

$$N_q = \frac{N_q^0}{1 + 2v_q N_q^0},$$

we find that also in the insulating state the small-$q$ behavior of $v_q$ is deeply related to the form of the corresponding structure factor $N_q \sim q^2$. Since the Jastrow term diverges at small $q$ as $v_q \sim \frac{1}{q^2}$, we can safely assume that $2v_q N_q^0 \gg 1$ and rewrite the above relation as $N_q \sim \frac{1}{v_q}$, which implies $N_q \sim q^2$. The fact that the approximate relation of Reatto and Chester holds for an insulator, i.e., a confined phase where generally perturbation theory does not apply, is quite unexpected. Indeed, we find that a more accurate empirical expression for small momenta is given by:

$$N_q \sim \frac{N_q^0}{1 + \gamma(U)\ v_q N_q^0}, \tag{4.8}$$

where the Jastrow coefficient $\gamma(U) > 2$ strongly depends upon the electronic in-

teraction. In the right inset of Figure 4.11, we report $\gamma(U)$ for different values of the ratio $U/t$ according to Eq. (4.8). Although for $q \to 0$ we have that $N_q \sim q^2$,

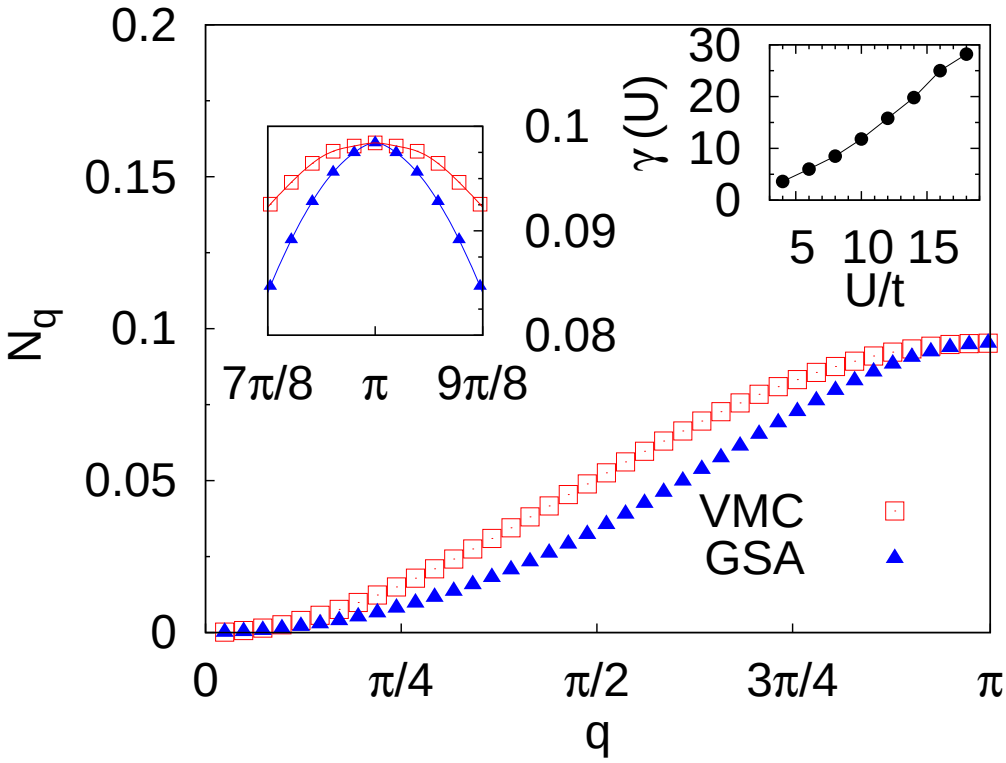


Figure 4.11: Charge structure factor for $L = 82$ and $U/t = 10$ at half filling: comparison between the variational result and the approximate expression (GSA) given by Eq. (4.8). The GSA results have been rescaled in order to have the same value as the variational ones at $q = \pi$. Left Inset: zoom of $N_q$ around $q = \pi$. Right Inset: The value of $\gamma$ from Eq. (4.8) at half filling for different ratios $U/t$.

the coefficient of the quadratic term in $N_q$ is not simply related to the Jastrow factor, like in the original Reatto-Chester approximate formula, but increases with the interaction. The important point is that, for the insulating phase, Eq. (4.8) is valid only at small $q$, since the presence of the singular Jastrow factor $v_q \sim 1/q^2$ determines a notable change in the qualitative behavior of the static structure factor at large momenta $q \sim 2k_F = \pi$. In fact, the cusp at $q \sim 2k_F$, which is present in $N_q^0$ and is responsible of the well-known Friedel oscillations in a metal, is completely removed by the singular Jastrow term: as shown in Figure 4.11, the charge

structure factor $N_q$ for the Jastrow WF shows a smooth behavior around $q \sim \pi$. Remarkably, this effect cannot be obtained within the Gaussian approximation. This clearly indicates the non-perturbative – and highly non-trivial – effect implied by the formation of a confined state between empty and doubly occupied sites in this correlated WF.

Finally, let us mention that the Gaskell RPA relation (2.13) of Section 2.3

$$2v(q) = -\frac{1}{N_0(q)} + \sqrt{\frac{1}{N_0^2(q)} + \frac{4mV(q)}{\hbar^2 q^2}} \ ,$$

does not predict a Jastrow of the form $v(q) \sim 1/q^2$ unless a long-range potential $V(q) \sim \frac{1}{q^2}$ is considered. The behavior of the minimized Jastrow parameters reported in Figure 4.10 shows that the Gaskell RPA relation does not hold in this case, since a singular Jastrow $v_q \sim \frac{1}{q^2}$ is stabilized with a short-range repulsion $U$. This is due to the fact that our variational problem is defined on a lattice, whereas the Gaskell relation has been obtained on the continuum. In addition to that, the discrepancy of our findings with respect to the Gaskell predictions could be addressed to the failure of RPA to approach an insulating state starting from a metallic determinant, stressing again that our variational findings are non-perturbative.

## 4.2 Results for the one-dimensional $t-t'$ Hubbard model at half-filling

The one-dimensional $t-t'$ Hubbard model is described by the following Hamiltonian:

$$H = -t\sum_{i,\sigma} c^\dagger_{i,\sigma} c_{i+1,\sigma} + h.c. + t'\sum_{i,\sigma} c^\dagger_{i,\sigma} c_{i+2,\sigma} + h.c. + U\sum_i n_{i,\uparrow} n_{i,\downarrow}, \quad (4.9)$$

where, compared to the standard Hubbard Hamiltonian of Eq. (1.1), a next-to-nearest neighbor hopping term with amplitude $t'$ is added. This model is commonly visualized as a two-chain model with zigzag coupling, as shown in Figure 4.12. In the following, we will assume $t$ and $t'$ positive, and we will consider the properties of this Hamiltonian at half filling.

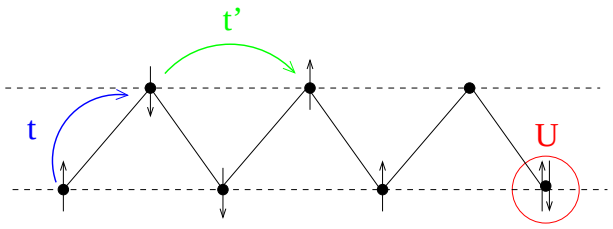


Figure 4.12: Schematic representation of the $t - t'$ Hubbard model.

For $U = 0$ the Hamiltonian (4.9) is characterized by the following dispersion relation:

$$\epsilon_k = -2t \cos k + 2t' \cos 2k \tag{4.10}$$

which has different properties according to the value of $t'/t$. If $t' < t/4$ the band minimum is at $k = 0$, and, similarly to the case with $t' = 0$, at half filling there are two Fermi points $\pm k_F = \pm\pi/2$ [see Figure 4.13 (a)]. If the interaction $U$ is turned on, the properties of the model are qualitatively similar to the standard Hubbard model with $t' = 0$ [83]. On the other hand, if $t' > t/4$, the band minima

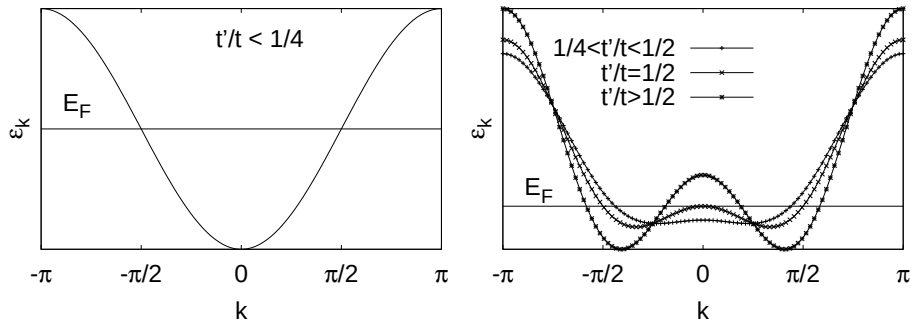


(a) (b)

Figure 4.13: Energy dispersion relation for the $t - t'$ non-interacting chain for $t' < t/4$ (a) and $t' > t/4$ (b).

move towards $k_{min} = \arccos\left(\frac{t}{4t'}\right)$ and $k = 0$ becomes a (relative) maximum [see Figure 4.13 (b)]. At half filling, this relative maximum reaches the Fermi level in correspondence of $t' = t/2$. As a consequence, for $t' > t/2$ there are four Fermi points, $\pm k_{F1}$ and $\pm k_{F2}$ such that $k_{F2} - k_{F1} = \pi/2$, and the model at low energy

behaves like a two-band model; the nesting property is lost and, when interaction is turned on, the corresponding phases show different properties from the standard Hubbard model [83].

When the interaction is very strong, the $t-t'$ Hubbard model at half filling can be mapped into an effective spin Hamiltonian, known as the $J_1-J_2$ *model*:

$$H_{J_1J_2} = J_1 \sum_{i=1}^{L} S_i \cdot S_{i+1} + J_2 \sum_{i=1}^{L} S_i \cdot S_{i+2} \tag{4.11}$$

where $J_1 = 4t^2/U$ and $J_2 = 4(t')^2/U$. For $J_2 = 0$ one recovers the well known Heisenberg model, which is characterized by gapless excitations and power-law decay of the spin correlations. When $J_2$ is turned on, it introduces a frustrating interaction that, if larger than a critical value, opens a spin gap. The critical value of the frustrating term is rather well known by very accurate numerical calculations, i.e., $(J_2/J_1)_c = 0.241167$ [84]. Moreover, for $J_2 = J_1/2$, called the Majumdar-Ghosh point, the ground state WF is exactly known [85] and consists of a product of singlets among nearest neighboring sites (dimers). This dimerized state is doubly degenerate, the two states being related among each other by the translation of one lattice spacing, and a finite energy gap exists between the ground state and the first excited ones [86].

By varying $U/t$, the properties of the $t-t'$ Hubbard model are influenced by the different topology of the energy dispersion relation at weak coupling and follow those of the $J_1-J_2$ at strong coupling. In particular, bosonization [83] and density-matrix renormalization group calculations [87, 88] predict that the ground state at half filling is an insulator with gapless spin excitations (labeled $C0S1$, where $CnSm$ indicates a state with $n$ gapless charge modes and $m$ gapless spin modes) for $t'/t < 1/2$, a spin-gapped metal ($C1S0$) with strong superconducting fluctuations for $t'/t > 1/2$ and small $U/t$, and a fully gapped spontaneously dimerized insulator ($C0S0$) for $t'/t > 1/2$ and large $U/t$. Therefore, since the phase diagram of the $t-t'$ Hubbard model, for $t'/t > 1/2$, shows a metal-insulator transition at a finite $U/t$, it offers the possibility to test our variational ansatz for the description of the Mott transition. The different spin properties of the phases involved, with a gapless and a gapped regime upon increasing $t'/t$ and $U$, can be correctly described by modifying only the determinantal part of the variational wavefunction. In particular, the $C1S0$ metallic phase suggests a variational WF

built out of a BCS Hamiltonian, namely:

$$|\Psi\rangle = \mathcal{P}_J \mathcal{P}_N \, |BCS\rangle = \mathcal{P}_J \mathcal{P}_N \exp\left(\sum_q f_q \, c^\dagger_{q\uparrow} c^\dagger_{-q\downarrow}\right)|0\rangle, \tag{4.12}$$

where $|BCS\rangle$ is the ground state of a BCS Hamiltonian with gap function $\Delta_q$ and dispersion

$$\epsilon_q = -2\cos(q) + 2t'\cos(2q) - \mu, \tag{4.13}$$

with $\mu$ being the free electron chemical potential. In all the variational calculations that follow, if not specified, the parameters $t'$ and $\mu$ of (4.13) are kept fixed, and, in order to have the exact solution for $U/t = 0$, correspond to those of the non-interacting $t - t'$ Hamiltonian. [1] The pairing function in (4.12) is defined by $f_q = \Delta_q/(\epsilon_q + E_q)$, with the BCS energy spectrum $E_q = \sqrt{\epsilon_q^2 + \Delta_q^2}$, and

$$\Delta_q = \Delta_1 \cos(q) + \Delta_2 \cos(2q) + \Delta_3 \cos(3q), \tag{4.14}$$

$\Delta_1$, $\Delta_2$, and $\Delta_3$ being variational parameters. Obviously $|BCS\rangle$ reduces to the Fermi sea for $\Delta_q = 0$. Finally, $\mathcal{P}_N$ projects onto the subspace with fixed number of electrons $N = L$ (see Appendix B) and $\mathcal{P}_J$ is the long-range Jastrow factor. In order to have a closed shell in the uncorrelated determinant, whenever $t'/t > 1/2$ we consider chains of $4n$ sites, with $n$ a positive integer.

### 4.2.1 Variational Mott transition for $t'/t = 0.75$

We first consider the properties of our WF for $t'/t = 0.75$ and different values of $U/t$. This value of $t'/t$ is very close to the corresponding value of $J_2/J_1$ where the spin-gap shows a maximum [89] and identifies a $C1S0$ metallic phase at weak-coupling and the $C0S0$ dimerized insulating phase at strong coupling. At half filling the non-interacting system is characterized by four Fermi points $\pm k_1$ and $\pm k_2$ as shown in Figure 4.13 (b).

In Figure 4.14 we consider the charge-density structure factor $N_q$ and the Fourier-transformed Jastrow parameters $v_q$ (multiplied by $q^2$) for different values of the interactions. Both the Jastrow and the structure factor show a different

[1] Indeed we find that the optimization of $t'$ and $\mu$ allows us to obtain a better accuracy in energy, but does not change the properties of the phases involved.

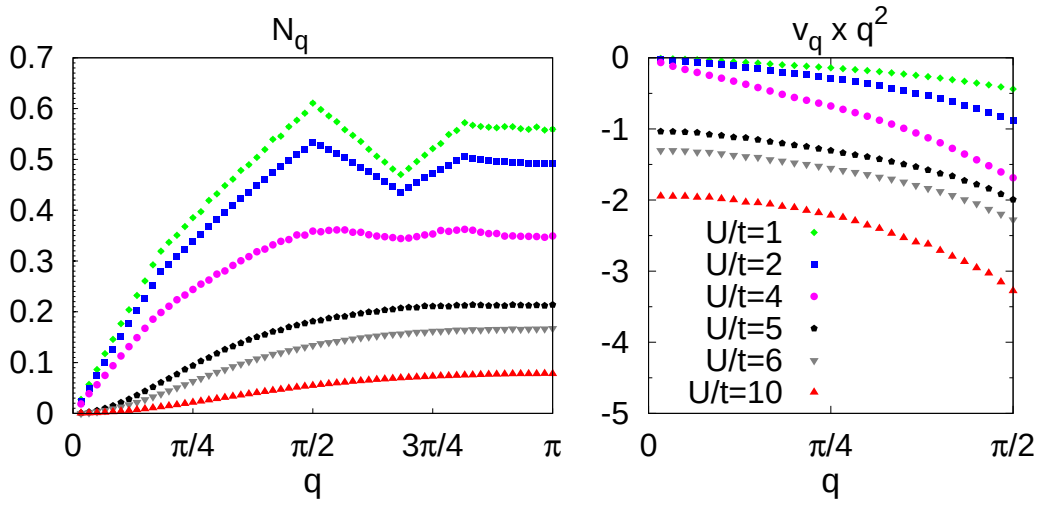


Figure 4.14: Charge-density structure factor $N_q$ and Jastrow parameters $v_q$ multiplied by $q^2$ for $t'/t = 0.75$ and $U/t = 1, 2, 4, 5, 6, 10$. A chain of 120 sites is considered. Notice the change of behavior between $U/t = 4$ and $U/t = 5$.

behavior for small and large $U/t$. Indeed, for $U/t \leq 4$ and small-$q$, the leading behavior of the Jastrow term is $v_q \sim \frac{1}{|q|}$, and the structure factor is linear, i.e., $N_q \sim |q|$, with strongly marked Friedel oscillations at $2k_{F1}$ and $2k_{F2}$. On the other hand, for $U/t \geq 5$, the leading behavior of the Jastrow factor turns into $v_q \sim \frac{1}{q^2}$ and the structure factor is quadratic, $N_q \sim q^2$, at small $q$, with the Friedel oscillations completely washed out. The change in the behavior of the Jastrow and the structure factor around $U/t \approx 5$ signals a metal-insulator transition at a finite value of $U/t$. This transition is further confirmed by looking at the Berry phase, as shown in Figure 4.15. It turns out that for $U/t \leq 4$ the Berry phase vanishes, i.e., the system is delocalized, hence metallic, while for $U/t \geq 5$ the Berry phase clearly changes its behavior, i.e., $z_L \to 1$ (see inset), signaling that the corresponding phase is localized.

Moreover, considering the spin sector, in Figure 4.16 we plot the spin-structure factor $S_q = \langle S^z_{-q} S^z_q \rangle$, $S^z_q$ being the Fourier-transformed $z$-component of the spin. Also in this case, the small-$q$ leading behavior of $S_q$ clearly changes around $U/t \approx 5$, turning from a linear to a quadratic behavior by increasing the interaction. Following the same arguments given for the charge modes, according to the analogous of the $f$-sum rule for the spin, the fact that $S_q \sim q^2$ at small $q$ for

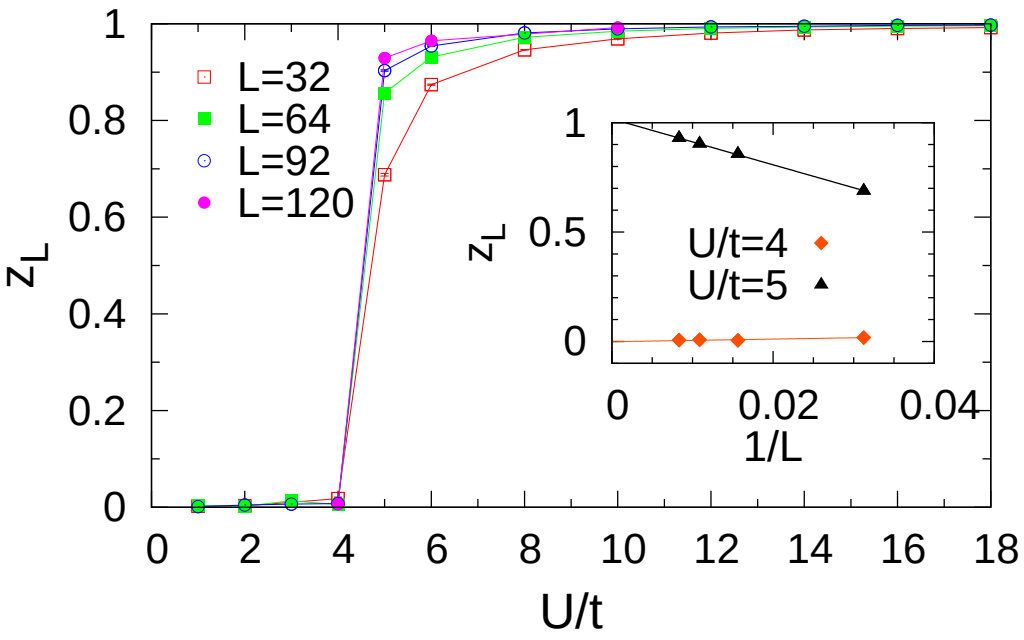


Figure 4.15: Berry phase as a function of $U/t$ for $t'/t = 0.75$ and different sizes. Inset: size scaling of $z_L$ for $U/t = 4$ and $U/t = 5$. Lines are two parameters fits.

$U \gtrsim 5$ signals the presence of a gap also in the spin sector. We would expect, according to previous calculations [83, 87, 88], the presence of a spin gap also at small couplings. Instead, from our variational calculations, it is very hard to detect a spin gap for $U \leq 4$, since the limited resolution in $q$ space does not allow us to clearly distinguish a linear from a quadratic behavior in $S_q$. Following the insight coming from spin systems [90], we argue that the behavior of the spin modes is determined by the spectrum $E_q$ of the BCS mean-field Hamiltonian that is used to construct the uncorrelated state. In particular, if $E_q$ is gapless, then the spin excitations are also gapless and the spin-structure factor $S_q \sim |q|$, whereas, if $\min(E_q) > 0$, the spin-excitation spectrum has a gap and $S_q \sim q^2$. In Figure 4.17 we plot the minimum value of the BCS energy spectrum for different $U/t$. Indeed, the BCS gap is very small for $U/t \leq 4$, as it turns out from the optimized BCS parameters (see inset). However, for $U/t = 4$, which, according to the Berry phase, is still in the metallic region, there is a clear evidence of a gap, signaling that the system is in the $C1S0$ phase. Moreover, by increasing the lattice size, the

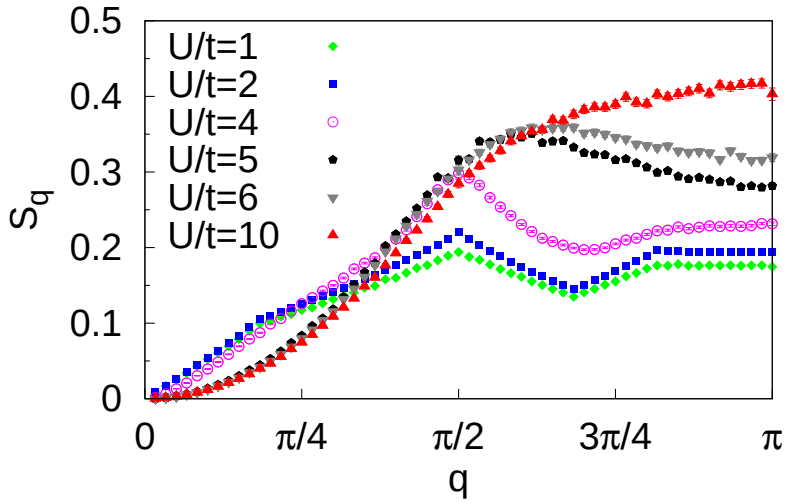


Figure 4.16: Spin structure factor $S_q$ for $t'/t = 0.75$ and different $U/t$ for 120 sites.

value of the BCS gap weakly increases for small $U/t$, giving the indication of a spin gap also for smaller interactions.

Let us remark at this point the important role of the Jastrow term when dealing with a BCS uncorrelated wavefunction. Indeed, whenever $\Delta_q \neq 0$, the density structure factor of a simple BCS determinant behaves like $N_q^0 \sim const$ at small $q$. Instead, the density structure factor of the Jastrow WF follows the correct behavior $\lim_{q\to 0} N_q = 0$, required for charge conservation (see Figure 4.14), in agreement with the Reatto-Chester predictions. Moreover, by calculating the pairing correlation functions, we find that there is no superconducting long-range order for any $U/t$ (not shown). Indeed, according to the generalized uncertainty-principle (see Section 2.4), in one dimension a singular Jastrow $v_q \sim \frac{1}{|q|}$ is sufficient to suppress the off-diagonal long-range order present in the BCS determinant.

Finally, in Figure 4.18, focusing on $U/t = 4$ and $U/t = 10$, where the behavior of the charge and spin-structure factor is more clear, we obtain a clear picture of the charge and spin properties of the two phases involved. Indeed, for $U/t = 4$ the charge is gapless, i.e. $N_q \sim |q|$ and the spin is gapped i.e. $S_q \sim q^2$, corresponding to the C1S0 spin-gapped metallic phase. On the other hand, for $U/t = 10$ we find that both the charge and spin-structure factors are quadratic,

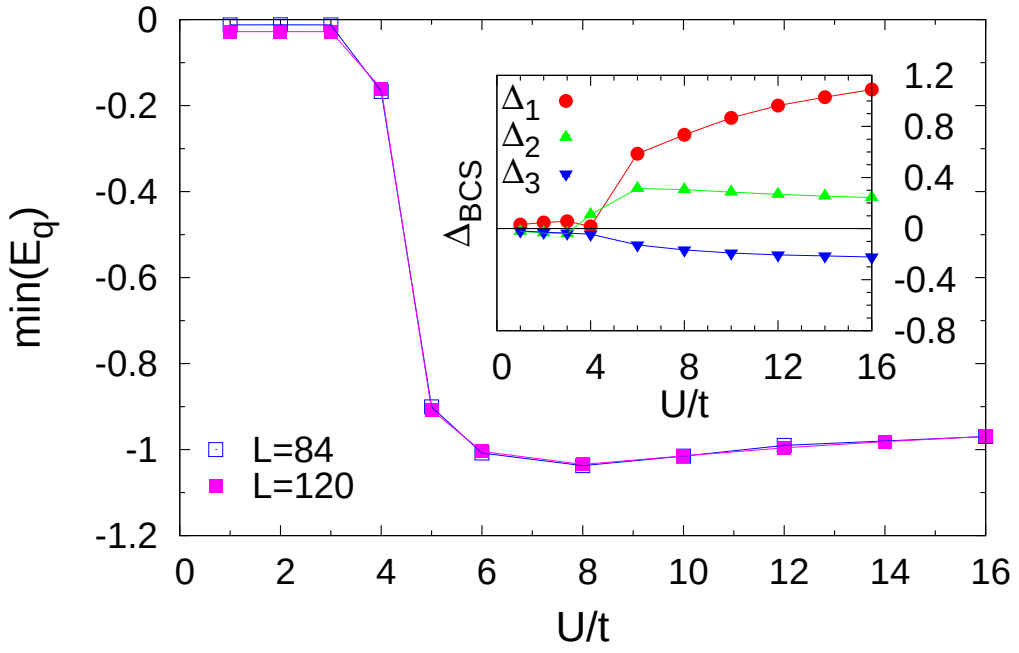


Figure 4.17: Minimum value of the BCS energy spectrum $E_q$ for different lattice sizes as a function of $U/t$. Inset: BCS gap parameters defined in Eq.(4.14) as a function of $U/t$ for 120 sites.

signaling that for this value of $U/t$ we are in the fully-gapped phase.

In order to further characterize the spin properties of the insulating phase $C0S0$, we check if dimerization takes place. Dimerization can be characterized by the long-distance asymptotic behavior of the following quantity [89]:

$$D_d^2 = \lim_{|i-j|\to\infty} |\chi(i-j-1) - 2\chi(i-j) + \chi(i-j+1)| \qquad (4.15)$$

where $\chi(i-j) = \langle S_i \cdot S_{i+1}\ S_j \cdot S_{j+1}\rangle$ gives the dimer-dimer correlation function. Considering spin rotationally-invariant WFs, one can approximate the above relation by writing $\chi(i-j) \simeq 9\langle S_i^z S_{i+1}^z\ S_j^z S_{j+1}^z\rangle$ where $S_i^z$ is the spin operator along z-axis at site $i$. Indeed, we find that for $U/t \geq 5$ the dimer-order parameter becomes finite, signaling that spontaneous dimerization occurs when the insulating state sets in (see Figure 4.19). Remarkably, even though our variational WF does not break any lattice symmetry, spontaneous symmetry-breaking occurs in the thermodynamic limit, due to the concomitant effect of a singular Jastrow

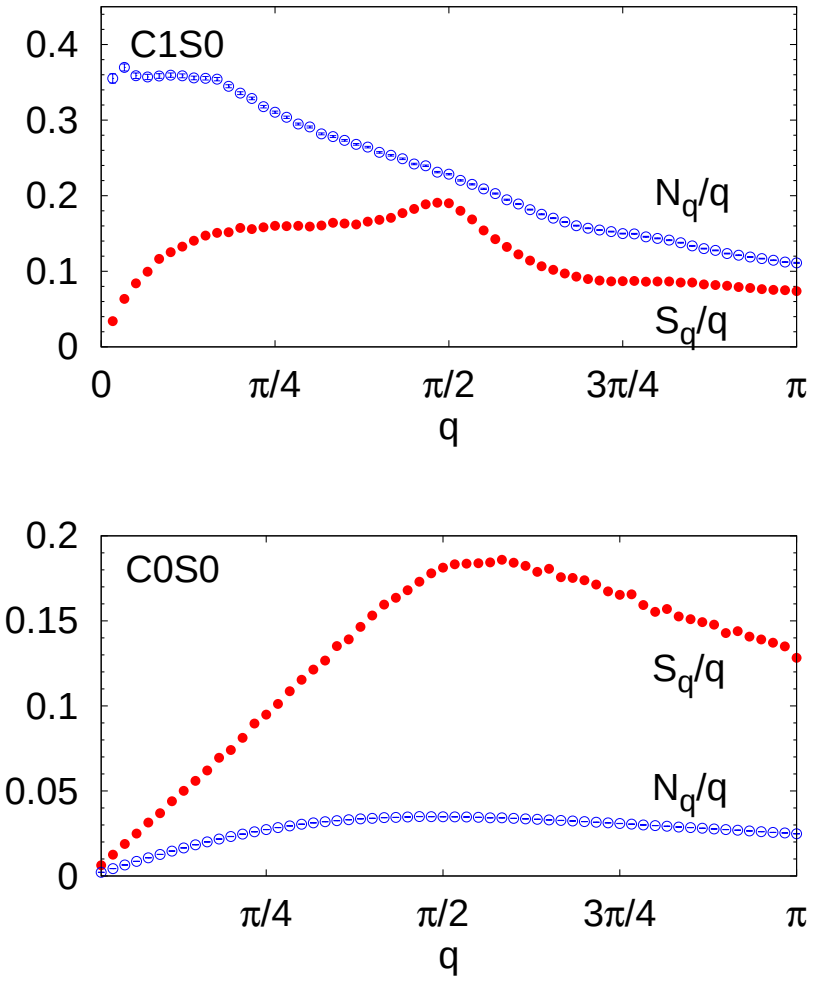


Figure 4.18: Charge and spin-structure factor divided by $q$ for $t'/t = 0.75$ and 120 sites. Two different couplings are considered: $U/t = 4$ (corresponding to the phase $C1S0$) and $U/t = 10$ (corresponding to the dimerized insulator $C0S0$)

$v_q \sim 1/q^2$ and a gapped BCS spectrum $E_q$.

At this point, let us draw some considerations about the accuracy of our WF. Indeed, we realized that, when looking at the behavior of the variational energy as a function of $U/t$, the accuracy is not as good as in the $t' = 0$ case, but it gets worse when increasing $U/t$. Namely, for $t' \neq 0$, the long-range Jastrow factor

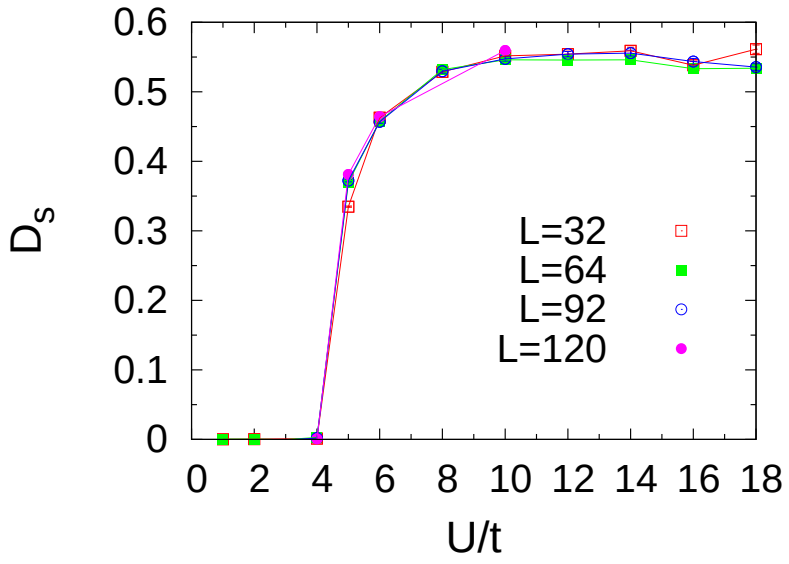


Figure 4.19: Dimer order parameter for different sizes for $t'/t = 0.75$ as a function of $U/t$.

does not allow us to connect to the energy of the fully-projected BCS determinant for the corresponding $J_1 - J_2$ model (see Figure 4.20). In order to improve the accuracy, we minimized also the $t'$ hopping term and the chemical potential $\mu$ in the energy dispersion (4.13). This allows us to recover a better variational energy, which nevertheless is still far from the exact one, and cannot reach the variational energy for the corresponding $J_1 - J_2$ model, where a the fully-projected BCS state is found to be very accurate. This is due to the complicate nodal structure of the finite-$U$ case: it turns out that, in presence of a finite number of holons and doublons, it is very difficult to find a variational WF that correctly describes the ground-state nodes in terms of a simple determinant. Since the Jastrow factor is able to correct *only* the amplitudes of the different configurations, but cannot act on the signs of the WF, the two limits cannot be connected with the only charge-density correlation factor. A possible route, to improve the simple BCS determinant at finite $U/t$, could be found in the addition of a backflow term [91].

However, even though for large $U/t$ we are less accurate than in the case of $t' = 0$, we show in Figure 4.21 that the Jastrow WF, with the BCS determinant, allows us to reproduce faithfully the phase diagram of the half-filled $t-t'$ Hubbard

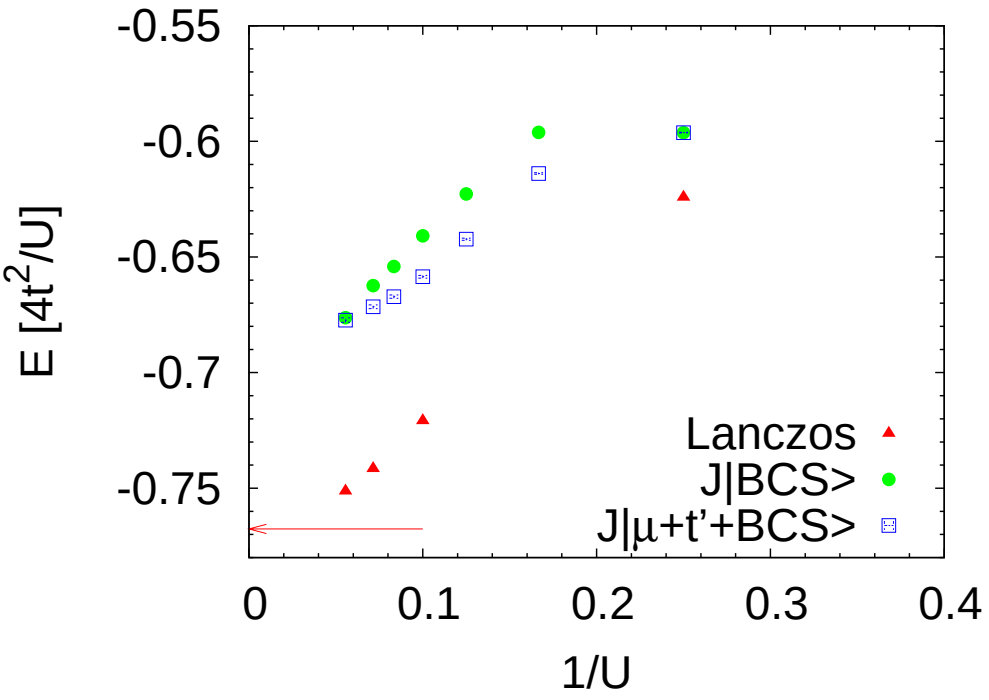


Figure 4.20: Energy in units of $4t^2/U$ vs. $1/U$ for $t'/t = 0.75$ for a chain of 16 sites. The variational energy for the Jastrow WF with BCS determinant (J|BCS$\rangle$) [with parameters $\Delta_1$, $\Delta_2$ and $\Delta_3$ in the gap function, see Eq.(4.14)] is compared with the variational energy of the WF where additionally also $t'$ and the chemical potential are optimized in the determinant (J|$\mu + t'$+BCS$\rangle$). The Lanczos energy is put for comparison. The arrow indicates the variational energy for the corresponding $J_1 - J_2$ model, obtained by optimizing the fully-projected BCS Slater determinant $\mathcal{P}_{g=\infty}|BCS\rangle$.

model. In the region of $t'/t < 0.5$, we find no evidence of a phase transition, apart from finite-size effects at small $U/t$. The best variational state has $N_q \sim q^2$, indicating a charge gap and $S_q \sim q$, i.e., gapless spin excitations: $\Delta_q$ connects only different sublattices (i.e., $\Delta_2 = 0$), making $E_q$ gapless. For $t'/t > 0.5$, there is a clear metal-insulator transition at finite $U/t$ between a spin-gapped metal, stable for small $U/t$ and a dimerized insulator, stable at large $U/t$. In the metallic phase, the variational WF has $N_q \sim q$, whereas $E_q$ is gapped (although $|\Delta_q|$ is small),

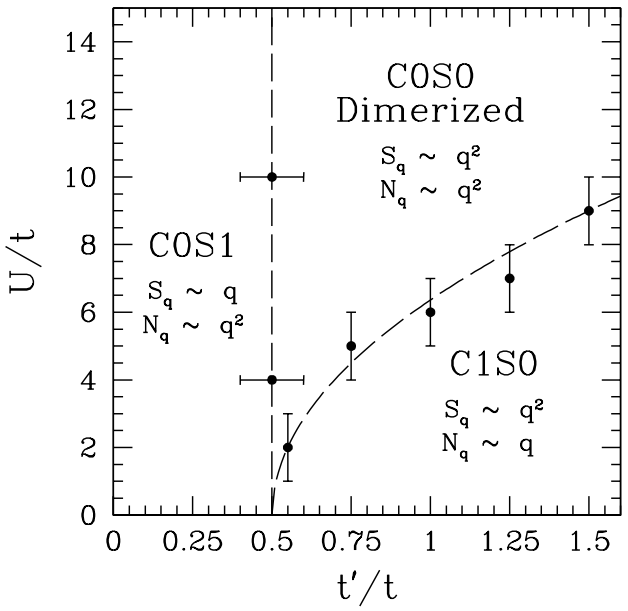


Figure 4.21: Variational phase diagram of the $1d$ $t$–$t'$ Hubbard model. The error bars keep into account finite-size effects and dashed lines are guides to the eye.

i.e., $S_q \sim q^2$, corresponding to exponentially decaying spin-spin correlations. By increasing $U/t$ and entering into the insulating phase, there is a fast increase of $\Delta_q$, with $E_q$ always fully gapped, and $v_q \sim 1/q^2$. In this phase therefore we find $N_q \sim q^2$ and $S_q \sim q^2$, with a finite dimerization in the thermodynamic limit.

## 4.3 Doping a one-dimensional Mott insulator: Luttinger liquid

A characteristic feature of one-dimensional interacting fermions is that, even if the system is gapless, they exhibit peculiar non-Fermi liquid properties. Indeed, due

to phase-space limitations, particle-hole excitations in one-dimensional models are exhausted by collective charge and spin modes, which are dynamically independent, realizing what is commonly referred to as *spin-charge separation*. When these modes are gapless, they propagate as acoustic waves (zero-sounds), hence can be identified by two parameters, the sound velocity $u_i$ and a dimensionless stiffness $K_i$, $i = \rho$ and $i = \sigma$ for charge and spin modes, respectively.

Besides spin-charge separation, another manifestation of the non-Fermi liquid behavior is the power-law decay with anomalous exponents of all correlation functions, when both spin and charge modes are gapless, or just some of them, when one of the two modes is gapped. Although these exponents are generically non universal, they all can be expressed in terms of the above mentioned $K_\rho$ and $K_\sigma$. Therefore, the finite set of parameters $u_\rho$, $u_\sigma$, $K_\rho$ and $K_\sigma$ is sufficient to characterize completely the asymptotic low-energy behavior of one-dimensional interacting electron models, similarly to the finite number of parameters which identify the low-energy behavior of Landau-Fermi liquids in higher dimensions [92]. Indeed, just in analogy with Fermi liquids, this kind of one-dimensional universal behavior was named "Luttinger liquid" by Haldane [93–95].

In the case of non interacting electrons $K_\rho = K_\sigma = 1$. Moreover, if spin SU(2) symmetry is unbroken and the spin modes are gapless, $K_\sigma = 1$ as for free fermions even in the presence of interaction and only $K_\rho$ parametrizes the anomalous exponents. When both charge and spin sectors are gapless, the asymptotic expressions of the charge and spin equal-time correlation functions are, apart from possible logarithmic corrections,

$$\langle n(x)n(0)\rangle \sim \frac{K_\rho}{(\pi x)^2} + A_1 \frac{\cos(2k_F x)}{x^{K_\rho+1}} + A_2 \frac{\cos(4k_F x)}{x^{4K_\rho}}, \tag{4.16}$$

$$\langle \mathbf{S}(x)\cdot\mathbf{S}(0)\rangle \sim \frac{1}{(\pi x)^2} + B \frac{\cos(2k_F x)}{x^{K_\rho+1}}, \tag{4.17}$$

where $n(x)$ and $\mathbf{S}(x)$ are the charge and spin density operators at position $x$, $k_F$ is the Fermi momentum, $A_1$, $A_2$, and $B$ are model-dependent constants. Analogously the singlet (and triplet) pairing correlations behave as

$$\langle \Delta^\dagger(x)\Delta(0)\rangle \sim \frac{1}{x^{K_\rho^{-1}+1}}, \tag{4.18}$$

where $\Delta^\dagger(x)$ creates a singlet (or triplet) pair at position $x$. Finally, the non-Fermi liquid character of one-dimensional interacting models shows up transparently in

the momentum distribution function near the Fermi momentum:

$$\mathtt{n}_k - \mathtt{n}_{k_F} \sim -\mathrm{sign}(k-k_F)|k-k_F|^{\theta}, \tag{4.19}$$

where $\theta$ is again expressed in terms of $K_\rho$ through the relation $\theta = (K_\rho + K_\rho^{-1} - 2)/4$. For any finite interaction $K_\rho \neq 1$, hence the momentum distribution function has a power-law singularity at the Fermi level, in contrast to the finite jump characteristic of Fermi liquids.

In the following, we show that in the Hubbard model at finite $U$ it is possible to design a consistent WF, which can faithfully describe the evolution from the Luttinger-liquid behavior at finite hole doping to the Mott insulating phase at half filling. Again the crucial ingredient turns out to be a density-density Jastrow factor applied to a simple Fermi sea Slater determinant $|FS\rangle$. The important role of the Jastrow factor for one-dimensional correlated metallic systems has been already discussed by Hellberg and Mele in the context of the one-dimensional $t-J$ model [60]. In that case, it is possible to show analytically that the momentum distribution function of the variational WF has an algebraic singularity at $k_F$, with an exponent related to the strength of the Jastrow factor [96]. In this section, we generalize this approach to a finite Coulomb repulsion $U$.

### 4.3.1 Properties of the quarter-filled Hubbard model

In order to demonstrate that the Jastrow WF is able to capture the Luttinger-liquid metallic properties, we consider the quarter-filled case. In Figure 4.22, we show the variational charge and spin structure factor for different values of $U/t$. For small momenta, the linear slope of $N_q$ is renormalized with respect to the non-interacting value, leading to $N_q \sim K_\rho |q|/\pi$. On the other hand, the small-$q$ behavior of the spin structure factor $S_q$ is not affected by the interaction and we have that $S_q \sim |q|/4\pi$. Notice that, in the presence of a strong interaction, the two singularities at $2k_F$ and $4k_F$ are clearly visible in $N_q$, whereas in $S_q$, only the singularity at $2k_F$ can be detected. From the small-$q$ linear part of $N_q$, it is possible to extract the value of $K_\rho$ (see Table 4.1), which is in very good agreement with the exact one [97].

Another characteristic feature of Luttinger liquids is the vanishing of quasi-

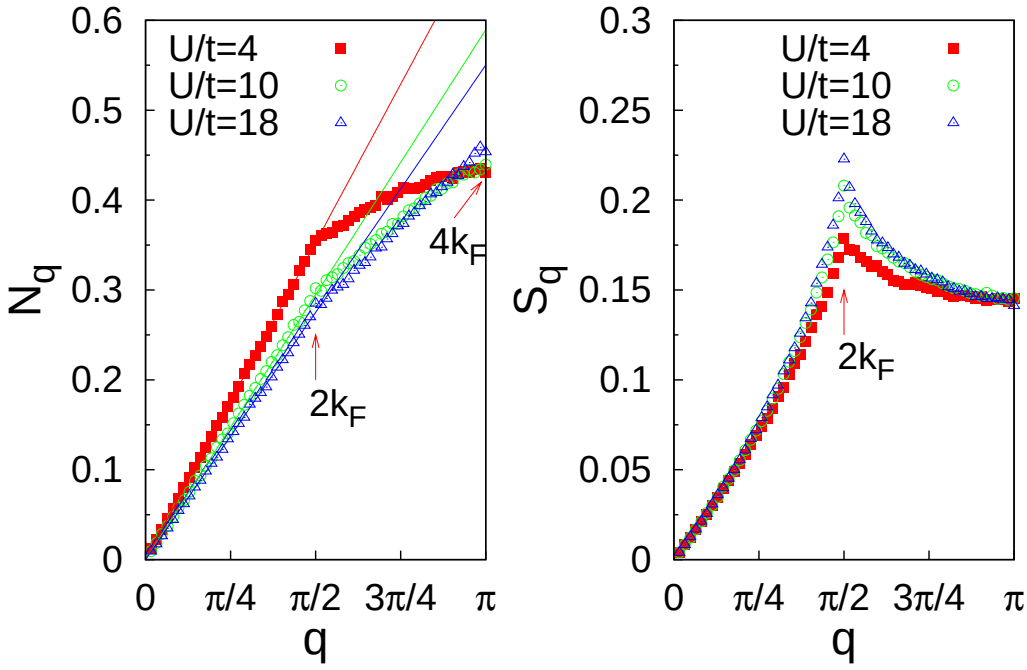


Figure 4.22: Left panel: charge structure factor $N_q$ for the Hubbard model at quarter filling for $L = 124$ and different $U/t$. Right panel: the same for the spin structure factor $S_q$.

particle weight:

$$Z_k = \frac{|\langle \Psi_{N-1}|c_{k,\sigma}|\Psi_N\rangle|^2}{\langle \Psi_N|\Psi_N\rangle\langle \Psi_{N-1}|\Psi_{N-1}\rangle}, \tag{4.20}$$

where $|\Psi_N\rangle$ and $|\Psi_{N-1}\rangle$ are the WFs with $N$ and $(N-1)$ particles, $c_{k,\sigma}$ is the annihilation operator of a particle of momentum $k$ and spin $\sigma$. Within our variational approach, the $(N-1)$-particle state is obtained by the $N$-particle one by removing an electron from the Slater determinant, i.e., $|\Psi_{N-1}\rangle = \mathcal{P}_J\, c_{k,\sigma}\, |FS\rangle$. The behavior of the quasiparticle weight allows us to show that the relationships among exponents of different correlation functions are correctly reproduced by our variational WF. Indeed, we can compare the value of the exponent $\theta$ found from a direct evaluation of the quasiparticle weight (4.20) at $k = k_F$, given by $Z_k \sim 1/L^\theta$ (see Figure 4.23), with the one obtained with $\theta = (K_\rho + K_\rho^{-1} - 2)/4$ by using the value of $K_\rho$ extracted from the linear slope of $N_q$. As reported in

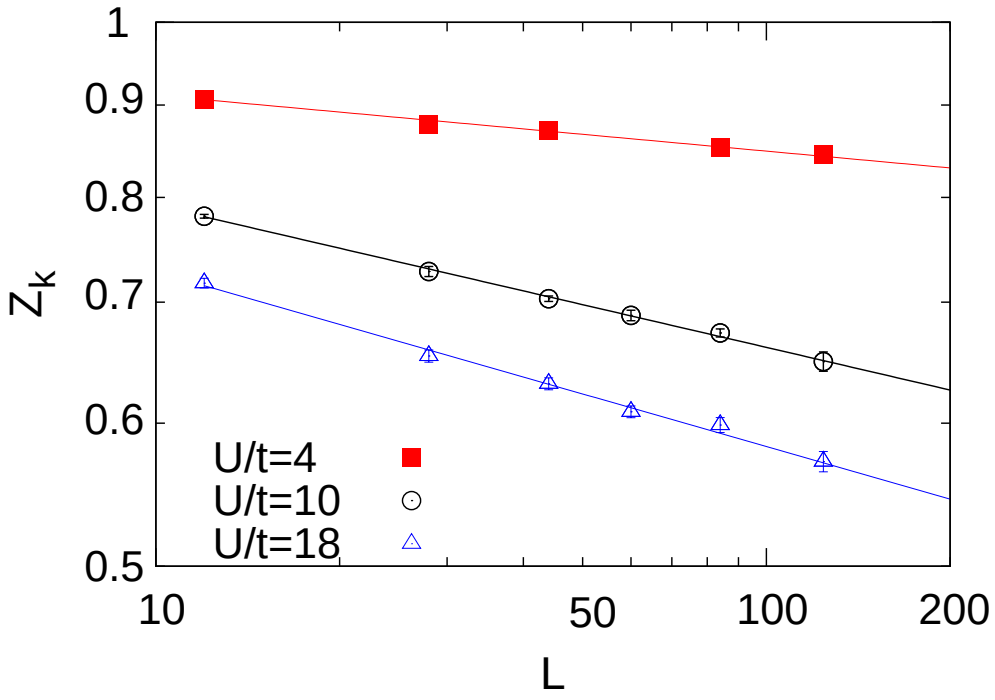


Figure 4.23: Log-log plot of the quasiparticle weight $Z_k$ at $k = k_F = \pi/4$ as a function of $L$ in the quarter-filled Hubbard model for different values of $U/t$. Lines are power-law fits.

Table 4.1, we obtain an excellent agreement for the values of the interaction $U/t$ considered. Finally, we can also calculate the singlet pairing correlations

$$P(r) = \frac{1}{L}\sum_i \frac{\langle \Psi_N | \Delta_{i+r} \Delta_i^\dagger | \Psi_N \rangle}{\langle \Psi_N | \Psi_N \rangle}, \tag{4.21}$$

where

$$\Delta_i^\dagger = c_{i,\uparrow}^\dagger c_{i+1,\downarrow}^\dagger - c_{i,\downarrow}^\dagger c_{i+1,\uparrow}^\dagger \tag{4.22}$$

creates a singlet pair of electrons at nearest neighbors. In order to calculate the exponent $\alpha$ related to the decay of $P(r) \sim 1/r^\alpha$, we consider the pairing correlation at the maximum distance $P(L/2)$ for different sizes, see Figure 4.24. In this case, the signal is very small and a precise determination of the critical exponent is quite difficult. Nonetheless, the results reported in Table 4.1 are rather satisfactory and not too far from the ones obtained with the exact relation $\alpha = K_\rho^{-1} + 1$ [97].

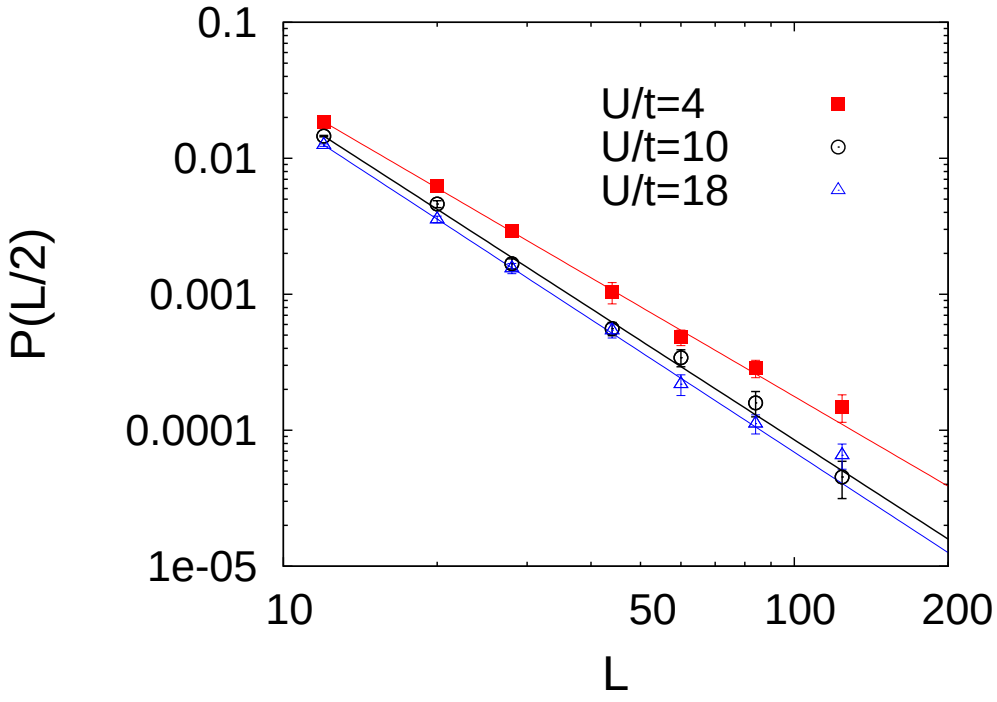


Figure 4.24: Log-log plot of the pairing correlation function at the maximum distance $P(L/2)$ as a function of $L$ in the quarter-filled Hubbard model for different values of $U/t$. Lines are power-law fits.

Table 4.1: Critical exponents for the $1d$ Hubbard model at quarter filling: $K_\rho$ is found from the low-$q$ behavior of $N_q$, $\theta_c = (K_\rho + K_\rho^{-1} - 2)/4$, and $\theta$ is found by fitting $Z_k$ with $Z_k \sim 1/L^\theta$. The last two columns refer to the critical exponent of the pairing correlations: $\alpha$ is found from the pairing correlation at the maximum distance $P(L/2) \sim 1/L^\alpha$ and $\alpha_c = K_\rho^{-1} + 1$. In the first column, we report the exact value of $K_\rho$.

| $U/t$ | $K_\rho^{exact}$ | $K_\rho$ | $\theta$ | $\theta_c$ | $\alpha$ | $\alpha_c$ |
|---|---|---|---|---|---|---|
| 4 | 0.711 | 0.705(3) | 0.031(5) | 0.031(3) | 2.1(1) | 2.42(6) |
| 10 | 0.594 | 0.595(3) | 0.078(5) | 0.072(3) | 2.4(1) | 2.68(9) |
| 18 | 0.551 | 0.550(3) | 0.097(5) | 0.092(3) | 2.5(2) | 2.82(9) |

### 4.3.2 From Luttinger liquid to Mott insulator

Let us consider how the insulating phase is reached by decreasing the hole concentration. First of all, it should be mentioned that, not too close to the insulating phase at half filling, the charge and spin structure factor have small size effects and, therefore, reliable calculations are possible even without using too large $L$. As an example, we report in Figure 4.25 (right panel), the case of doping $\delta = 2/11$, where we can see that there are no appreciable differences in $N_q$ from $L = 22$ to $L = 154$. In the doped region, the system is always conducting, $N_q$

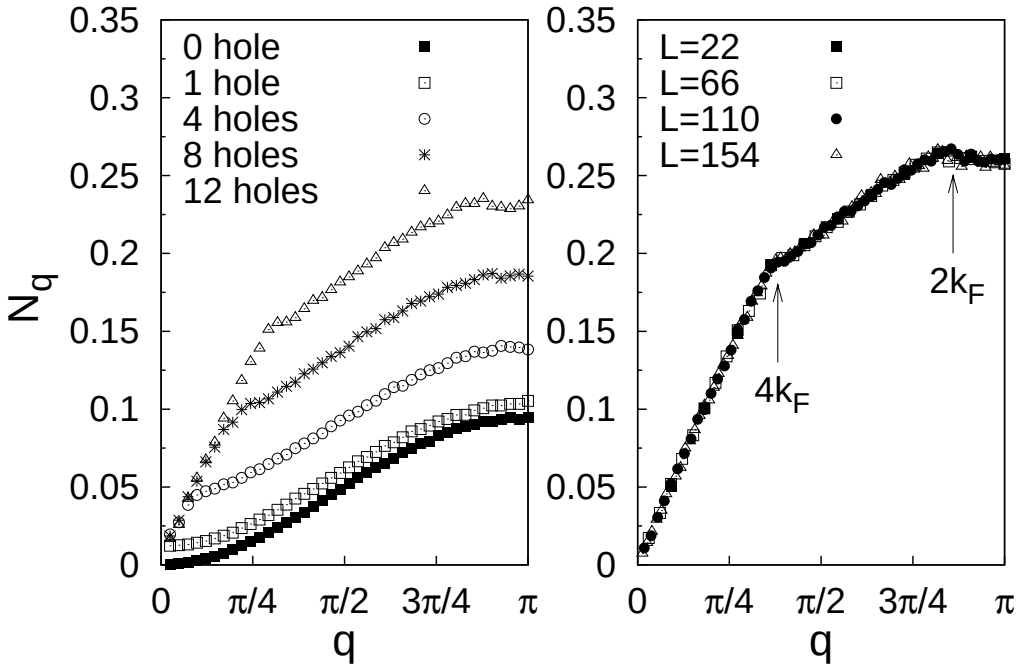


Figure 4.25: Left panel: charge structure factor $N_q$ for $L = 82$, $U/t = 10$, and different hole dopings. Right panel: $N_q$ for $\delta = 2/11$ and different $L$.

having a linear behavior for small momenta, with a slope that depends upon $U/t$ and $\delta$. For sufficiently small hole doping, it turns out that the linear regime is limited to a small window around $q = 0$, whereas for larger momenta, $N_q$ acquires a finite curvature, see Figure 4.25 (left panel). The two different regimes are separated by the singularity at $q = 4k_F = 2\pi\delta$, and, therefore, by decreasing $\delta$, the width of the linear regime shrinks, the slope being almost constant. Therefore, we

arrive at the empirical result:

$$N_q \sim \frac{K_\rho |q|}{\pi} \Theta(4k_F - q) + (c + q^2)\Theta(q - 4k_F), \tag{4.23}$$

where $k_F = (1-\delta)\pi/2$, $\Theta(x)$ indicates the Heaviside step function and $c$ is a constant determined by imposing continuity of $N_q$ at $q = 4k_F$. This singular behavior, with the kink at $q = 4k_F$, is entirely due to correlation and it is compatible with the exact result that $K_\rho$ remains finite, more precisely $K_\rho \to 1/2$, for $\delta \to 0$ [97].

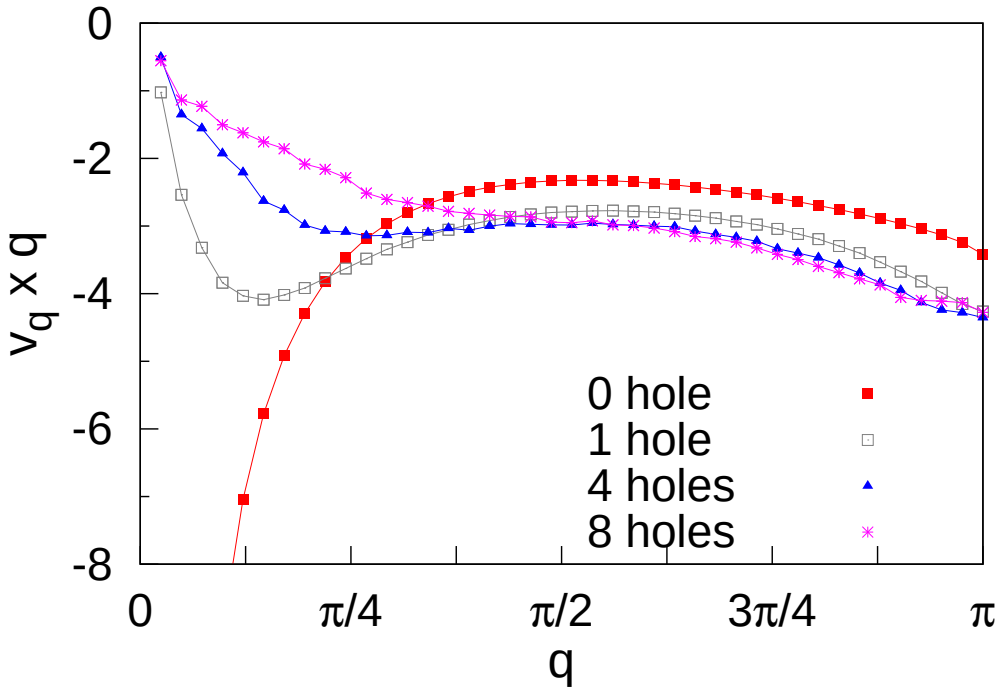


Figure 4.26: Jastrow factor $v_q$ (multiplied by $q$) for different hole dopings, obtained by a careful minimization of the energy for $U/t = 10$ and $L = 82$.

Let us now consider the behavior of the Jastrow parameters when the doping $\delta$ is varied. In Figure 4.26 we report the form of the Jastrow factor at half filling and for small concentration of holes considered in Figure 4.25. Starting from the insulating phase, upon doping, $v_q$ moves away from $v_q \sim 1/q^2$, and becomes less singular, i.e., $v_q \sim 1/|q|$. Clearly, at very small doping, the size effects affect the small-$q$ part, and, in particular, for the smallest momentum we can have

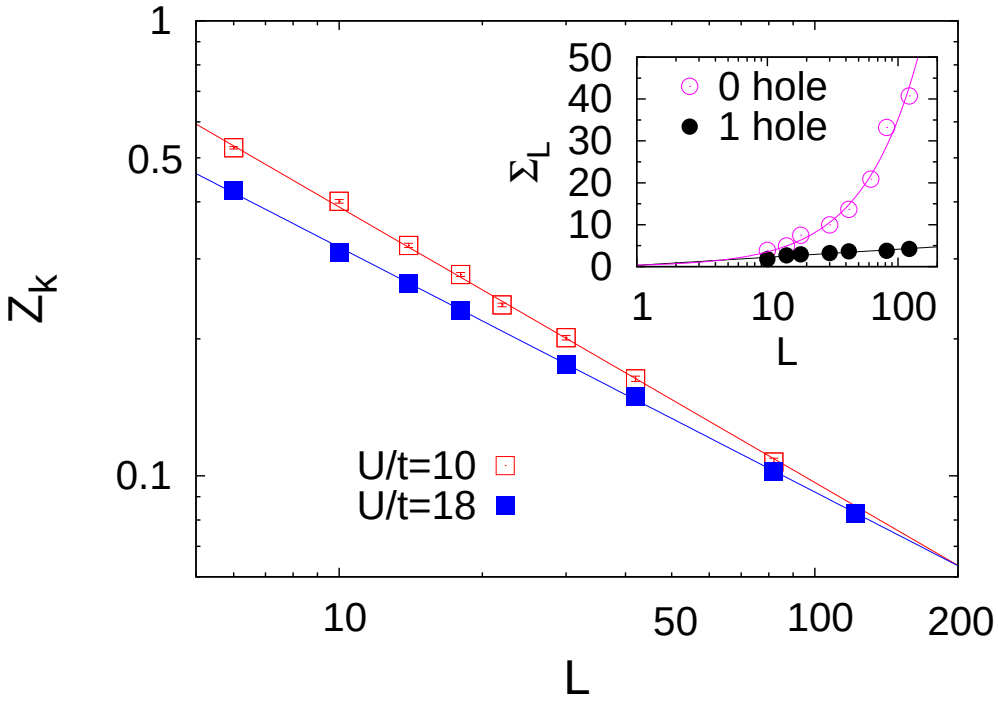


Figure 4.27: Log-log plot of $Z_k$ as a function of $L$ for $U/t = 10$ and $18$ at half-filling. Lines are power-law fits. Inset: the quantity $\Sigma_L = -1/L \sum_{q\neq 0} v_q$ (see text) as a function of $L$ at half-filling and for one hole. Lines are fit of the data.

some deviations from the expected $v_q \sim 1/|q|$ behavior. The remarkable thing is that for any non-vanishing hole doping $\delta$ and interaction $U/t$, by optimizing the variational WF, the Jastrow factor is singular, i.e., $v_q \sim 1/|q|$. This fact is crucial to recover the correct low-$q$ behavior of $N_q$, whose linear slope is renormalized by the interaction, leading to $N_q \sim K_\rho |q|/\pi$. Therefore, the Jastrow factor has to be intrinsically long range also at finite doping. Moreover we find that the small-$q$ behavior of $v_q$ follows the Reatto-Chester predictions (2.7), not only qualitatively but also with the correct coefficient, signaling that the Gaussian approximation in this case is exact at long wavelengths.

Notice that the correct minimization of the Jastrow factor is particularly important for an accurate description of $Z_k$, especially when approaching half filling. Indeed, in this case, the Jastrow factor for one hole is considerably different from the insulating one for small $q$'s (see Figure 4.26), and one has to optimize both

WFs with $N$ and $(N-1)$ particles. This difference can be appreciated by considering $\Sigma_L = -1/L \sum_{q\neq 0} v_q$, which diverges linearly with the system size $L$ if $v_q \sim 1/q^2$ and, instead, diverges only logarithmically if $v_q \sim 1/|q|$. In Figure 4.27 (inset), we report $\Sigma_L$ as a function of $L$ for the insulating state and for the one-hole case: the difference between the two cases clearly demonstrates the different behavior of $v_q$ for small momenta. By a careful minimization of both the WFs, it is possible to recover the result that $\theta = 1/2$ independently of $U/t$ [98]. Indeed, upon increasing $U/t$, our variational WF gives a rather accurate description of the insulating phase, the size effects being strongly reduced due to the small correlation length expected at large $U/t$. In this limit, we obtain a reasonable good agreement with the exact exponent for the quasiparticle weight (see Figure 4.27): $\theta = 0.60 \pm 0.05$ and $\theta = 0.55 \pm 0.05$ for $U/t = 10$ and $U/t = 18$, respectively. On the other hand, it should be mentioned that a naive calculation with a singular Jastrow $v_q \sim 1/q^2$ for both WFs would lead to a wrong exponential behavior of the quasiparticle weight.

# Chapter 5

# The Jastrow wavefunction in two dimensions

In Chapter 4 we have shown that the long-range Jastrow wavefunction (WF), optimized for the one-dimensional Hubbard model, faithfully describes both the Mott insulating state and the Luttinger-liquid metallic state. The two leading behaviors for the Jastrow parameters are $v_q \sim \frac{1}{q^2}$ for the insulator and $v_q \sim \frac{1}{|q|}$ for the correlated metal. This form of the Jastrow factor gives the correct charge-density structure factor in the two cases, namely $N_q \sim q^2$ in the insulator and $N_q \sim |q|$ in the metal.

In this chapter we generalize our approach to the two-dimensional case. Following general arguments, we show that a wavefunction with a two-body long-range Jastrow factor $v_q \sim \frac{1}{q^2}$ naturally arises from the condition imposed on the behavior of the structure factor for an insulating state, i.e., $N_q \sim q^2$. Indeed, in the regime of large Coulomb interaction, the quantum problem can be mapped into a classical problem at finite temperature, the classical Coulomb gas model, where particles with positive and negative charges interact with a Coulomb potential. Within this mapping, the temperature of the classical model corresponds to the Jastrow strength in the quantum system. Therefore, we can learn about the physical properties of the Jastrow WF from the known results of this classical model. In particular, the Coulomb gas model in two dimensions ($2d$) shows a Kosterlitz-Thouless transition by reducing the temperature, turning from a metallic phase (plasma phase) at high temperature to an insulating confined phase at low temper-

ature. This suggests that also in the quantum problem, in two dimensions, a similar transition might occur, when the Jastrow strength is varied. However, the quantum fermionic problem is characterized not only by the Jastrow factor, but also by the presence of the uncorrelated determinant. We show that the action of a singular Jastrow factor $v_q \sim \frac{1}{q^2}$ on the determinant induces anomalous properties, which depend on the Jastrow strength and are deeply related to the corresponding phase in the classical Coulomb gas model. In particular, for small Jastrow strengths, we find that the corresponding phase is a non-Fermi liquid metal, characterized by a vanishing quasiparticle weight. On the other hand, for large correlations, we find an insulating phase, characterized by a singular power-law behavior in the photoemission spectrum, that can be continuously connected to the fully-projected Gutzwiller state. This opens the possibility for an unconventional metal-insulator transition in two dimensions, where both the metallic and the insulating phase are characterized by a vanishing quasiparticle weight.

In order to see whether this scenario occurs in some microscopic model, we optimize the Jastrow WF on the two-dimensional Hubbard model. In particular, we consider the paramagnetic sector, where we show that the Jastrow WF allows us to obtain a metal-insulator transition at a finite $U/t$ and we characterize the metallic and the insulating phase that are obtained. Since the metallic phase is described by $v_q \sim \frac{1}{|q|}$ and has a finite quasiparticle peak, we find that the appealing scenario for an unconventional metal-insulator transition does not occur in this case.

Finally, besides the paramagnetic solution, we compare the accuracy of different WFs which allow us to describe also the magnetic properties of the model. This is done in view of the possibility to connect the infinite-$U$ limit to the finite-$U$ case. Indeed, in the corresponding two-dimensional Heisenberg model, the use of fully-projected determinants can give very accurate variational energies. In particular, on the square lattice, the antiferromagnetic state has the lowest energy, but the RVB state obtained by fully-projecting a BCS state is also remarkably accurate [9, 10, 99]. At this point, since the presence of the long-range charge-density Jastrow factor ensures the correct insulating behavior, independently on the choice of the determinant, it is very interesting to evaluate the accuracy of these different wavefunctions in the finite-$U$ case.

## 5.1 Mapping on the classical Coulomb gas model

In Chapter 4 we have applied the $f$-sum rule in different cases and we have shown that, in order to have an insulator, a necessary condition is that for small momenta $N_q \sim q^2$. In the following, we show that this argument has very general consequences on the form of the corresponding ground-state WF $|\Psi_0\rangle$, that do not depend on the particular microscopic model. To this purpose, let us denote an electronic configuration by the positions $\{x\}$ of the particles. For all the operators $F$ that depend only on such positions, e.g., the charge-density structure factor itself, the quantum average

$$\langle F \rangle = \frac{\langle \Psi_0 | F | \Psi_0 \rangle}{\langle \Psi_0 | \Psi_0 \rangle} \tag{5.1}$$

can be written in terms of the *classical* distribution $|\Psi_0(x)|^2 = \frac{|\langle x|\Psi_0\rangle|^2}{\sum_{x'} |\langle x'|\Psi_0\rangle|^2}$, as:

$$\langle F \rangle = \sum_x \langle x|F|x\rangle |\Psi_0(x)|^2. \tag{5.2}$$

Since $|\Psi_0(x)|^2$ is a positive quantity, we can define an appropriate correspondence between the wavefunction $|\Psi_0\rangle$ and an effective potential $V(x)$:

$$|\Psi_0(x)|^2 = e^{-V(x)}. \tag{5.3}$$

Focusing on the charge properties, if the system is subject to small charge fluctuations (e.g., in the limit of strong Coulomb interaction), we can safely assume that only the two-body term is relevant and all multi-particle interactions are negligible. This leads to the quadratic potential:

$$V(x) = \sum_{q \neq 0} v_q^{eff} n_q(x) n_{-q}(x), \tag{5.4}$$

being $n_q(x)$ the Fourier transform of the local density of the configuration $|x\rangle$.

In order to obtain the expected behavior of the charge-density structure factor, given in terms of the classical distribution by $N_q = \sum_x n_q(x) n_{-q}(x) e^{-V(x)} \sim q^2$, the effective potential (5.4) must diverge as:

$$v_q^{eff} = \frac{\pi}{T^{eff} q^2} + \text{less singular terms}. \tag{5.5}$$

Here, $T^{eff}$ can be considered as the effective temperature of classical particles interacting through a potential $\pi/q^2$. Within this choice of $v_q^{eff}$, $N_q \sim q^2$ is generally valid. The form of $v_q^{eff}$ can be understood by considering $n_q$ as a complex continuous variable, so that the classical average $\langle n_q n_{-q} \rangle$ turns into a standard Gaussian integral, yielding:

$$N_q \sim \frac{1}{v_q^{eff}} = \frac{T^{eff} q^2}{\pi}. \tag{5.6}$$

If we now consider the Jastrow WF, $|\Psi_J\rangle = \mathcal{P}_J |D\rangle$ as a variational ansatz for the true ground state $|\Psi_0\rangle$ of a fermionic system, it turns out immediately that the potential $V(x)$ of Eq.(5.3) now contains the contributions coming from both the determinant and the Jastrow potential. Here, we are interested in describing Mott insulators that do not break any symmetry and, therefore, the uncorrelated determinant represents a metallic state at half-filling. A straightforward way to modify the effective potential associated to $|D\rangle$ is obtained by taking into account an appropriate Jastrow factor:

$$\mathcal{P}_J = \exp\left[-\frac{1}{2}\sum_q v_q n_q n_{-q}\right] \qquad \text{with} \quad v_q \sim \frac{\pi\beta}{q^2} \tag{5.7}$$

$\beta$ fixing its strength. This form of the Jastrow allows us to reproduce the behavior of the effective potential (5.5) necessary to describe an insulator. In this picture the metallic determinant will contribute only with less singular terms (typically $O(1/q)$) as reported in Eq.(5.5). Comparing Eqs.(5.5) and (5.7) it turns out that there is a correspondence between the inverse of the effective temperature $1/T^{eff}$ of the classical model and the Jastrow strength $\beta$ of the quantum system.

Within this approach, the potential $V(x)$ of Eq. (5.3-5.4) turns out to be the one of the classical Coulomb gas model (CGM) [100], which describes a two-component system of positive and negative charges interacting with a potential $V(q) \sim 1/q^2$. Considering the quantum system described by the Jastrow WF, let us recall that it is possible to write the density-density operator contained in the Jastrow factor in terms of holons and doublons, namely:

$$(n_i - 1)(n_j - 1) = h_i h_j + d_i d_j - h_i d_j - d_i h_j \tag{5.8}$$

where $h_i = (1 - n_{i\uparrow})(1 - n_{i\downarrow})$ counts the holons on site $i$ and $d_j = n_{j\uparrow} n_{j\downarrow}$ counts the doublons. Therefore, the corresponding charged objects in the quantum

system are the holons and the doublons created by charge fluctuations. [1] The interaction $v_q \sim \frac{1}{q^2}$ turns out to be attractive among holons and doublons, and repulsive among holon-holon and doublon-doublon. In particular, in the half-filled case, there is an equal number of empty and doubly occupied sites, implying the charge neutrality of the CGM. The fugacity $z$ of the CGM, that sets the average number of the charges, can be identified with the on-site Gutzwiller term in the Jastrow potential, i.e., $z = \exp(-g)$, where $g$ is the Gutzwiller parameter.

Finally, let us comment on the quadratic form of the potential (5.4), that was assumed to be valid in the limit of small charge fluctuations. In the quantum system, this assumption corresponds to the low-density regime of holons and doublons, condition which is surely fulfilled in the limit of large interactions, where the Mott insulating phase is stabilized.

### 5.1.1 Unconventional metal-insulator transition in $2d$

The mapping among the quantum system and the classical Coulomb gas model described above, has several implications on the phases characterized by the Jastrow WF, which depend on the dimensionality. In particular, the two-dimensional classical CGM shows a Kosterlitz-Thouless (KT) transition at a finite temperature $T_c^{CGM}$ [100] (see Figure 5.1). This transition is transparent from the classical dielectric function:

$$\frac{1}{\epsilon} = \lim_{q \to 0} \left[ 1 - \frac{2\pi}{T^{eff} q^2} N_q \right], \tag{5.9}$$

where $T^{eff}$ is the temperature of the classical model. The charge structure factor is quadratic at small momenta, i.e., $N_q \sim \alpha q^2$, for all temperatures, but the coefficient $\alpha$ changes discontinuously at $T_c^{CGM}$. Above $T_c^{CGM}$, the CGM is in the *plasma phase*, i.e., a metallic phase with infinite dielectric function, perfect screening, and exponential correlation functions. On the other hand, below $T_c^{CGM}$, the CGM is in the *confined phase*, with a finite dielectric constant. In this phase the charges are bound together forming dipoles, that, because of their residual interaction, induce power-law correlations. At the transition, the inverse of the dielectric function has a finite jump, changing from zero, in the plasma phase, to a finite value, in the confined phase.

[1] Let us stress that the above arguments have not been obtained for a particular model, but are valid for a generic one-band fermionic model at half-filling.

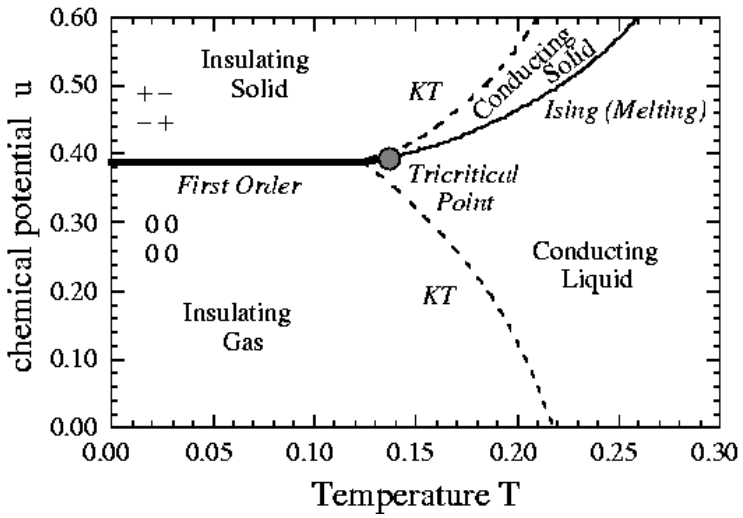


Figure 5.1: Phase diagram of the two-dimensional Classical Coulomb gas model on a square lattice [101]. In the low-density limit, there is a KT transition among a confined phase (denoted as Insulating Gas) and a plasma phase (named Conducting Liquid).

In the following we show that, in analogy with the classical CGM, also in the case of fermionic systems at zero temperature, a KT-like transition is found by varying the correlation strength $\beta$. However, the existence of the fermionic determinant induces non-trivial properties for the two phases involved, that are not present in the classical problem. For example, the uncorrelated part of the WF may contribute to the expression of the effective temperature $T^{eff}$, as shown below. Whenever the square of the WF describes the plasma phase of the corresponding classical model, the Gaussian fluctuations are exact for small $q$'s and the classical temperature can be determined by imposing $1/\epsilon = 0$ in Eq. (5.9), namely $T^{eff} = 2\pi \lim_{q\to 0} N_q/q^2$. In the language of quantum states, the Gaussian approximation leads to the well-known Reatto-Chester relation:

$$N_q = \frac{N_q^0}{1 + 2v_q N_q^0}, \tag{5.10}$$

where $N_q^0$ is the charge structure factor of the uncorrelated determinant $|D\rangle$. The

previous form of $N_q$ allows us to identify the effective temperature as:

$$\frac{1}{T^{eff}} = \beta + \frac{\alpha_0}{2\pi} \tag{5.11}$$

where $\alpha_0 = \lim_{q\to 0} q^2/N_q^0$ is the contribution to the effective temperature coming from the uncorrelated determinant.

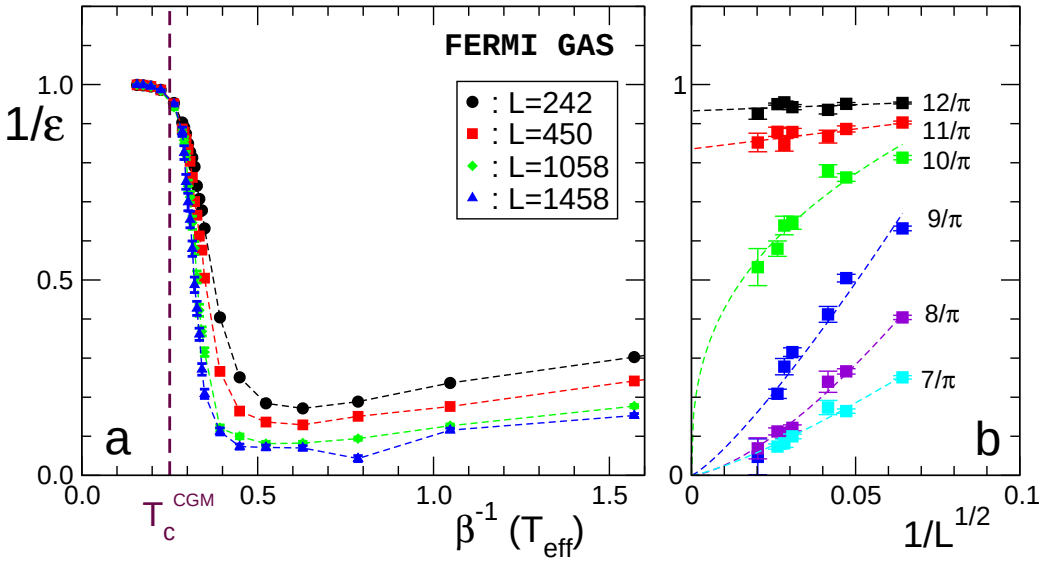


Figure 5.2: Inverse of the dielectric function $1/\epsilon$ [see Eq. (5.9)] for the free-electron determinant. Left panel: $1/\epsilon$ as a function of the effective temperature $1/\beta$ and for different sizes $L$ of the cluster. The critical temperature of the classical Coulomb gas model $T_c^{CGM}$ is marked with a dashed line for a comparison. Right panel: size scaling of $1/\epsilon$ for various $\beta$.

In order to show the general validity of our approach, we consider the case of a free-electron determinant, obtained by occupying the lowest-energy states in the tight-binding model with dispersion $E_k = -2t(\cos k_x + \cos k_y)$ and a gapless BCS state with a superconducting order parameter $\Delta_k = \Delta(\cos k_x - \cos k_y)$. In these cases $\alpha_0 = 0$ and, therefore, the effective temperature in Eq. (5.11) is determined only by the Jastrow coefficient, namely $T^{eff} = 1/\beta$. In Figure 5.2, we report the inverse of the dielectric function for the free-electron determinant and different sizes $L$ of the system at half filling, i.e., $N = L$. In order to have closed-shell states for $|D\rangle$, we used square lattices tilted by $45°$ (i.e., with $L = 2l_x^2$ and $l_x$ odd)

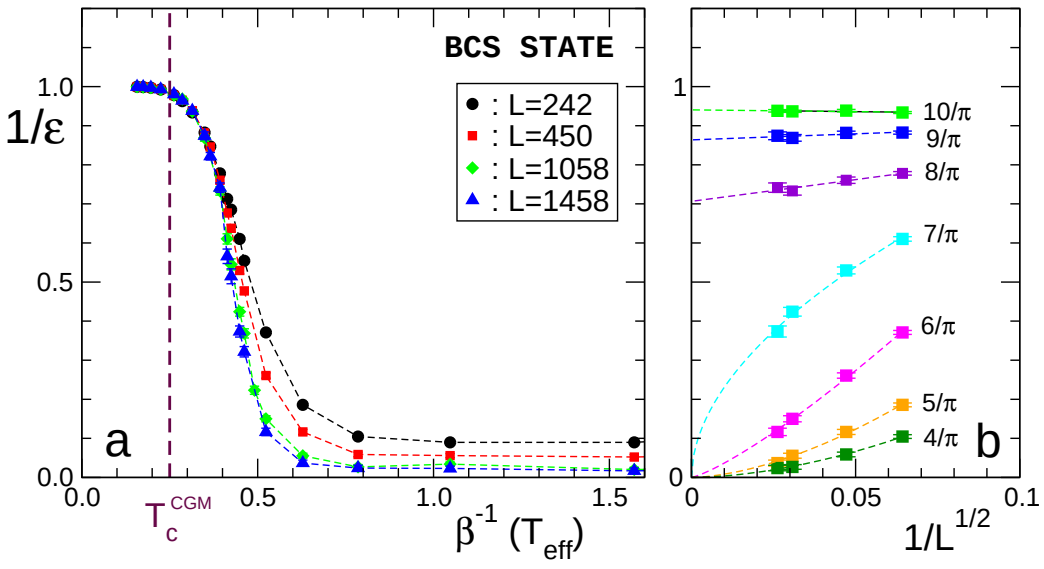


Figure 5.3: The same as in Figure 5.2 for a gapless BCS state with $\Delta/t = 1.1$ and $d_{x^2-y^2}$ symmetry.

and periodic boundary conditions. By increasing $L$, the curves show a steeper and steeper shape in the vicinity of the critical temperature $T_c$. This result is further confirmed by the size scaling of $1/\epsilon$, which clearly supports the existence of a finite jump in the thermodynamic limit: $1/\epsilon \to 0$ for $T^{eff} > T_c$, whereas $1/\epsilon \to \text{const}$ for $T^{eff} < T_c$. Interestingly, $T_c$ depends slightly upon the choice of the uncorrelated determinant (see for comparison Figure 5.3 for the gapless BCS state) and is quite close to the CGM critical temperature $T_c^{CGM} = 1/4$. These results give an important and transparent insight into the strong-coupling limit described by the fully-projected WF [8], that can be connected to our WF by letting $\beta \to \infty$, i.e., $T^{eff} \to 0$. Indeed, in the confined phase for $T^{eff} < T_c$, the classical KT scaling equations of the CGM flow to fixed points with zero fugacity: this translates into the fact that the fully-projected state represents the fixed-point of the correlated WFs describing the two-dimensional Mott insulating phase. Therefore, in the confined regime, the ground-state properties are universal and represented by the ones of the fully-projected WF. In this respect, the total projection is not an unrealistic assumption and can accurately reproduce the low-energy physical properties of a strongly-correlated system. On the other hand, for $T^{eff} > T_c$ the classical KT scaling equations flow to strong coupling and are

useful only close to the transition.

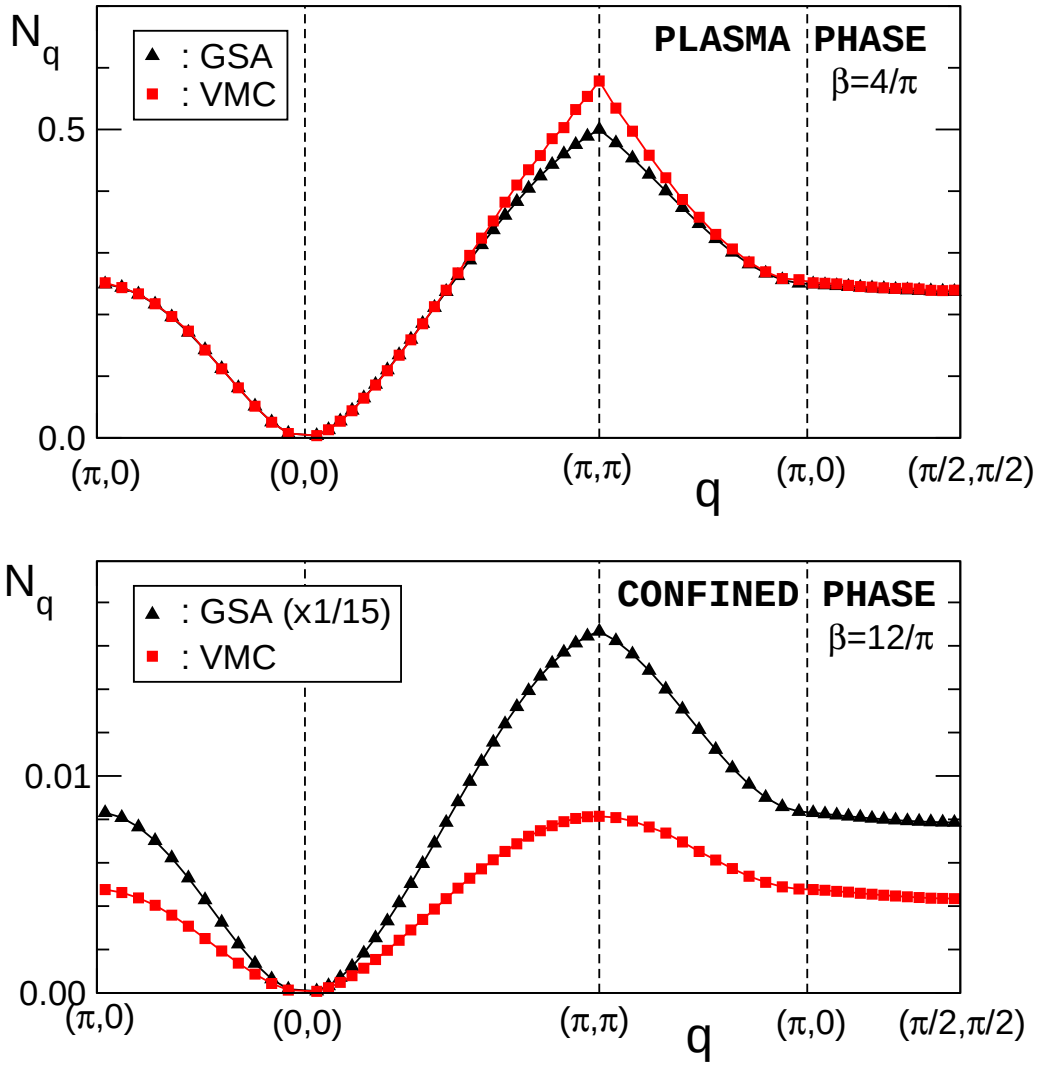


Figure 5.4: Equal-time density structure factor $N_q$ for the correlated Jastrow wave function (with $FS\rangle$ determinant) (full squares), compared to the same quantity calculated within the Gaussian approximation [indicated as GSA and given by Eq. (5.10)], (full triangles) for $\beta = 4/\pi$ (upper panel) and $\beta = 12/\pi$ (lower panel, notice the different scale of the GSA data).

Let us now characterize the two phases involved. In Figure 5.4 we show that

in the plasma phase (i.e., for $\beta < \beta_c$) the Gaussian approximation, given by Eq. (5.10), is very accurate, not only for small $q$'s (where it is exact) but also for large momenta. In this case, the cusp singularity in $N_q$ for $Q = (\pi, \pi)$, related to the Friedel oscillations inherited from the uncorrelated Slater determinant, is not removed, even though $N_q \sim q^2$ at low momenta. Thus, for $\beta < \beta_c$ ($T^{eff} > T_c$), the Jastrow WF with $v_q = \pi\beta/q^2$ describes a "Coulomb metal", with $N_q \sim q^2$ at small $q$'s but with the sign of the Fermi surface at large momenta. As shown previously in the low-density regime [102], this WF has low-energy properties similar to one-dimensional Luttinger liquid conductors, where the absence of a jump in the momentum distribution is replaced by a weaker singularity, yielding to $2k_F$ and $4k_F$ power-law density correlations. It is important to emphasize that, in the quantum case, the power-law correlations come from the large momentum singularity and are absent in the classical CGM [100]. Indeed, in the quantum state, the subleading corrections in the classical potential of Eq. (5.3) are very important and can actually turn the CGM exponential correlations to power laws in the plasma phase, and *vice-versa* in the confined phase. On the other hand, in the confined phase the Gaussian approximation is not adequate both at small and large momenta, see Figure 5.4. Indeed, at small $q$'s, the coefficient of the quadratic term is not simply given by the Gaussian approximation and, more importantly, the strong Jastrow factor washes out completely the singularities of $N_q^0$, leading to a smooth charge-structure factor, a genuine fingerprint of an insulating phase.

In order to further characterize the two phases, we consider the quasiparticle weight

$$Z_k = \frac{|\langle \Psi_{N-1}|c_{k,\sigma}|\Psi_N\rangle|^2}{\langle \Psi_N|\Psi_N\rangle\langle \Psi_{N-1}|\Psi_{N-1}\rangle}, \tag{5.12}$$

where $|\Psi_N\rangle$ and $|\Psi_{N-1}\rangle$ are the WF with $N$ and $(N-1)$ particles, $c_{k,\sigma}$ is the destruction operator of a particle of momentum $k$ and spin $\sigma$. In particular, the wave function with $N-1$ particles is constructed from $|\Psi_N\rangle$ as:

$$|\Psi_{N-1}\rangle = \mathcal{P}_J c_{k,\sigma}|D\rangle. \tag{5.13}$$

In previous works [102, 103], it was argued that the singular Jastrow factor can induce non-Fermi liquid properties, and in particular a vanishing $Z_k$ at the Fermi surface. In Figure 5.5, we report $Z_k$ for $k = (\pi/2, \pi/2)$ and for different Jastrow strengths $\beta$. We find that the quasiparticle weight vanishes with a power-law

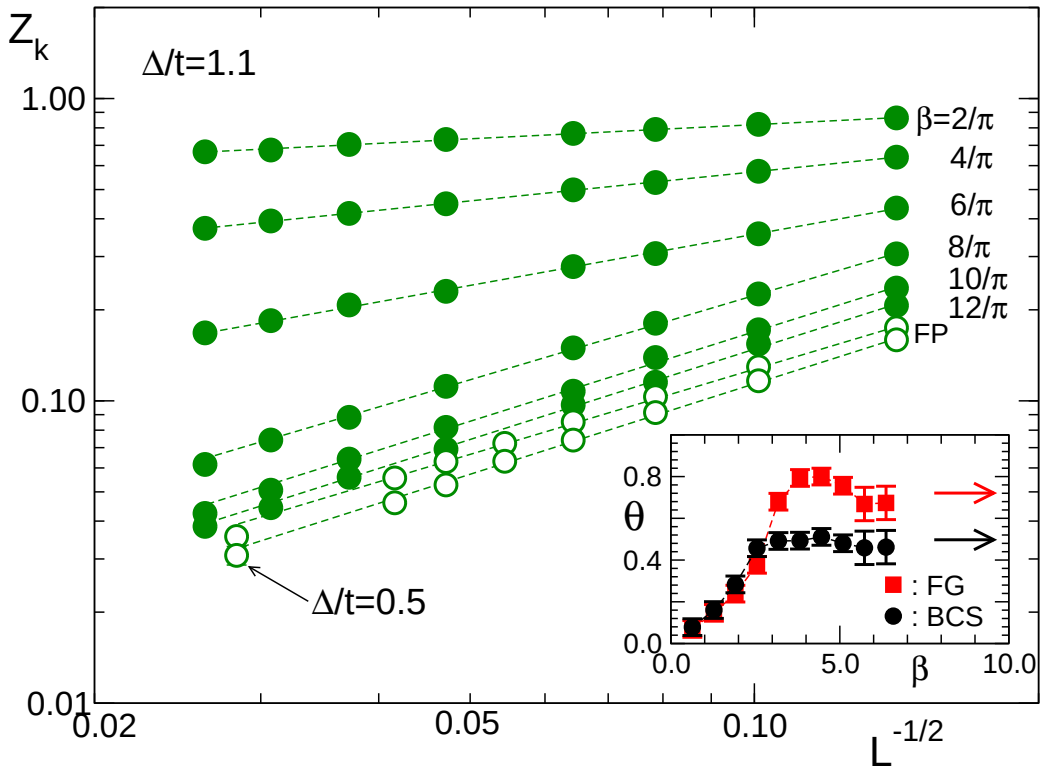


Figure 5.5: Quasiparticle weight $Z_k$ at $k = (\pi/2, \pi/2)$ for the gapless BCS state with $\Delta/t = 1.1$ and $d_{x^2-y^2}$ symmetry as a function of $L$ and for different Jastrow strengths $\beta$ (full circles). The case of the fully-projected wave function (empty circles) is also reported for $\Delta/t = 1.1$ and $0.5$. Inset: The behavior of $\theta$ [the exponent of the quasiparticle weight, see Eq. (5.14)] as a function of $\beta$ for BCS state (full circles) and the Fermi gas (FG) determinant (full squares). The value of the fully-projected states are also reported (arrows).

behavior:

$$Z_k \sim L^{-\theta} \tag{5.14}$$

both in the confined and in the plasma phase, with an exponent $\theta$ that depends upon $\beta$ and the type of the uncorrelated state. In the plasma phase, $\theta$ varies continuously with the Jastrow strength $\beta$ and there is no appreciable dependence on the uncorrelated determinant. On the other hand, in the confined phase, the exponent is constant, i.e., $\theta \simeq 1/2$ for the BCS state and $\theta \simeq 3/4$ for the free-electron state, and equal to the value found for the fully projected WF, as shown in the in-

set of Figure 5.5. It must be mentioned that, for the BCS state, $\theta$ does not depend upon the value of the superconducting order parameter $\Delta$, indicating the universal properties of the confined phase.

Let us finally comment on the possible occurrence of the above scenario for a microscopic Hamiltonian. In Section 5.2.1 we will test if a metal-insulator transition of this type occurs in the two-dimensional Hubbard model, by considering the paramagnetic solution. We find that this novel scenario does not occur in this case. On the other hand, we can safely predict the occurrence of the novel KT-like scenario in two-dimensional systems with long-range (logarithmic) interaction. In this case, the application of the Gaussian approximation for small interaction and our ansatz for the insulating phase imply the presence of a transition of the type considered here. It is remarkable that the proposed picture crucially depends on the long-range nature of the Coulomb interaction, recalling Mott's original idea.

### 5.1.2 Kosterlitz-Thouless transition with AF and BCS

The novel scenario presented in the previous section shows that the Jastrow factor $v_q \sim \frac{1}{q^2}$ determines anomalous properties in the resulting phases, both in presence of a simple uncorrelated Slater determinant for free electrons and with a BCS mean-field determinant. In these two cases, the uncorrelated starting point is a metallic (superconducting) state. However, the Jastrow factor could be of the form $v_q \sim \frac{1}{q^2}$ also in presence of an insulating antiferromagnetic (AF) Slater determinant, since it enables to obtain the correct density-density correlations. Moreover, the numerical evidence of an attractive $d$-wave pairing interaction even for the half-filled Hubbard model on the square lattice [104–106], suggests that a natural choice for the variational ground state of this model might contain both the BCS and the AF parameter. In this case, the Jastrow factor $v_q \sim \frac{1}{q^2}$ is necessary, in order to restore the correct behavior of the charge-density structure factor $\lim_{q\to 0} N_q = 0$, required to ensure charge conservation. [2]

At this point, one could ask about the effect of the singular Jastrow $v_q \sim \frac{1}{q^2}$ on this kind of insulating determinants, and characterize the properties of the

[2] Indeed, as discussed for the one-dimensional case, the presence of a BCS Slater determinant induces the wrong behavior $N_q^0 \sim const$ and a Jastrow factor is needed in order to set the correct small-$q$ behavior.

corresponding phases when the Jastrow strength is varied.

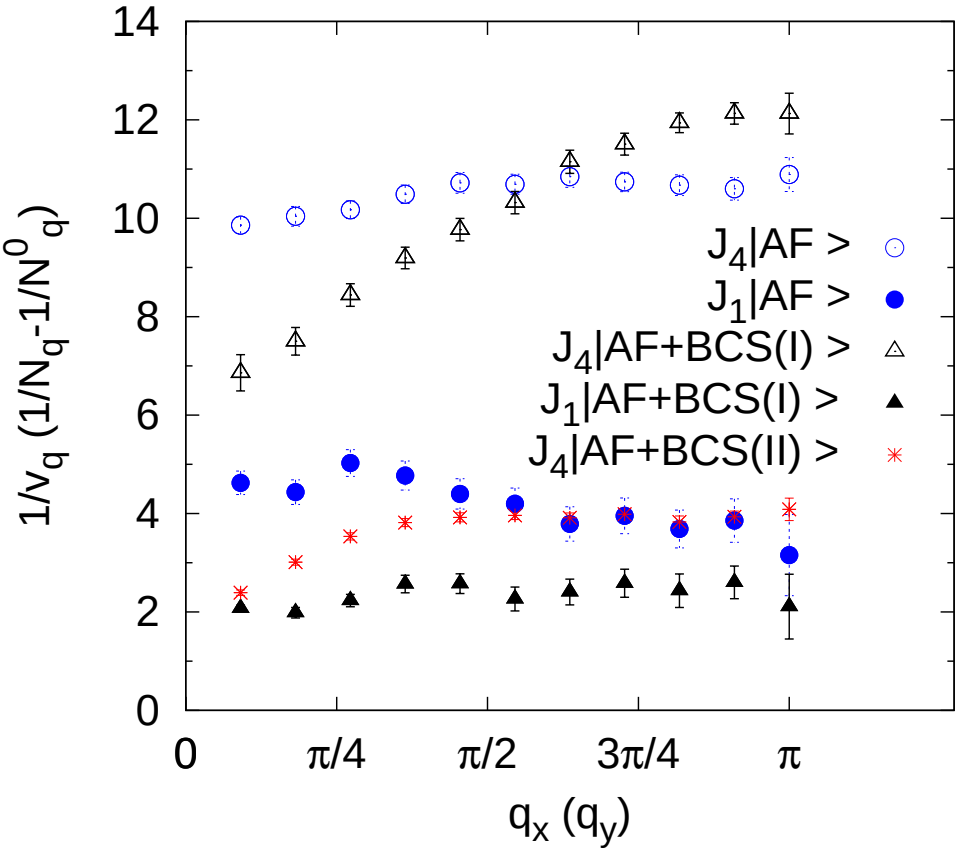


Figure 5.6: Validity of the Gaussian approximation for different Slater determinants and Jastrow strengths for a lattice of 242 sites. Two different Jastrow strengths are considered. $J_4$ corresponds to $\beta = 4/\pi$ and $J_1$ to $\beta = 1/\pi$, with $\beta$ fixing as usual the Jastrow strength $v_q = \frac{\beta\pi}{q^2}$. The determinant denoted with $|AF\rangle$ is obtained for a mean-field Hamiltonian with a staggered antiferromagnetic term [see (1.15)] with antiferromagnetic gap $\Delta_{AF} = 2.0$, while $|AF + BCS\rangle$ corresponds to the ground state of a mean-field Hamiltonian containing both AF and BCS terms. In particular $|AF + BCS(I)\rangle$ denotes the determinant obtained with $\Delta_{AF} = 2.0$ and $\Delta_{d_{x^2-y^2}} = 2.0$ and $|AF + BCS(II)\rangle$ corresponds to $\Delta_{AF} = 0.5$ and $\Delta_{d_{x^2-y^2}} = 1.1$. Points are taken along the diagonal direction.

First, let us consider the validity of the Gaussian approximation for different Jastrow strengths in presence of an AF Slater determinant, with and without the

BCS term. This is done by calculating the coefficient $\gamma$ appearing in the following expression, valid at small $q$:

$$N_q \sim \frac{N_q^0}{1+\gamma\, v_q N_q^0}. \tag{5.15}$$

Whenever $\gamma = 2$, one recovers the Reatto-Chester relation, which holds when the Gaussian approximation is valid. The validity of the Gaussian approximation implies, as discussed in the previous section, that the system properties have the fingerprint of the CGM plasma phase, with additional corrections due to the presence of the Slater determinant; otherwise, if $\gamma > 2$, the Gaussian approximation is valid only qualitatively and the corresponding state is related to the confined phase of the CGM. [3] The value of $\gamma$ is obtained from Eq.(5.15) by taking:

$$\gamma = \lim_{q\to 0}\left[\frac{1}{v_q}\left(\frac{1}{N_q}-\frac{1}{N_q^0}\right)\right]. \tag{5.16}$$

In Figure 5.6 we plot the quantity on the r.h.s. of (5.16) for different determinants and different Jastrow strengths $\beta$, focusing on very small $\beta$, where the plasma phase was previously found in the case of the $|FS\rangle$ and $|BCS\rangle$ states (see Section 5.1.1). The corresponding value of $\gamma$ can be obtained by looking at the limit of small $q$.

In the case of an antiferromagnetic determinant $|AF\rangle$, we find $\gamma > 2$ even for very small Jastrow strengths, namely the system is always in the confined phase and the Gaussian approximation never holds. Indeed, even though the value of $\gamma$ becomes smaller by decreasing the Jastrow strength (see the two cases with $v_q = 4/q^2$ and $v_q = 1/q^2$ reported in Figure 5.6), we find that $\gamma$ is *always* different from 2. The fact that the AF wavefunction always corresponds to the confined phase implies that it has the same universal properties independently from $\beta$ (according to the Kosterlitz-Thouless scaling equations) and we expect that this phase does not differ substantially from the simple AF Slater determinant. Viceversa, in presence of both BCS and AF ($|$AF+BCS$\rangle$), the validity of the Gaussian approximation can be recast for small enough $\beta$ and we find $\gamma \to 2$ (see Figure 5.6). Moreover, for larger $\beta$, the value of $\gamma$ increases, signaling that, contrarily to the

[3] Indeed let us recall that in one dimension, for the minimized Jastrow WF on the Hubbard model, we found that $\gamma$ depends on the value of $U$ as reported in Eq.(4.8) and $\gamma > 2$ at half-filling, while $\gamma = 2$ at finite doping.

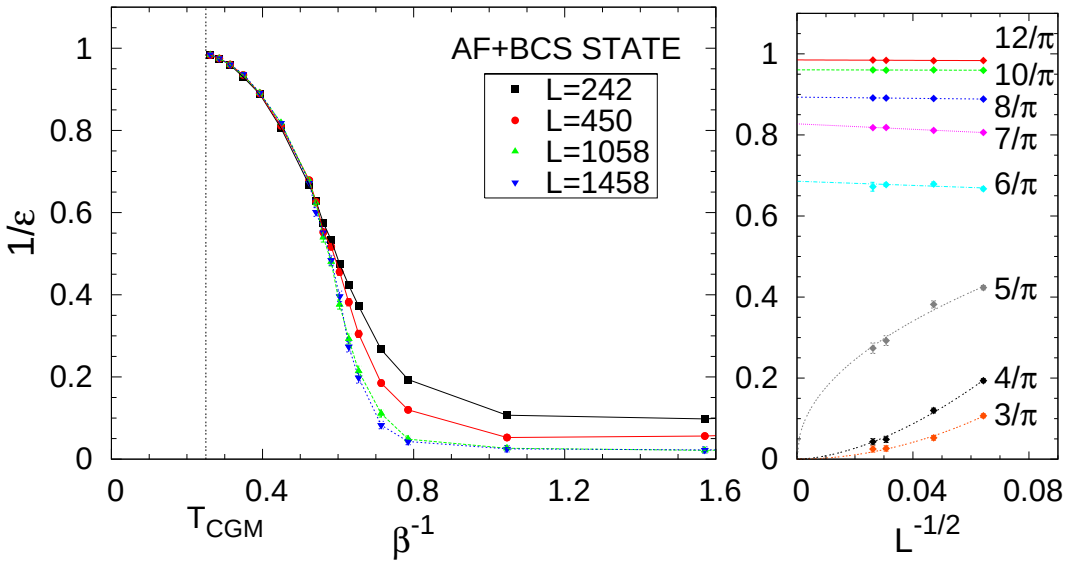


Figure 5.7: The same as in Figure 5.2 for a state with $\Delta_{AF} = 0.5$ and $\Delta_{d_{x^2-y^2}} = 1.1$.

simple AF determinant, a Kosterlitz-Thouless transition might occur in this case. In particular, we find that the values of $\beta$ where the Gaussian approximation holds depend on the ratio among the values of the BCS and the AF gaps, namely, the larger is $\Delta_{AF}/\Delta_{BCS}$, the smaller is the range of validity of the Gaussian approximation, i.e., $\beta_c \to 0$ by increasing the ratio $\Delta_{AF}/\Delta_{BCS}$.

Let us now investigate the possible occurrence of a Kosterlitz-Thouless transition for this latter case in more detail. In Figure 5.7 we plot the inverse dielectric constant as a function of the inverse Jastrow strength for a correlated WF that contains both AF and BCS in the determinant. From the behavior of $1/\epsilon$ for the different sizes it turns out that there is a jump, signaling that the Kosterlitz-Thouless transition occurs also in this case. Notice that the critical value of $\beta$ is much smaller than the classical case, contrarily to what happens for the BCS and FS states. Let us remark that, whenever $\Delta_{AF} \neq 0$, we find that this jump occurs *only when the BCS pairing term is present*, otherwise the system remains in the same phase characterized by a finite dielectric constant for any $\beta$, and no transition occurs.

Finally, in order to further characterize the correlated state built with the long-range Jastrow factor and finite $\Delta_{AF}$ and $\Delta_{BCS}$, we calculate the quasiparticle

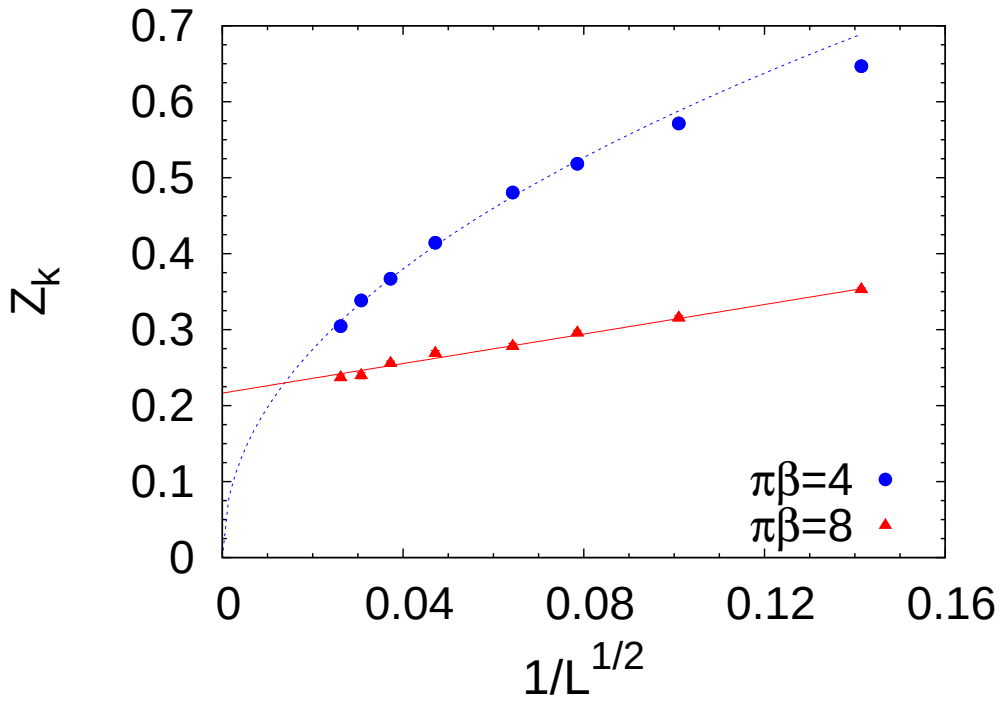


Figure 5.8: Quasiparticle weight $Z_k$ as a function of the inverse square root of the volume $L$ for a Jastrow WF with $\Delta_{AF} = 0.5$ and $\Delta_{d_{x^2-y^2}} = 1.1$, for two different values of the Jastrow strength. Here $\pi\beta = 8$ corresponds to the confined phase and $\pi\beta = 4$ to the plasma phase. Lines are three parameters fits.

weight for two different Jastrow strengths on the two sides of the transition. We find that the quasiparticle weight is finite for $\beta > \beta_c$, whereas, by increasing the size, the value of $Z_k$ strongly decreases in the plasma region, suggesting the possible occurrence of a vanishing quasiparticle weight in this case (see Figure 5.8).

The above scenario, suggests the possible existence of an insulating state, that we denote as “plasma insulator”, which appears at small correlations and is characterized by a vanishing quasiparticle weight and finite antiferromagnetic gap. This strange insulator occurs only if the corresponding mean-field state contains both AF and BCS parameters. It would be very interesting to verify if this state can be stabilized in a microscopic model.

## 5.2 Variational results for the Hubbard model in 2$d$

### 5.2.1 Paramagnetic Jastrow WF

In the previous section we have shown that, within the variational approach, the use of a long-range Jastrow factor admits the possible occurrence of an unconventional metal-insulator transition in two dimensions, with a metallic phase with anomalous non-Fermi liquid properties. Here we verify whether this scenario occurs by considering the two-dimensional Hubbard model in the paramagnetic sector.

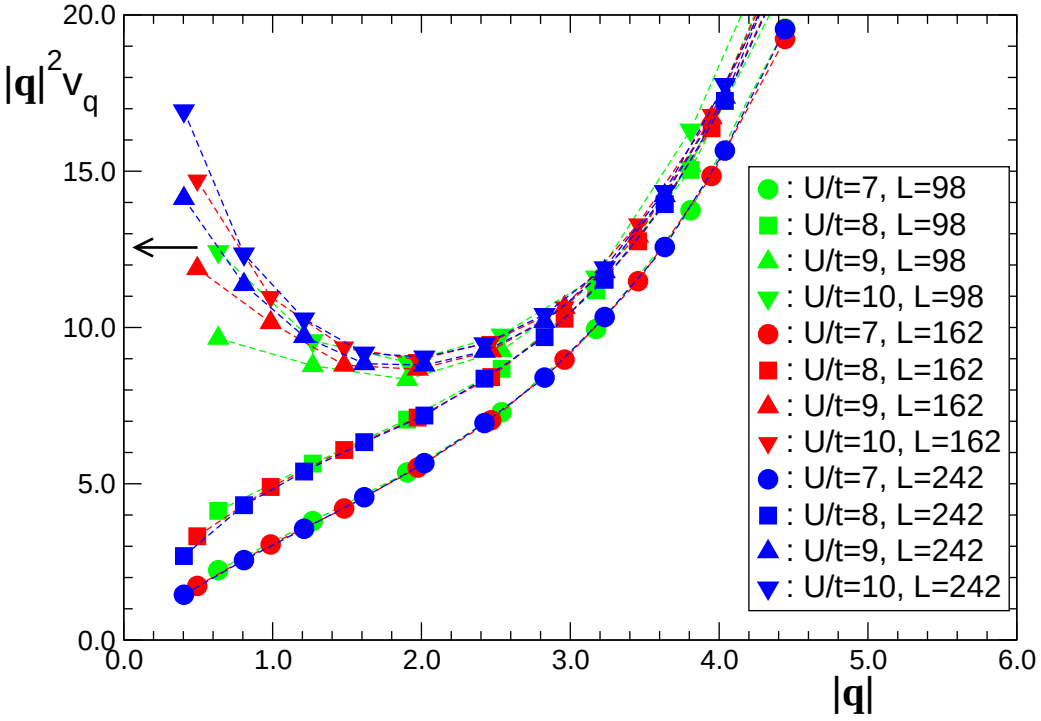


Figure 5.9: Optimized Jastrow potential $v_q$, multiplied by $|q|^2$, for the Hubbard model as a function of $|q|$ [in the (1,1) direction] for different sizes of the cluster and ratios $U/t$. The arrow indicates $\pi/T_c^{CGM}$, the expected value of $\lim_{q\to 0} v_q|q|^2$ at the classical transition point.

Within this approach, that neglects magnetic phases, we obtain a metal-insulator

transition for $U_c/t = 8.5 \pm 0.5$. In the weak coupling regime, we find that the Jastrow strength is $v_q \sim 1/|q|$ (see Figure 5.9) and the WF describes a correlated metal. As soon as we enter in the insulating phase, $v_q$ becomes more singular and $\lim_{q\to 0} v_q \ |q|^2$ defines an effective $\beta$ which is larger than the critical value for the KT transition. Therefore, no evidence for the "Coulomb metal" is found. Indeed, we expect that the optimized Jastrow factor $v_q$, containing subleading corrections with respect to Eq. (5.5), will define a critical $\beta$ very close to the value of the classical CGM, i.e., $\beta_c = 1/T_c^{CGM} = 4$. Although there are large size effects around $U_c$, we have a clear evidence that $\lim_{q\to 0} v_q|q|^2 \to 0$ for $U < U_c$ and $\lim_{q\to 0} v_q|q|^2 \gtrsim 4\pi$ for $U > U_c$. In order to further characterize the two

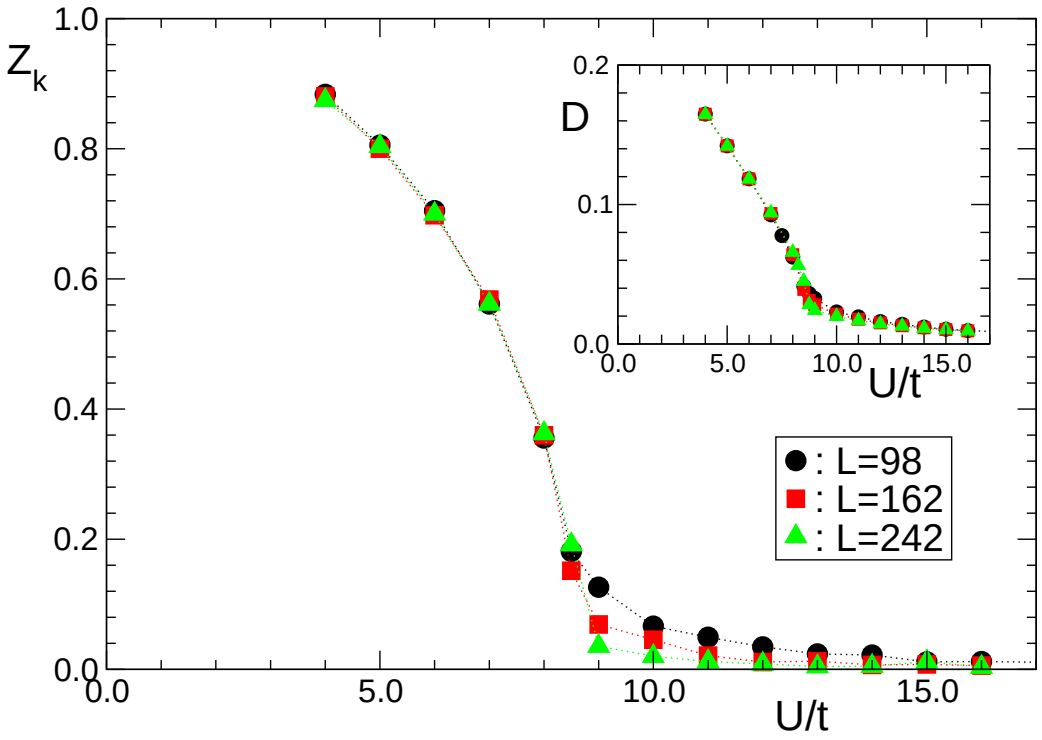


Figure 5.10: Quasiparticle weight $Z_k$ at $k = (\pi/2, \pi/2)$ of the optimized *paramagnetic* wave function containing a Jastrow factor applied to the Fermi gas as a function of the interaction $U/t$ in the Hubbard model, for three different sizes of the system. Inset: the number of double occupancies $D$ as a function of $U/t$.

phases, we calculate the quasiparticle weight for different $U/t$. In the weak coupling regime, for $U < U_c$, we obtain a Fermi liquid with a finite quasiparticle weight, whereas at strong couplings, i.e., for $U > U_c$, we have an insulating phase with a vanishing $Z_k$, see Figure 5.10. [4] In addition, the calculation of the double occupancy $D$ clearly indicates that the transition is continuous and the insulating phase still possess finite charge fluctuations, see the inset of Figure 5.10.

Therefore, in light of the above results, the stabilization of the "Coulomb metal" seems to be very unlikely. This was expected since at weak coupling the Random-Phase Approximation holds, and, according to previous RPA calculations, a metallic phase with $N_q \sim q^2$ and zero quasiparticle weight can be found only for long-range potentials [102].

### 5.2.2 Comparison among different variational wavefunctions

Let us finally compare the accuracy of different WFs obtained with the long-range density Jastrow factor and different uncorrelated states for the two-dimensional Hubbard model. In particular, we consider the mean-field solutions of the BCS and antiferromagnetic Hamiltonians of Section 1.4.1. Moreover, we also evaluate the accuracy of a determinant with in-plane staggered magnetization, which is the ground state of the mean-field Hamiltonian:

$$H_{AF_x} = \sum_{k,\sigma} \epsilon_k c^\dagger_{k,\sigma} c_{k,\sigma} + \Delta_{AF_x} \sum_i (-1)^{r_i} (c^\dagger_{i\uparrow} c_{i\downarrow} + h.c.) \qquad (5.17)$$

where $\Delta_{AF_x}$ is a variational parameter. Furthermore, in order to describe correctly the spin properties of the system, we consider the effect of a long-range spin-Jastrow factor along the $z$ direction $J_{S_z} = \exp\left[\frac{1}{2}\sum_{ij} v^z_{ij} S^z_i S^z_j\right]$. Let us emphasize that, in the mean-field Hamiltonian (5.17), the magnetic order parameter is in the $x-y$ plane and not along the $z$ direction like in $H_{AF}$ of (1.15). Only in this case the presence of the spin Jastrow factor $J_{S_z}$ can introduce relevant fluctuations over the mean-field order parameter $\Delta_{AF_x}$, leading to an accurate description of the spin properties [63, 107].

Figure 5.11 shows the variational energy of the different WFs, as a function of $1/U$. We plot for a comparison the behavior of the energy of the paramagnetic

[4] In order to minimize the size effects on $Z_k$, we calculate the momentum distribution $n_k$ and extract, by fitting around the known Fermi surface, the value of the jump.

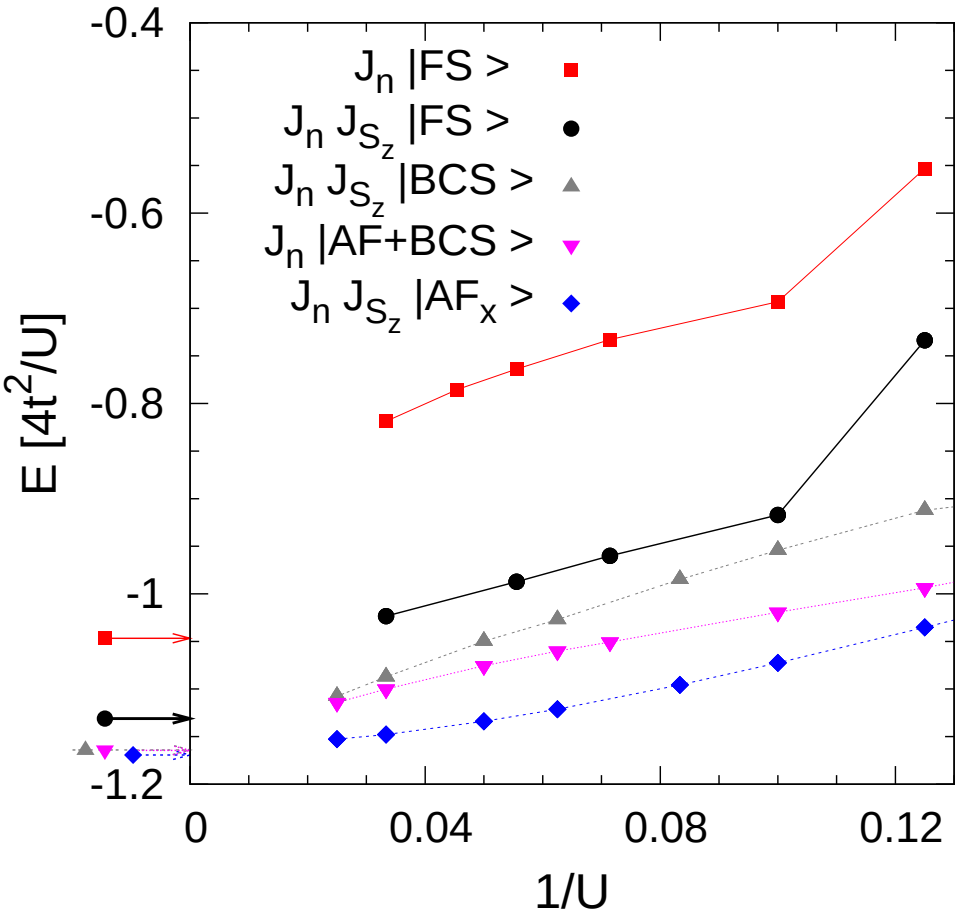


Figure 5.11: Energy vs $1/U$ for different WFs for a lattice of 98 sites. $J_n$ ($J_{S_z}$) denotes the charge-density (spin) Jastrow factor. $|FS\rangle$ is the uncorrelated Fermi sea determinant, $|AF\rangle$ is the determinant obtained from a mean-field antiferromagnetic Hamiltonian (see Eq.(1.15)), $|BCS\rangle$ is the ground state of a BCS Hamiltonian (see Eq.(1.14)) with a gap parameter having $d_{x^2-y^2}$ symmetry. Finally, $|AF+BCS\rangle$ corresponds to a mean-field Hamiltonian containing both the antiferromagnetic gap $\Delta_{AF}$ and the BCS gap $\Delta_{d_{x^2-y^2}}$ and $|AF_x\rangle$ corresponds the ground state of Hamiltonian (5.17). Arrows (marked with different points according to the caption) indicate the infinite-$U$ variational energy obtained for the Heisenberg model by optimizing the corresponding fully-projected determinants.

variational state $J_n|FS\rangle$ described in the previous section, which turns out to be much higher than the other variational energies, since in that case the magnetic

contributions are completely neglected. The WF with the lowest energy corresponds to the determinant with in-plane magnetization and a long-range spin and charge Jastrow factor. Quite surprisingly, the WFs coming from the BCS mean-field solution, with and without antiferromagnetism, are far less close in energy at finite $U$ with respect to the infinite-$U$ limit. However, when discussing these find-

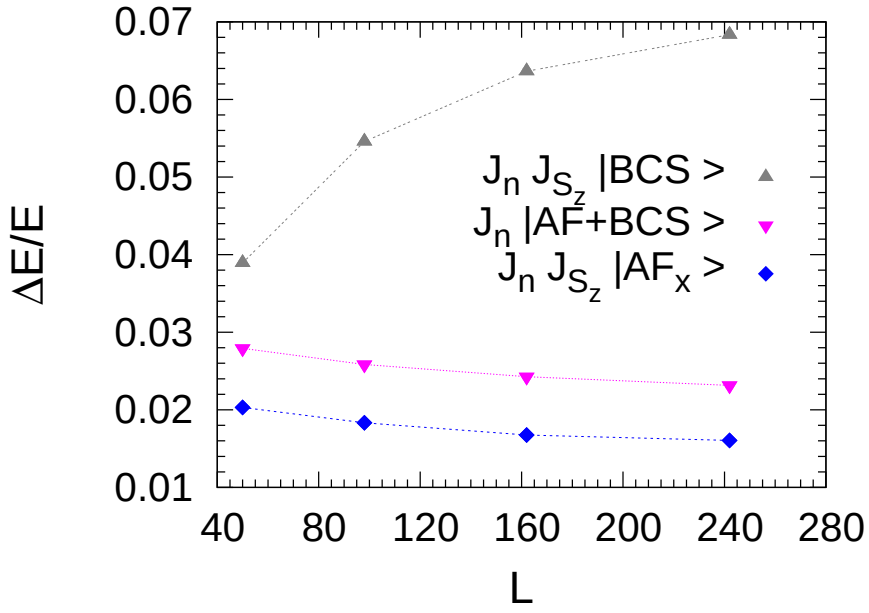


Figure 5.12: Energy accuracy for different WFs (see the caption of Figure 5.11) for $U/t = 4$ as a function of the lattice size. $\Delta E = \frac{E_{HS}-E_T}{E_{HS}}$ where $E_{HS}$ is the energy calculated with the Hubbard-Stratonovich algorithm.

ings, it is necessary to remark that, as we already observed for the one-dimensional $t-t'$ Hubbard model, also in two dimensions the Jastrow factor does not generally allow us to connect with a good accuracy to the infinite-$U$ limit. This happens because the Jastrow term can only change the amplitudes of the configurations given by the determinant, but is not capable to change the nodes of the WF, which turn out to be remarkably different for finite $U$ with respect to the infinite-$U$ limit. We find that the possibility to connect the two limits deeply depends on the accuracy of the variational WF in the corresponding infinite-$U$ model. For example, by considering the wavefunction built with the fully-projected Slater determinant $|FS\rangle$, whose variational energy is very far from the ground-state energy of the

Heisenberg Hamiltonian, we find that at finite $U$ the corresponding Jastrow wavefunction $J_n|FS\rangle$ fails to connect to the infinite-$U$ limit. Instead, the wavefunction with spin Jastrow factor and in-plane magnetization, which is the most accurate for the Heisenberg model, reaches the infinite-$U$ limit with a good accuracy.

Finally, in order to check the size dependence of the above results, in Figure 5.12 we show the accuracy of the three WFs that mostly approach the Heisenberg limit for $U/t = 4$ and different sizes. This is obtained by comparing the variational energy with the one calculated through the Hubbard-Stratonovich algorithm, which is exact within the statistical error. As expected, the WF with the in-plane magnetization and the charge and spin Jastrow factors has the best accuracy, which increases by increasing the lattice size. This behavior is found also for the WF built with a long-range Jastrow factor and a mean-field determinant containing both the AF and BCS parameters. On the other hand, for $U/t = 4$ the simple BCS state with charge and spin Jastrow factors, which is the finite-$U$ version of the RVB state with a further magnetic contribution coming from the spin correlation factor, looses accuracy by increasing the lattice size.

From the above results we expect that a WF containing both in-plane AF and BCS, with a long-range spin and Jastrow factor, could give remarkably accurate results for the two-dimensional Hubbard model on the square lattice. In that case, the uncorrelated part can be written in terms of a Pfaffian instead of a simple determinant [107, 108].

# Chapter 6

# The Jastrow WF for bosonic systems: comparison with exact results

In this chapter we study the bosonic Hubbard model in one and two spatial dimensions, by using the variational approach and the numerically exact Green's function quantum Monte Carlo technique(GFMC) [39, 109]. With respect to the fermionic case, where the so-called sign problem prevents one to have access to the exact ground-state properties on fairly large sizes, in the bosonic case the ground-state wavefunction (WF) can be sampled by using quantum Monte Carlo techniques. Therefore, the non-frustrated bosonic models give the opportunity to compare our variational ansatz with the exact ground state.

Following the ideas of the previous chapters on fermionic systems, we show that, in order to obtain an accurate approximation of the ground state, it is necessary to include a long-range Jastrow factor. In this case, its singular behavior at small momenta may turn a non-interacting superfluid into an insulator that still possess density fluctuations. Moreover, thanks to the mapping between this quantum state to the classical Coulomb gas model, shown in Chapter 5, important insight into the insulating phase are possible. Finally, considering additional long-range repulsive interactions added to the Hamiltonian, we report the evidence for different scenarios for the superfluid-insulator transition.

## 6.1 The Bose-Hubbard model

The Bose-Hubbard model is described by the following Hamiltonian:

$$\mathcal{H} = -\frac{t}{2}\sum_{\langle i,j\rangle} b_i^\dagger b_j + h.c. + \frac{U}{2}\sum_i n_i(n_i - 1), \tag{6.1}$$

where $\langle \dots \rangle$ indicates nearest-neighbor sites, $b_i^\dagger$ ($b_i$) creates (destroys) a boson on site $i$, and $n_i = b_i^\dagger b_i$ is the local density operator. In the following, we consider $N$ particles on a lattice of $L$ sites with periodic boundary conditions. At zero temperature and integer densities $\rho = N/L$, this model shows a superfluid-insulator transition when the ratio $U/t$ between the kinetic energy and the on-site interaction is varied. Otherwise, for non-integer fillings, the ground state is always a superfluid. In a seminal paper [110], by using a field theoretical approach, Fisher and coworkers proposed that the transition of the $d$-dimensional clean system belongs to the $XY$ universality class in $d + 1$. This scenario has been confirmed mostly in one an two dimensions by using different numerical techniques, such as quantum Monte Carlo and density-matrix renormalization group [111–115]. In particular, it has been verified that in one dimension ($1d$) at $\rho = 1$ there is a Kosterlitz-Thouless transition and the estimation of the critical value of the on-site interaction ranges between $U_c/t \sim 1.8$ and $U_c/t \sim 2.3$ [112, 114]. Instead, in two dimensions ($2d$), there is a second-order phase transition at $U_c/t \sim 8.5$ [111].

Besides the numerically exact techniques, important informations on the various phases can be obtained by considering simplified variational WFs. The simplest example is given by the celebrated Gutzwiller state, where the on-site repulsive term disfavors density fluctuations. In this case, contrary to the fermionic case, it is possible to tackle exactly this wave function [116, 117] and to describe the superfluid-insulator transition with reasonably accurate values of $U_c/t$, i.e., $U_c/t = d(\sqrt{n_c} + \sqrt{n_c + 1})^2$, for commensurate fillings $\rho = n_c$. The main drawback of this approach is that, similarly to what happens with fermions, the transition is reached with a vanishing of the kinetic energy and the insulating state does not possess density fluctuations, all the particles being frozen on the lattice sites. Of course, this gives a rather inaccurate description of the insulator, whenever the local interaction is finite.

### 6.1.1 The bosonic variational WF and the GFMC approach

For bosonic systems, the variational Jastrow WF is defined by applying a density Jastrow factor to a state with all the bosons condensed into the $q = 0$ state, namely:

$$|\Psi_J\rangle = \exp\left(\frac{1}{2}\sum_{ij} v_{i,j} n_i n_j\right)|\Phi_0\rangle, \tag{6.2}$$

where $|\Phi_0\rangle = (\sum_i b_i^\dagger)^N|0\rangle$ is the non-interacting boson ground state with $N$ particles and $v_{i,j}$ are translationally invariant parameters that can be optimized to minimize the variational energy. On the other hand, as we showed in Section 1.4, previous studies for fermionic systems stressed the importance of short-range many-body terms [13], where the on-site Gutzwiller projector is supplied by a holon-doublon term acting for nearest-neighbor sites. A simple generalization of this state for bosonic systems is given by

$$|\Psi_{g,MB}\rangle = \exp\left(g\sum_i n_i^2 + g_{MB}\sum_i \xi_i\right)|\Phi_0\rangle, \tag{6.3}$$

where $g$ and $g_{MB}$ are variational parameters and the many-body operator is defined by

$$\xi_i = h_i \prod_\delta (1 - d_{i+\delta}) + d_i \prod_\delta (1 - h_{i+\delta}), \tag{6.4}$$

where $h_i = 1$ ($d_i = 1$) if the site $i$ is empty (doubly occupied) and $0$ otherwise, $\delta = \pm x, \pm y$; therefore, $\xi_i$ counts the number of isolated holons and doublons. Even though this projector has been originally introduced for fermionic systems, where the maximum occupancy at each site is given by two electrons, it can be used also for bosons, where in the limit of large interaction the number of sites with an occupation larger than two is negligible.

Then, it is straightforward to combine the two previous variational wave functions and consider

$$|\Psi_{J,MB}\rangle = \exp\left(\frac{1}{2}\sum_i v_{i,j} n_i n_j + g_{MB}\sum_i \xi_i\right)|\Phi_0\rangle, \tag{6.5}$$

containing both the long-range Jastrow factor and a short-range many-body term. As it will be shown in the next sections, in two dimensions the presence of the latter term helps to increase the accuracy in the strong-coupling regime. Instead,

in one dimension, the many-body term does not improve the accuracy of the long-range Jastrow state, and there is no appreciable difference between the WF (6.2) and (6.5).

In the following, we will present the results obtained by considering the variational WFs described above and, in order to verify their accuracy, we will compare their properties with those found with the numerically exact GFMC. This technique allows one to sample the distribution:

$$\Pi_x \propto \langle x|\Psi^G\rangle\langle x|\Psi_0\rangle, \tag{6.6}$$

where $|\Psi_0\rangle$ is the exact ground state and $|\Psi^G\rangle$ is the so-called guiding function that helps the convergence and may be chosen to be the best variational state. In particular, following the power method:

$$\Pi \propto \lim_{n\to\infty} G^n \Pi^0, \tag{6.7}$$

where $\Pi^0$ is a starting distribution and

$$G_{x',x} = \Psi^G_{x'}(\Lambda\delta_{x',x} - \mathcal{H}_{x',x})/\Psi^G_x, \tag{6.8}$$

is the so-called Green's function, defined with a large or even infinite [118] positive constant $\Lambda$, $\delta_{x',x}$ being the Kronecker symbol. The GFMC statistical method is very efficient for non-frustrated bosonic systems, since in this case all the matrix elements of $G$ are non-negative and the ground state is node-less. Therefore, $G$ can represent a transition probability in configuration space, apart from a normalization factor $b_x = \sum_{x'} G_{x',x}$. In this case, it follows immediately that the asymptotic distribution $\Pi$ is also positive and, therefore, we have a direct access to the ground-state energy $E_0$ by sampling the local energy $e_L(x) = \langle x|\mathcal{H}|\Psi^G\rangle/\langle x|\Psi^G\rangle$ over the distribution $\Pi_x$. Finally, the static correlations, like the density structure factor, can be obtained by using the forward-walking technique introduced in Ref. [39]

### 6.1.2 Results for the 1$d$ Bose-Hubbard model

First, in Figure 6.1 we compare the variational accuracy of the WFs (6.2), (6.3) and (6.5) for different values of $U/t$. Remarkably, in one dimension and in presence of a long-range Jastrow, the many-body term parametrized by $g_{MB}$ is irrelevant and there is no an appreciable difference between the WFs (6.2) and (6.5)

for all the on-site interactions considered. By contrast, the Gutzwiller state, even when supplied by the many-body term, is much less accurate by increasing $U/t$. Therefore, in the following, we will consider the state with long-range Jastrow

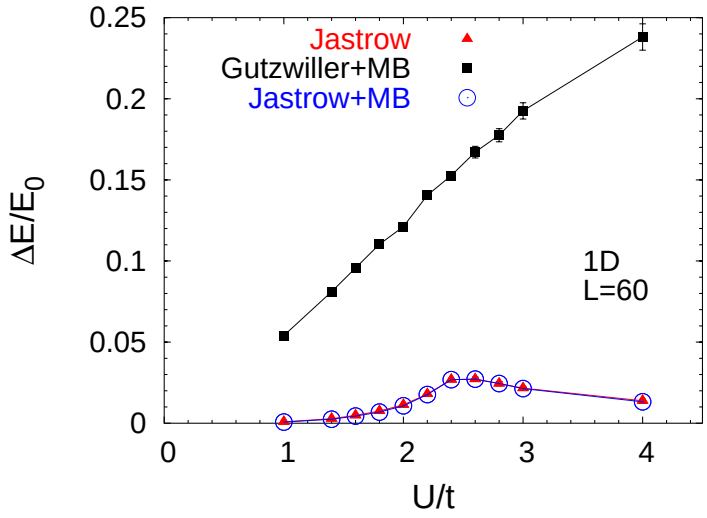


Figure 6.1: Accuracy of different variational WFs as a function of $U/t$ for 60 sites and 60 bosons. $\Delta E = E_{VMC} - E_0$, where $E_{VMC}$ is the variational energy and $E_0$ is the ground-state one, obtained by GFMC. The state of Eq. (6.2) is denoted by "Jastrow", the one of Eq. (6.3) by "Gutzwiller+MB", and the one of Eq. (6.5) by "Jastrow+MB".

given by Eq. (6.2), since the fact of dealing with the many-body term makes the algorithm much slower than the case with the Jastrow factor alone and does not improve the quality of the variational state.

In Figure 6.2, we report the minimized Jastrow parameters $v_q$ multiplied by $q^2$ for different $U/t$: There is a clear difference in the small-$q$ behavior for $U/t \lesssim 2.4$, where $v_q \sim \alpha/|q|$ and for $U/t \gtrsim 2.5$, where $v_q \sim \beta/q^2$. At the variational level, the change of the singular behavior of the Jastrow parameters for $U/t \sim 2.4$ marks the superfluid-insulator transition. Indeed, as discussed in the previous chapters, $v_q \sim \alpha/|q|$ implies a gapless systems, whereas $v_q \sim \beta/q^2$ indicates a finite gap in the excitation spectrum and, therefore, an insulating character. These variational findings will be confirmed by the comparison with the exact results in the following. Let us now concentrate on the insulating phase. As discussed in Chapter 5,

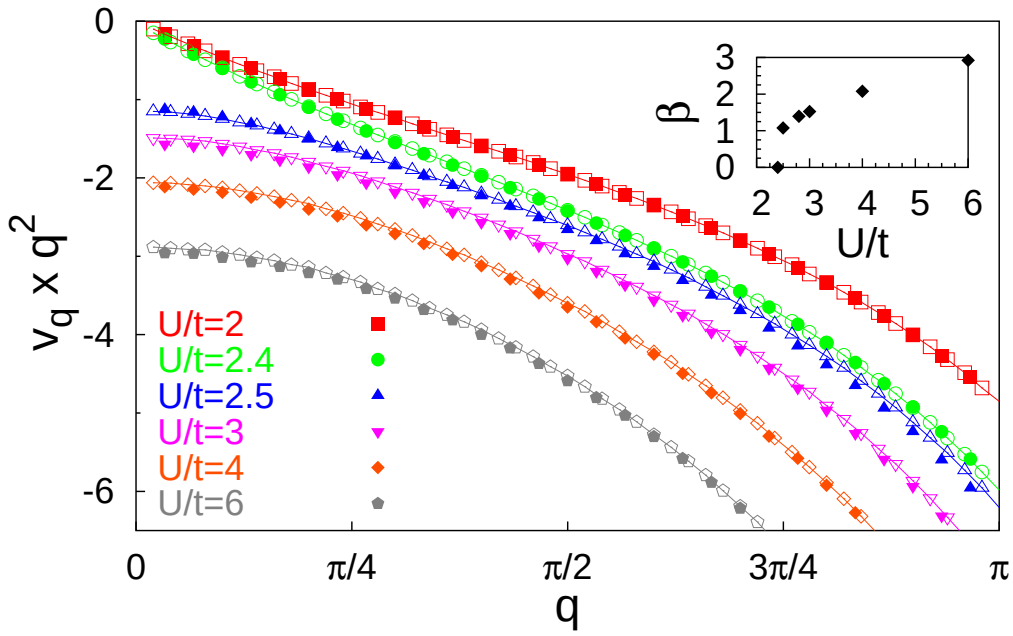


Figure 6.2: Variational results for the Jastrow parameters in $q$ space $v_q$ multiplied by $q^2$, for different $U/t$, for $60$ sites (full symbols) and $100$ sites (empty symbols). Inset: The extrapolated value of $\beta = \lim_{q\to 0} v_q \times q^2$ as a function of $U/t$.

the Jastrow WF (6.2) can be mapped onto the partition function of an effective classical Coulomb gas model (CGM) and $\beta$ plays the role of the inverse classical temperature $\beta = \pi/T_{eff}$. In $1d$ the CGM is in the confined phase for any finite temperature, with exponential correlations [119]. This outcome is consistent with the fact of having, in the quantum model, a finite gap in the excitation spectrum. Remarkably, in the $1d$ case, close to the superfluid-insulator transition, the value of $\beta$ obtained from the optimized Jastrow potential is very small (see inset of Figure 6.2) and approaches zero when $U \to U_c$ from above, thus giving a strong indication in favor of a continuous transition between the superfluid and the insulating phase.

Let us now analyze the transition by considering the density structure factor $N_q$. In the small-$q$ regime, we can generally write that

$$N_q = \gamma_1 |q| + \gamma_2 q^2, \tag{6.9}$$

where $\gamma_1$ and $\gamma_2$ depend upon the Jastrow parameters. Since $v_q \sim \alpha/|q|$ in the

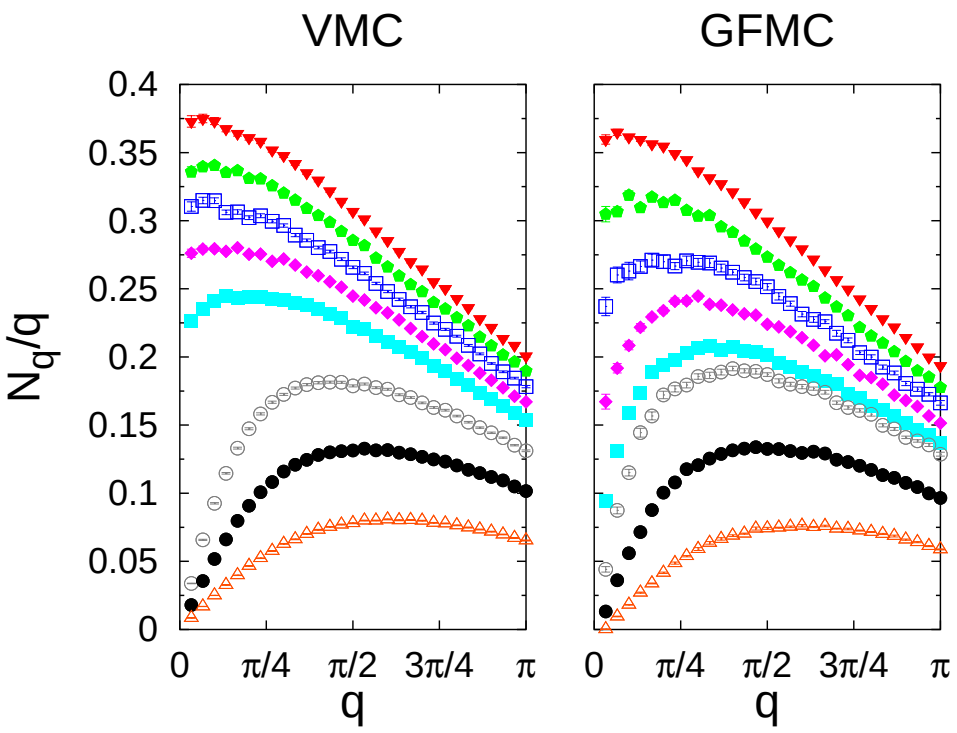


Figure 6.3: Density structure factor $N_q$ divided by $q$ calculated with variational Monte Carlo (left panel) and GFMC (right panel) for different $U/t$ and $L = 60$. From top to bottom $U/t = 1.6$, $1.8$, $2$, $2.2$, $2.4$, $2.5$, $3$, and $4$.

superfluid and $v_q \sim \beta/q^2$ in the insulator, from the Reatto-Chester relation [16] it follows that $\gamma_1 \neq 0$ in the superfluid, whereas $\gamma_1 = 0$ in the insulating phase, where $\gamma_2 \propto 1/\beta$. In analogy with spin systems, we have that $\gamma_1 = v_c\chi$, with $v_c$ and $\chi$ being the sound velocity and the compressibility, respectively. The fact of having $\gamma_1 = 0$ in the Mott insulating regime indicates that this state is incompressible. The Reatto-Chester predictions are confirmed in Figure 6.3, where moreover we obtain that $\gamma_1$ has a jump from a finite value to zero across the transition. This outcome is consistent with the fact that the compressibility also has a finite jump in the $1d$ quantum phase transition [120]. Moreover, just above $U_c$ in the insulating regime, $\gamma_2$ is very large (infinite when $\beta \to 0$) for both the variational and the GFMC calculations, indicating the peculiar character of the $1d$ transition. According to the different small-$q$ behavior of the density structure factor, the superfluid-insulator transition can be located at $U_c/t \sim 2.4$ for the variational

calculation, whereas the GFMC gives $U_c/t \sim 2.2$.

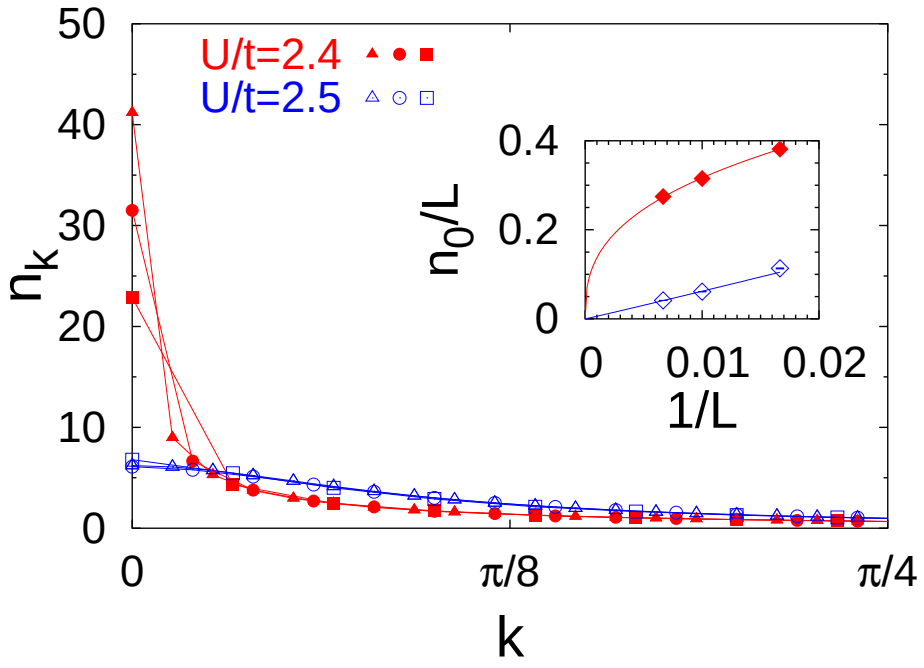


Figure 6.4: Variational results for the momentum distribution $\mathtt{n}_k$ in $1d$ for $L = 60$, $100$, and $150$ and different values of $U/t$. Inset: Size scaling of the condensate fraction $\mathtt{n}_0/L$.

At the variational level, the superfluid-insulator transition can be also easily detected by considering the momentum distribution:

$$\mathtt{n}_k = \frac{\langle \Psi_J | b_k^\dagger b_k | \Psi_J \rangle}{\langle \Psi_J | \Psi_J \rangle}, \tag{6.10}$$

where $b_k^\dagger$ is the creation operator of a boson of momentum $k$. It turns out that the momentum distribution has a radically different behavior below and above the transition: in the superfluid phase, it has a cusp at $k = 0$, although there is no condensate fraction, i.e., $\mathtt{n}_0/L \to 0$ for $L \to \infty$, while in the insulating phase it is a smooth function, see Figure 6.4. These facts naturally implies a power-law/exponential decay of the density matrix in the former/latter phase.

Finally, we consider the superfluid stiffness $D_s$. In analogy to what has been done by Pollock and Ceperley at finite temperature [121], this quantity can be

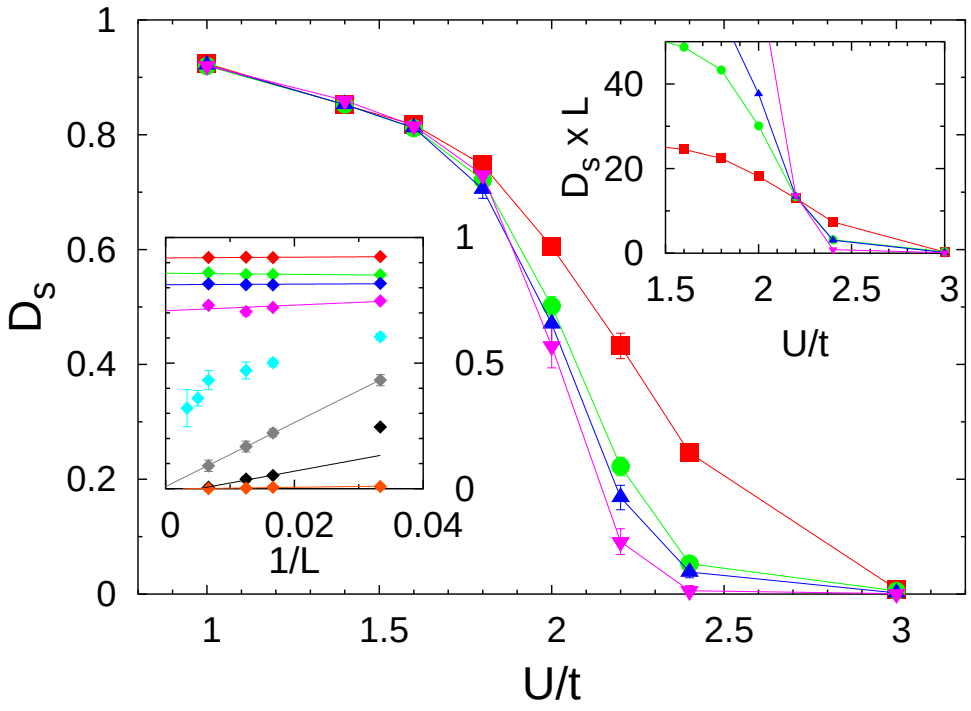


Figure 6.5: Superfluid stiffness calculated by GFMC as a function of $U/t$ for different sizes ($L = 30, 60, 80, 150$). Lower inset: Size scaling of $D_s$ for different $U/t$ (From top to bottom $U/t = 1,\ 1.4,\ 1.6,\ 1.8,\ 2,\ 2.2,\ 2.4,\ 3$). Upper inset: $D_s \times L$ as a function of $U/t$ for the same sizes. The point where the different curves cross marks the transition point.

also calculated directly at zero temperature by using the GFMC and the winding numbers:

$$D_s = \lim_{\tau\to\infty} \frac{W^2(\tau)}{d\ L\ \tau}, \tag{6.11}$$

where $W(\tau) = \sum_i [r_i(\tau) - r_i(0)]$, $r_i(\tau)$ being the position of the $i$-th particle at diffusion time $\tau$, and $d$ is the dimension of the system. It should be stressed that, exactly at zero temperature, $D_s$ can only give information about the presence of a gap in the excitation spectrum, and, therefore, it can discriminate between conducting and insulating phases. In analogy with the Drude weight, $D_s \neq 0$ for a metal and $D_s = 0$ for an insulator. In Figure 6.5, we show $D_s$ for different sizes of the system as a function of the ratio $U/t$. The superfluid stiffness is finite and large in the weak-coupling regime, whereas it vanishes for $U/t \gtrsim 2.2$. In analogy

with spin systems (hard-core bosons) and from general scaling arguments valid for $1d$ boson models, we expect a finite jump at the transition [122], which however it is very difficult to detect by using numerical methods.

### 6.1.3 Results for the $2d$ Bose-Hubbard model

Let us now turn to the $2d$ case of the Hubbard model of Eq. (6.1) and consider square clusters with $L = l^2$ sites and again $N = L$ bosons. The accuracy of

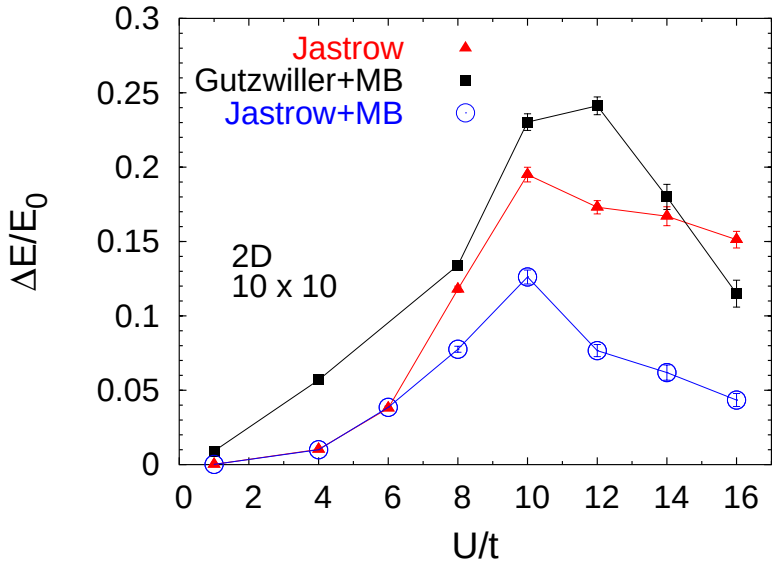


Figure 6.6: Accuracy of different variational WFs as a function of $U/t$ for the $10 \times 10$ cluster and $100$ bosons. The symbols are the same as in Figure 6.1.

the three WFs (6.2), (6.3) and (6.5) are reported in Figure 6.6. The situation is different from the previous $1d$ case: the Gutzwiller state with the many-body term, which in $1d$ is not accurate for large $U/t$, in $2d$ becomes competitive with the Jastrow WF for $U/t \gtrsim 14$. Moreover, the presence of the many-body term strongly improves the accuracy of the Jastrow state as soon as $U/t \gtrsim 8$. Then, in the following, we will consider the state of Eq. (6.5) for both the variational and the GFMC calculations.

Similarly to the $1d$ case, we show in Figure 6.7 the behavior of the optimized $v_q$ as a function of the interaction strength: $v_q \sim \alpha/|q|$ for $U/t \lesssim 10.5$, while $v_q \sim$

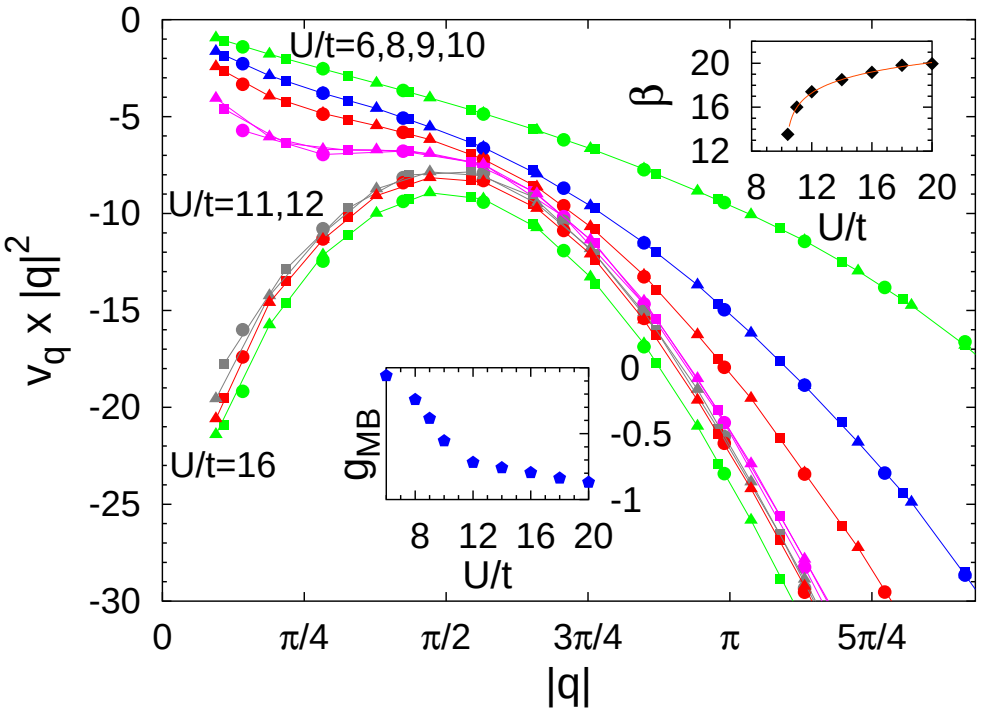


Figure 6.7: Variational results for the Jastrow parameters $v_q$ multiplied by $q^2$ as a function of $q_x$ (or $q_y$) for different $U/t$ and $L = 400$ (circles), $676$ (squares), and $900$ (triangles). Upper inset: The extrapolated value of $\beta = \lim_{q\to 0} v_q \times q^2$ as a function of $U/t$. Lower inset: The many-body variational parameter $G_{MB}$ as a function of $U/t$.

$\beta/q^2$ for $U/t \gtrsim 10.5$, corresponding to the superfluid and the insulating phase, respectively. Therefore, at the variational level, the superfluid-insulator transition is located at $U_c/t \sim 10.5$; this value is close, but slightly better, to the one obtained by using the simple Gutzwiller state, for which $U_c/t \sim 11.33$ [111]. It should be noticed that, in contrast with the $1d$ case, here in the strong-coupling regime there are subleading corrections to the $1/q^2$ behavior of the Jastrow parameters. These corrections can in principle turn the power-law correlations typical of the classical CGM to exponential ones, more suitable for gapped insulators. Unfortunately, for the sizes available with our variational approach, it is not possible to distinguish a true exponential decay from a power-law behavior with a large exponent.

The fingerprint of the transition is also given by the momentum distribution.

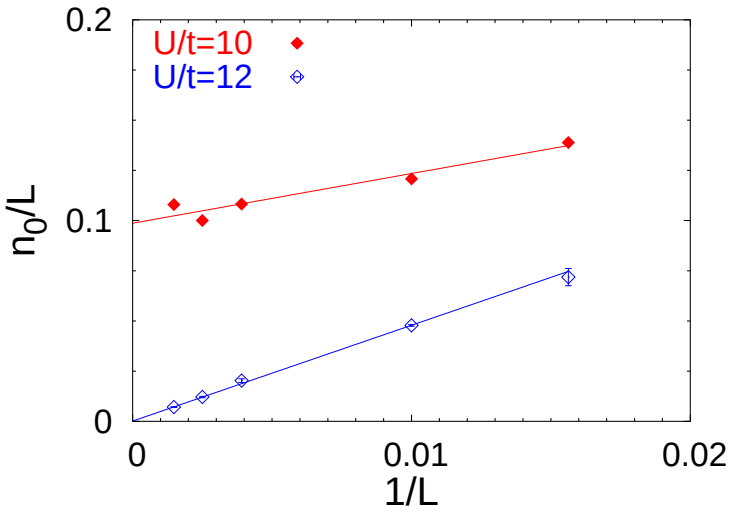


Figure 6.8: Size scaling of the condensate fraction $\mathtt{n}_0/L$ ($L = 100$,256, 400, and 676) for two different values of $U/t$.

For this quantity, a striking difference is observed below and above $U_c$. In the former case, a cusp-like behavior with a finite condensate fraction, is found, whereas in the latter case a smooth behavior is detected, with a vanishing $\mathtt{n}_0/L$. Notice the vanishing condensate fraction in the thermodynamic limit when $v_q \sim 1/q^2$ (see Figure 6.8). Indeed, since $N_q \sim q^2$, the fact that $\mathtt{n}_0/L \to 0$ in the insulator immediately follows from the generalized uncertainty principle derived by Pitaevskii and Stringari [66].

At this point, it is instructive to consider the classical mapping from the quantum WF with $v_q \sim \beta/q^2$ to the classical CGM. We recall that in $2d$, the CGM shows a Kosterlitz-Thouless transition from a plasma phase, stable at high temperatures and a confined phase, stable at low temperatures. The large-$U$ limit corresponds to the confined phase, with $\beta > \beta_c$. By decreasing the ratio $U/t$, the coefficient $\beta$ diminishes, and eventually we enter into the superfluid phase, parametrized by $v_q \sim \alpha/|q|$, where the mapping onto the CGM is no longer valid. Within this framework, a natural question arises: is it possible to stabilize an "intermediate" phase, for $U > U_c$, which has $v_q \sim \beta/q^2$ and $\beta < \beta_c$, the quantum equivalent of the plasma phase? This scenario would imply two successive phase transitions by increasing $U/t$: the first one from the superfluid to the quantum plasma phase and the second one from this "intermediate" phase to the Mott in-

sulating state. In analogy with the $1d$ case, in order to answer this question, we

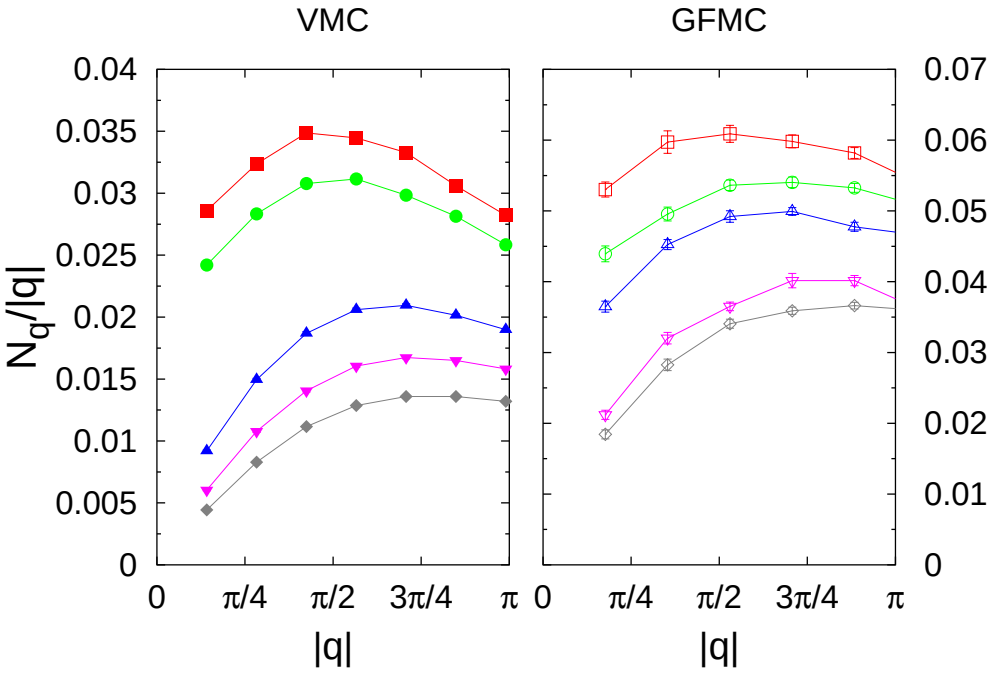


Figure 6.9: Left panel: Density structure factor $N_q$ divided by $q$ calculated by the variational Monte Carlo for different $U/t$ and $L = 20 \times 20$. From top to bottom $U/t = 10$, $10.2$, $10.4$, $11$, and $12$. Right panel: The same for the GFMC on the $L = 16 \times 16$ cluster. From top to bottom $U/t = 8$, $8.2$, $8.4$, $8.6$, and $8.8$.

have to look closely to the optimized Jastrow parameters, having in mind that the classical value for the transition temperature between the confined and the plasma phase is $\beta_c = 4\pi$ and that, since the optimized $v_q$ is not in general exactly equal to the CGM potential, a small change in the classical critical temperature is still possible, i.e., $T_c \neq T_c^{CGM} = 1/4$. From the small-$q$ behavior of $v_q$ (see Figure 6.7), we find that the value of $\beta$ at the superfluid-insulator transition is $\beta \sim 13.5$ and, therefore, very close to $\beta_c$. Reasonably, this fact completely rules out the possibility that, when optimized for the Hubbard model of Eq. (6.1), the Jastrow WF (6.5) can describe a stable plasma phase close to the superfluid-insulator. So, our variational Jastrow state correctly describes a direct transition between a superfluid and a Mott insulator. Of course, the Kosterlitz-Thouless character of the classical transition is expected to be spoiled in the quantum model, since on one side the superfluid phase is parametrized by a less singular interaction $v_q \sim \alpha/|q|$.

In analogy with what we did for the $1d$ case, the superfluid-insulator transition can be also analyzed by considering the small-$q$ behavior of the structure factor $N_q$. In Figure 6.9, we show the results for the variational and the GFMC calculations as a function of $U/t$. In both cases, we find a different small-$q$ behavior for large and small couplings. In the variational calculations, for $U/t \lesssim 10.3$ the structure factor goes like $N_q \sim \gamma_1 |q|$ while for $U/t \gtrsim 10.3$ we get $N_q \sim \gamma_2 q^2$. The critical value of the on-site interaction is rather different within GFMC, for which we obtain $U_c/t \sim 8.5$, in close agreement with the value found in the literature [117]. More specifically, coming from the weak-coupling region, $\gamma_1$ goes smoothly to zero, in contrast with the results of the $1d$ model, where we observed an abrupt jump. Moreover, since at the transition $\beta_c \sim 13.5$, the quadratic term $\gamma_2$ in the insulating state close to $U_c$ is finite, and not diverging like in $1d$. These

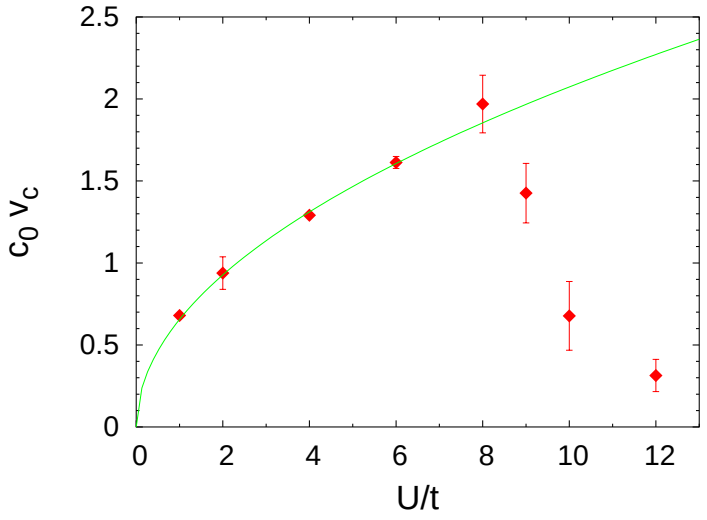


Figure 6.10: GFMC results for the sound velocity $v_c$ obtained through a finite size scaling of the ground-state energy, Eq. (6.12).

results, based upon the variational WF, are confirmed by the GFMC calculations, see Figure 6.9. Since, $\gamma_1 = v_c \chi$, the vanishing linear coefficient of $N_q$ can be ascribed either to $v_c$ or to $\chi$. In order to clarify which one of these quantities goes to zero at the transition, we can extract the sound velocity $v_c$ from the finite-size scaling of the exact ground-state energy by

$$E_0(L) = E_0(\infty) - \frac{c_0 v_c}{L^{3/2}}, \tag{6.12}$$

where $E_0(L)$ is the ground-state energy for a cluster with $L$ sites, $E_0(\infty)$ is the extrapolated value in the thermodynamic limit, and $c_0$ is a given model-dependent constant. Our results of Figure 6.10 clearly indicate that $v_c$ stays finite across the superfluid-insulator transition, thus implying a vanishing compressibility when approaching the Mott insulator.

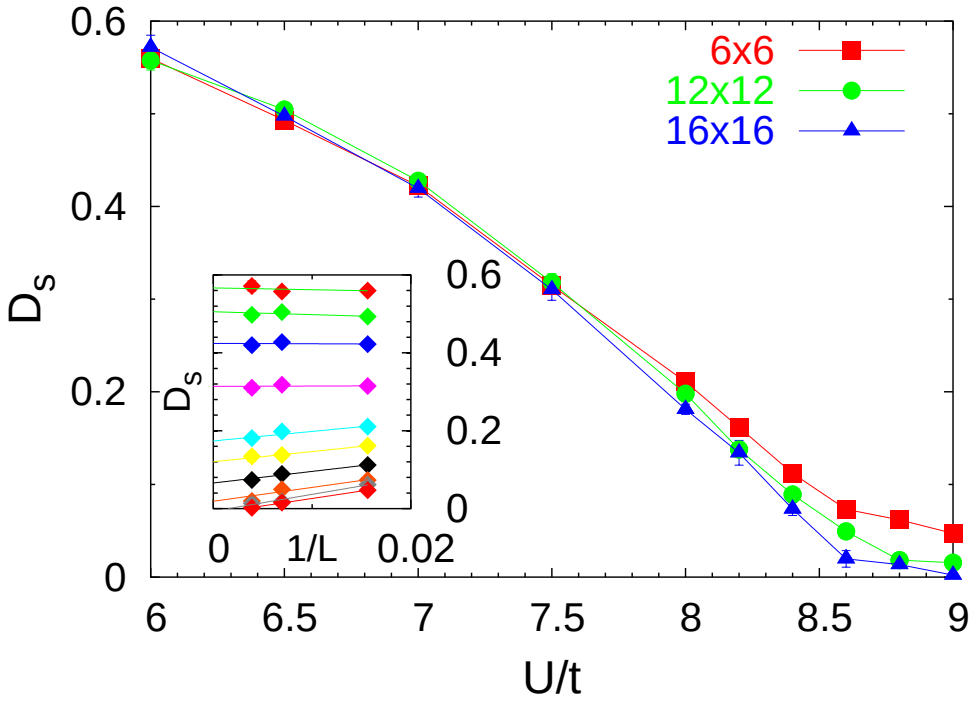


Figure 6.11: Superfluid stiffness as a function of $U/t$ for different sizes. Inset: Size scaling of $D_s$ for the sampled values of $U/t$, namely, from top to bottom, $U/t = 6, 6.5, 7, 7.5, 8, 8.2, 8.4, 8.6, 8.8, 9$.

Finally, we calculate the stiffness $D_s$ with GFMC: Also for this quantity we have a different behavior with respect to the $1d$ case, where a finite jump is rather clear at the superfluid-insulator transition. Indeed, in this case evaluation of the stiffness for different sizes confirms the absence of the jump in $2d$, see Figure 6.11.

## 6.2 Bosons with long-range interaction in $2d$

In the previous paragraphs, we have shown that, in the Hubbard model, the superfluid regime can be described by a long-range Jastrow WF with $v_q \sim \alpha/q$. By increasing the on-site interaction, our variational approach describes a continuous transition to a Mott insulating phase that corresponds to the confined phase of the classical CGM, parametrized by a more singular Jastrow potential $v_q \sim \beta/q^2$. Remarkably, this approach correctly reproduces the behavior of the exact results both in $1d$ and $2d$. However, in $2d$ the classical CGM possess another phase, the plasma one, which cannot be stabilized on the microscopic quantum Hubbard model. Indeed, we have seen that, whenever the Jastrow parameters present the singular behavior $v_q \sim \beta/q^2$, then $\beta \gtrsim \beta_c$ and the ground state is found to be in the confined phase. In the following, we generalize the Hubbard model of Eq. (6.1) to have long-range interactions, like Eq. (6.13), in order to understand under which circumstances it is possible to stabilize this quantum plasma phase. The cases with long-range interactions have been considered mostly in the continuum, where a transition between a charged bosonic fluid and a Wigner crystal is found by varying the density [123–126]. In particular, in presence of the logarithmic interaction, the $2d$ Bose liquid has no condensate, due to the predominance of long-wavelength plasmon excitations [123].

Let us now consider a generalization of the Bose-Hubbard model in presence of a long-range interaction:

$$\mathcal{H}_{LR} = -\frac{t}{2}\sum_{\langle i,j\rangle} b_i^\dagger b_j + h.c. + \frac{V}{2}\sum_{i,j}\Omega(r_i,r_j)n_i n_j, \tag{6.13}$$

where $\Omega(r_i,r_j)$ is a long-range potential that only depends upon the relative distance $|r_i - r_j|$ between two particles and $V$ represents its strength. In particular, we will consider two possibilities for the long-range potential. The first one is given by taking the Coulomb interaction between (charged) bosons moving in a $2d$ lattice embedded in a three-dimensional environment. In practice, this can be done by taking the Poisson equation in three dimensions and projecting the particles onto the $2d$ layer, i.e., by integrating the $z$ component of the momentum $q$. This leads to the potential in the $q$ space:

$$\Omega(q_x,q_y) = \frac{\pi}{\sqrt{(\cos q_x + \cos q_y - 3)^2 - 1}}. \tag{6.14}$$

Notice that the small-$q$ behavior is given by $\Omega(q) \sim 1/|q|$, as expected for the Coulomb potential, which behaves like $\Omega(r) \sim 1/r$ at long distance. The second possibility is instead given by directly considering the solution of the Poisson equation in $2d$:

$$\Omega(q_x, q_y) = \frac{1}{2 - (\cos q_x + \cos q_y)}, \tag{6.15}$$

which for small momenta behaves like $\Omega(q) \sim 1/q^2$, leading to a logarithmic interaction in real space, i.e., $\Omega(r) \sim \log(r)$. In both cases, a uniform background is considered, in order to cancel the divergent $q = 0$ component of the potential.

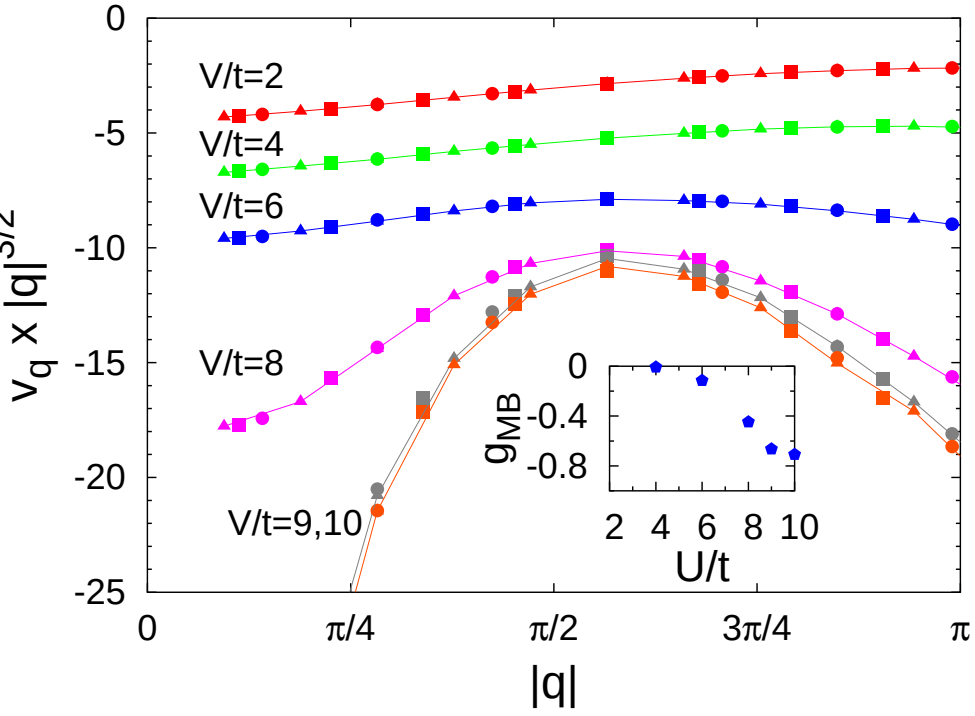


Figure 6.12: Variational results for the Jastrow parameters $v_q$ multiplied by $|q|^{3/2}$ for the potential of Eq. (6.14) with different $V/t$ and $L = 400$ (circles), $676$ (squares), and $900$ (triangles). Inset: The many-body variational parameter $g_{MB}$ as a function of $U/t$.

Let us start by considering the realistic case of the Coulomb potential, i.e., $\Omega(r) \sim 1/r$ that in $2d$ leads to Eq. (6.14). Then we vary its strength $V$ to drive the system across a superfluid-insulator transition. The small-$q$ behavior of the

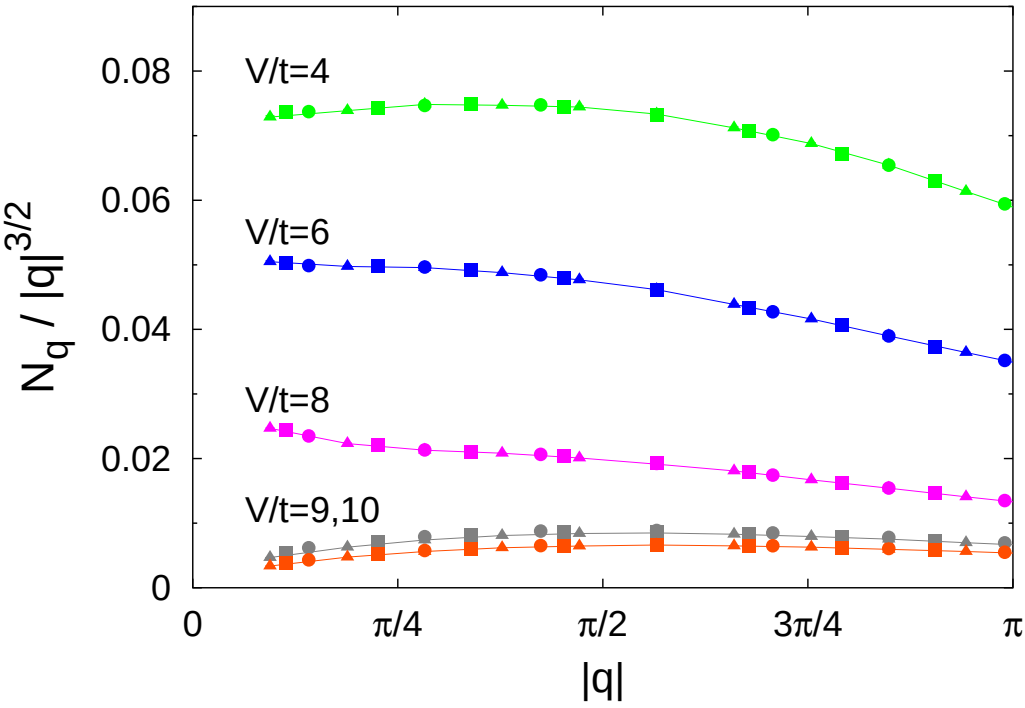


Figure 6.13: Variational results for the density structure factor $N(q)$ divided by $|q|^{3/2}$ for the potential of Eq. (6.14) with different $V/t$ and $L = 400$ (circles), $676$ (squares), and $900$ (triangles).

optimized Jastrow parameters is shown in Figure 6.12: For $V/t \lesssim 8$, we obtain that $v_q \sim 1/|q|^{3/2}$, whereas, for larger values of the interactions, we turn into $v_q \sim \beta/q^2$. In this case, the singular behavior of the weak-coupling region leads to $N_q \sim |q|^{3/2}$, whereas, for large couplings, the well known insulating behavior $N_q \sim q^2$ is recovered (see Figure 6.13). These results are confirmed by GFMC (not shown), though the critical $V/t$ is slightly decreased, i.e., $V_c/t \sim 7$. It should be stressed that the same behavior of the superfluid phase has been found in continuum models at high densities both analytically [127] and numerically [126]. Unfortunately, also in this case, the plasma phase with $v_q \sim \frac{\pi\beta}{q^2}$ and $\beta < \beta_c$ cannot be stabilized by varying the Coulomb strength, and we obtain a standard superfluid-insulator transition.

Then, we turn to the more singular interaction given by Eq. (6.15), leading to $\Omega(r) \sim \log(r)$. In this case the potential in $q$-space is given by $\Omega(q) \sim 1/q^2$

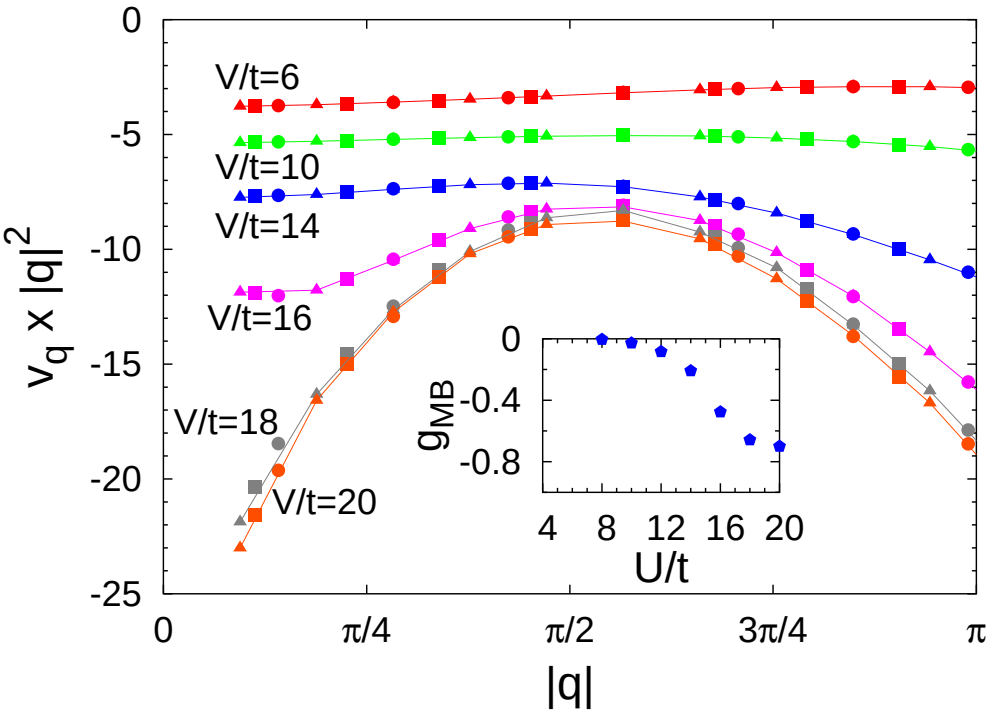


Figure 6.14: The same as in Figure 6.12, for the potential of Eq. (6.15).

and, in continuum models, by using the Gaussian approximation, it is possible to obtain: [123]

$$v_q \sim \Omega(q). \tag{6.16}$$

Then, with a logarithmic interaction, we expect that also in the weak-coupling regime $v_q \sim 1/q^2$. Indeed, as shown in Figure 6.14, this is the case and the behavior of the Jastrow potential for small $V/t$ is compatible with the predictions of Eq. (6.16). Therefore, with such a singular potential, we have that $\beta < \beta_c$ for $V/t \lesssim 16$ and it is possible to stabilize the quantum equivalent of the plasma phase. Moreover, with this kind of long-range potential, we observe a direct transition between this plasma state and the Mott insulator stable for large interactions. Also the structure factor behaves like $N_q \sim q^2$ for all the coupling strength $V/t$, see Figure 6.15. Again, similarly to the previous cases with on-site and Coulomb interactions, in the insulating regime we observe important subleading corrections of $v_q \sim 1/q^2$ (see Figure 6.14) that may restore the correct exponential behavior of the correlation functions.

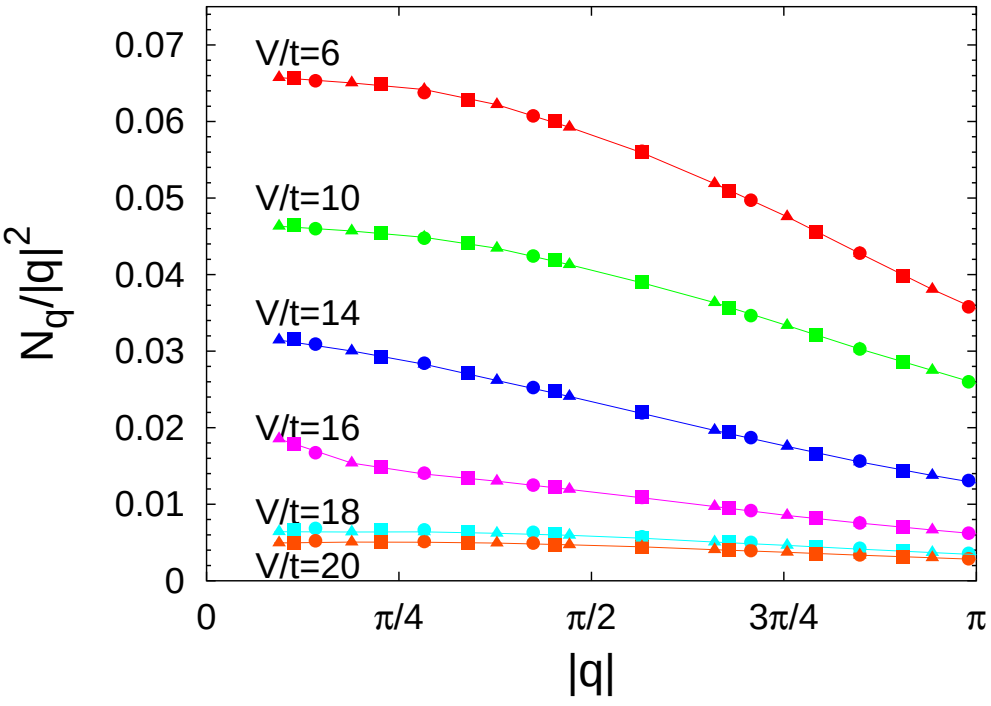


Figure 6.15: The same as in Figure 6.13, for the potential of Eq. (6.15).

# Conclusions and perspectives

In this thesis we have shown, by using a robust variational approach, that the long-range spatial density correlations are crucial for describing the Mott transition at zero temperature.

This understanding has been achieved by considering a long-range Jastrow correlation factor applied on top of an uncorrelated wavefunction. We have found that the long-range Jastrow factor is able to turn a metallic (superconducting) uncorrelated state into an insulating one. Indeed, within this scheme, for the first time we are able to recover an insulating state that does not break any lattice symmetry, but still allows for charge fluctuations, corresponding to Mott's original idea where the localization of charges is purely driven by strong correlation.

We have carefully tested the accuracy of our variational ansatz in the half-filled one-dimensional Hubbard model, where a comparison with exact results is possible. We have found that the Jastrow wavefunction does contain the essential ingredients to capture the physical properties of one-dimensional Mott insulators [128]. Furthermore, we have shown that this kind of wavefunction smoothly connects to the fully-projected Gutzwiller wavefunction, which describes very accurately the limit of infinite repulsion. With respect to the latter, the long-range Jastrow wavefunction offers a more realistic description of insulators, where charge fluctuations are still allowed.

In addition, we have established the capability of the Jastrow wavefunction to describe the correlation-induced metal-insulator transition in the one-dimensional $t-t'$ Hubbard model. In this case, with a proper choice of the uncorrelated wavefunction, corresponding to a BCS state, it is possible to stabilize a metallic state that has a gap in the spin excitations, and an insulator that dimerizes in the thermodynamic limit, with finite charge and spin gaps. By considering the properties of our wavefunction for the different phases, we have generalized at strong cou-

pling the weak-coupling relations known from the previous applications of the Jastrow wavefunction in liquid Helium. In this way, we obtained a deep understanding on the relation among the long-range behavior of the Jastrow factor and the low-energy properties of the corresponding correlated system [128, 129].

Then, we have applied our variational findings to two dimensions. Here, we have realized that the quantum problem can be mapped, for strong enough correlations, onto a classical Coulomb gas. This mapping is particularly transparent and useful when applied to the variational Jastrow wavefunction. In fact, the well known behavior of the classical Coulomb gas suggests the intriguing possibility of an unconventional transition from an anomalous metal, the analogous of the Coulomb gas plasma phase, into a Mott insulator, corresponding to the confined phase of the Coulomb gas [130]. We have found that the properties of both these phases are deeply connected to those of the underlying classical model, although they maintain fingerprints of the quantum state encoded in the uncorrelated determinant. In particular, we have shown that both the unconventional metal and the insulator display anomalous properties, like the vanishing quasiparticle weight, a typical manifestations of the "Mottness" of many strongly correlated materials. In order to check whether this anomalous metallic phase may emerge in realistic models, we have optimized the Jastrow wavefunction in the particular example of a two-dimensional Hubbard model. By considering the paramagnetic sector, we have shown that also in two dimensions the long-range Jastrow factor is able by its own to describe the Mott transition without recurring to any symmetry breaking, providing us with an insulating state of purely "Mott type". In this specific example, we found no evidence of the above mentioned anomalous metallic phase, the metallic region being always characterized by a finite quasiparticle weight, that vanishes only upon approaching the insulating state at strong coupling. This suggests that the stabilization of the anomalous metal may require the presence of a long-range interaction. Moreover, we have compared the accuracy of different variational wavefunctions for the two-dimensional Hubbard model and how they connect to the fully-projected determinants. We have found that the density Jastrow factor is able to approach the insulating state independently of the choice of the determinant. However, the possibility to accurately connect to the infinite-$U$ limit in two dimensions depends crucially upon the choice of the uncorrelated state and its nodal structure.

Finally, we have applied our variational wavefunction for bosonic models. We have found that our approach beautifully agrees with the exact numerical solution on finite-size systems and with the generally accepted theoretical predictions [131].

The above results strongly indicate that the long-range correlations induced by the Jastrow factor are the essential ingredient in order to describe the physical properties of Mott insulators and their parent compounds.

The future implications of this work can range among the whole series of phenomena where strong-correlation effects dominate and determine the physical properties of the system. Remarkably, by considering the role of the long-range Jastrow factor on different uncorrelated states, we have recently found an anomalous phase, characterized by the concomitant presence of both the antiferromagnetic order parameter and a BCS pairing term. This phase, which corresponds to an antiferromagnetic insulator with paired electrons and a vanishing quasiparticle weight, turns out to be very promising in explaining the still debated photoemission spectra in High-temperature superconductors at zero doping. The possible stabilization of this anomalous insulator in a microscopic model constitutes a very interesting future application of our variational approach.

Moreover, a remarkable improvement of our variational wavefunction could reside in the insertion of a backflow term into the determinantal part, in order to have access, in the regime of finite interaction, to the low-energy physics that is observed in the corresponding two-dimensional spin models.

Another interesting development of our approach might also consist in the inclusion of both in-plane antiferromagnetism and BCS pairing in the wavefunction. This state requires an uncorrelated wave-function which is written in terms of a pfaffian instead of a usual determinant. The main advantage would be the possibility to handle a spin-Jastrow factor, that could allow us to treat correctly the spin fluctuations, giving very accurate properties for the Hubbard model.

# Appendix A

# Cumulant expansion and Gaussian approximation

Given a probability density $p(x)$, its Fourier transform $f(q)$, called characteristic function, is given by:

$$f(q) = \langle e^{iqx} \rangle = \int_{-\infty}^{\infty} dx \, \mathrm{e}^{iqx} p(x). \tag{A.1}$$

The cumulant expansion of $f(q)$ can be obtained by taking the Taylor series expansion of $\ln[f(q)]$:

$$\ln[f(q)] = \left( \sum_{n=1}^{\infty} \frac{(iq)^n}{n!} C_n \right), \tag{A.2}$$

where $C_n$ corresponds to the $n$-th cumulant:

$$C_1 = \langle x \rangle \quad C_2 = \langle x^2 \rangle - \langle x \rangle^2 \quad ....$$

Now consider a wavefunction $|\Psi^0\rangle$ describing a system of bosons on a lattice of $L$ sites, and a set of $L$ continuous variables $\{\rho_j\}$. Let us define the function $p(\{\rho_j\})$ as:

$$p(\{\rho_j\}) = \frac{\langle \Psi^0 | \prod_j \delta(\rho_j - n_j) | \Psi^0 \rangle}{\langle \Psi^0 | \Psi^0 \rangle} \tag{A.3}$$

where as usual $n_j = c_j^\dagger c_j$ is the operator that counts the number of particles on site $j$. The function $p(\{\rho_j\})$ defined above, satisfies the two conditions required for a probability density:

$$\int [\{d\rho_j\}] p(\{\rho_j\}) = 1 \; ; \quad p(\{\rho_j\}) \geq 0$$

Consider the Fourier transform $f(\{Q_j\})$ of $p(\{\rho_j\})$, in the variables $\{Q_j\}$:

$$f(\{Q_j\}) = \int [\{d\rho_j\}]\, \mathrm{e}^{i\sum_j Q_j\rho_j}\; p(\{\rho_j\}) = \frac{\langle\Psi^0|\mathrm{e}^{i\sum_j Q_j n_j}|\Psi^0\rangle}{\langle\Psi^0|\Psi^0\rangle}. \tag{A.4}$$

The cumulant expansion of $\ln[f(\{Q_j\})]$ truncated to second order is:

$$\ln[f(\{Q_j\})] \simeq i\sum_j Q_j\langle n_j\rangle - \frac{1}{2}\sum_{jj'} Q_jQ_{j'}\left(\langle n_jn_{j'}\rangle - \langle n_j\rangle\langle n_{j'}\rangle\right), \tag{A.5}$$

which corresponds to:

$$f(\{Q_j\}) \simeq \exp\left[i\sum_j Q_j\langle n_j\rangle - \frac{1}{2}\sum_{jj'}\chi_{jj'}Q_jQ_{j'}\right], \tag{A.6}$$

where we have defined $\chi_{jj'} = \langle n_jn_{j'}\rangle - \langle n_j\rangle\langle n_{j'}\rangle$. The fact that the cumulant expansion of $f(\{Q_j\})$ is truncated to second order, is based on the assumption that the Gaussian fluctuations of the charge give the dominant contribution. This approximation, called *Gaussian approximation*, is surely valid for weakly-interacting systems at large distances.

Now let us inverse Fourier transform Eq. (A.6) in order to express the probability $p(\{\rho_j\})$ in Gaussian approximation:

$$p(\{\rho_j\}) \simeq \int [\{dQ_j\}] \exp\left[-i\sum_j Q_j(\rho_j - \langle n_j\rangle) - \frac{1}{2}\sum_{jj'}\chi_{jj'}Q_jQ_{j'}\right] \tag{A.7}$$

By performing the Gaussian integral in the variables $\{dQ_j\}$, apart from normalization constants, we get:

$$p(\{\rho_j\}) \simeq \exp\left[-\frac{1}{2}\sum_{jj'}\chi^{-1}_{jj'}(\rho_j - \langle n_j\rangle)(\rho_{j'} - \langle n_{j'}\rangle)\right] \tag{A.8}$$

Now, since we are interested in the probability associated to the Fourier-transformed particle-density $\rho_q = \frac{1}{\sqrt{L}}\sum_j \mathrm{e}^{iqr_j}\rho_j$ we put:

$$\chi^{-1}_{jj'} = \frac{1}{L}\sum_q \mathrm{e}^{iq(r_j - r'_j)}\chi_q^{-1}. \tag{A.9}$$

Substituting (A.9) in (A.8) we find, neglecting the normalization constants:

$$p(\{\rho_q\}) \simeq \exp\left[-\frac{1}{2}\sum_q \chi_q^{-1}\rho_q\rho_{-q}\right] \tag{A.10}$$

which is the Gaussian approximation of the probability $p(\{\rho_q\})$ in the variables $\{\rho_q\}$. This approximate formula is used to derive the Reatto-Chester approximate formula given in Eq.(2.7).

# Appendix B

# Technical details for an efficient QMC algorithm

## B.1 Ratio among the Slater determinants

The fermionic uncorrelated wavefunction $\Psi^0(x) = \langle x|D\rangle$ describing $N$ fermions located on a lattice of $L$ sites at positions $|x\rangle$ can be written as a determinant of a $N \times N$ matrix [1]:

$$\Psi^0(x) = \det(D).$$

In the following we assume that the first index of $D_{ij}$ refers to the position of the particle and the second index indicates the occupied orbital. [2] Consider now another configuration $|x'\rangle$, which differs from $|x\rangle$ only by the displacement of one particle, from the $k$-th site to the $l$-th site.

If we want to calculate the ratio among the two wavefunctions, this corresponds to:

$$\frac{\Psi^0(x')}{\Psi^0(x)} = \frac{\det(D')}{\det(D)}. \tag{B.1}$$

Consider now the $L \times L$ matrix $M$ associated to the $L$ orbitals and the possible $L$ positions of the particles. The matrices $D$ and $D'$ are constructed from $M$ by taking $N$ rows corresponding to the positions occupied by the electrons and $N$

[1] Let us consider for simplicity spinless fermions, the generalization to the spinfull case will be discussed in the following

[2] For example, for free fermions, $D_{ij} = \frac{\exp(ik_j \cdot R_i)}{\sqrt{L}}$.

columns corresponding to the occupied orbitals. Consider the following identity:

$$D'_{ij} = D_{ij} + \delta_{ik}(D'_{kj} - D_{kj}),$$

where we remark that $k$ corresponds to the old position left by the displaced electron. The above identity means that the new matrix $D'$ is constructed from the old matrix $D$ by replacing the $k$-th row. The $k$-th row of $D'_{kj}$ is taken from the $L \times L$ matrix $M$, by taking the $l$-th row, associated to the new position:

$$D'_{ij} = D_{ij} + \delta_{ik}(M_{lj} - D_{kj}) = D_{ij} + \delta_{ik} v_j^{(lk)}$$

where we have defined the vector $v_j^{(lk)} = (M_{lj} - D_{kj})$, having the apex indices $(lk)$ fixed from the initial and final position of the displaced electron. The above equation can be written as:

$$D'_{ij} = D_{ij} + \sum_m D_{im} D^{-1}_{mk}\, v_j^{(lk)} = \sum_m D_{im}(\delta_{mj} + D^{-1}_{mk} v_j^{(lk)}) \tag{B.2}$$

where $D^{-1}$ is the inverse of $D$. By defining:

$$K_{mj} = \delta_{mj} + D^{-1}_{mk} v_j^{(lk)} \tag{B.3}$$

we can write Eq. (B.2) in the compact form:

$$D' = D \cdot K \tag{B.4}$$

Therefore the ratio among the determinants (B.1) correspond to the calculation of the determinant of $K$. Since the matrix $K$, defined in (B.3), has elements in which the dependence on the indexes is factorized, one can show that:

$$\det(K) = 1 + \sum_q v_q^{(lk)} D^{-1}_{qk} = 1 + \sum_q (M_{lq} - D_{kq}) D^{-1}_{qk} \tag{B.5}$$

Therefore:

$$\frac{\det(D')}{\det(D)} = \det(K) = \sum_q M_{lq} D^{-1}_{qk} = W_{lk} \tag{B.6}$$

The calculation of the ratio among the two determinants reduces to calculate the matrix element $W_{lm}$, i.e. the dot product among the $l$-th row of the matrix $M$ and the $k$-th column of the inverse matrix $D^{-1}$. By storing and updating the matrix $W_{ij}$, we can calculate the ratio (B.6) for any Monte Carlo move by simply looking

at the corresponding matrix element $W_{ij}$. This corresponds to $O(1)$ operations instead of the $O(N^3)$ required for the brute-force calculation of a determinant. The largest computational effort is spent, each time the Monte Carlo move is accepted, for updating the matrix $W$. This, as we show in the next paragraph, can be done with $O(N^2)$ operations.

## B.2 Updating of the matrix $W_{ij}$

Once the move is accepted, the matrix $D$ is substituted by $D'$ and one should calculate again its inverse, in order to apply (B.6) and find $W_{ij}$ for another Monte Carlo move. In the following we show how the inverse $D'^{-1}$ can be obtained from $D^{-1}$ in a more efficient way, reducing to $O(N^2)$ operations. Consider again Eq.(B.2), inserting the definition of $K$:

$$D'_{ij} = \sum_m D_{im}(\delta_{mj} + D^{-1}_{mk} v^{(lk)}_j) = \sum_m D_{im} K_{mj}.$$

The inverse is given by:

$$D'^{-1}_{ij} = \sum_m K^{-1}_{im} D^{-1}_{mj}. \tag{B.7}$$

The inverse $K^{-1}$ corresponds to:

$$K^{-1}_{im} = \delta_{im} + g^{(lk)} D^{-1}_{ik} v^{(lk)}_m, \tag{B.8}$$

with [3]:

$$g^{(lk)} = \frac{1}{\sum_q M_{lq} D^{-1}_{qk}} = \frac{1}{W_{lk}}. \tag{B.9}$$

Therefore, substituting (B.8) in (B.7), we find:

$$D'^{-1}_{ij} = \sum_m (\delta_{im} + g^{(lk)} D^{-1}_{ik} v^{(lk)}_m) D^{-1}_{mj} = D^{-1}_{ij} + g^{(lk)} D^{-1}_{ik} \sum_m v^{(lk)}_m D^{-1}_{mj}. \tag{B.10}$$

The updated matrix $W'_{ij}$ can be easily obtained:

$$W'_{ij} = \sum_q M_{iq} D'^{-1}_{qj} = \sum_q M_{iq} D^{-1}_{qj} + g^{(lk)} \sum_q M_{iq} D^{-1}_{qk} \sum_m v^{(lk)}_m D^{-1}_{mj} \tag{B.11}$$

[3] Substituting (B.8) and (B.2) in the condition for having an inverse $\sum_j D'^{-1}_{ij} D'_{jh} = \delta_{ih}$ one finds the value of $g^{(lk)}$ given in (B.9).

and, substituting the definition $v_m^{(lk)} = M_{lm} - D_{km}$, we find:

$$W'_{ij} = W_{ij} + \frac{W_{ik}(W_{lj} - \delta_{jk})}{W_{lk}}. \tag{B.12}$$

In conclusion, we make $O(N^3)$ operations for constructing the matrix $W_{ij}$ from scratch. This is done at the beginning of the Monte Carlo run and after a certain number of samplings, in order to avoid the bias introduced by truncation errors. The great advantage is that, for any trial proposal, instead of calculating the Metropolis ratio $\mathcal{R}$ each time, which would require $O(N^3)$ operations, we only need to look at the corresponding matrix element $W_{lk}$, implying an irrelevant computational time, if the move is not accepted. Moreover, each time the move is accepted, we make only $O(N^2)$ operations (instead of $O(N^3)$) to update $W_{ij}$.

In this way, we can simulate a fermionic system without dealing, at each Metropolis step, with the bottle-neck of the $O(N^3)$ operations required for the calculation of the Slater determinants.

## B.3 Spinfull case and BCS Slater determinant

The generalization of the approach described in the previous Sections to the spinfull case is straightforward. Instead of considering $N \times N$ matrices, one must take $2N \times 2N$ matrices, since one must indicate not only the particle position and orbital, but also its spin. In the case in which particles have a defined spin (e.g. in the Fermi sea and in the antiferromagnetic Slater determinants), these are block diagonal matrices, the first (last) $N$ rows and columns indicating the positions and orbitals occupied by the spin-up (down) electrons (or viceversa). The same happens for the $L \times L$ matrix $M_{ij}$ defined above, which in the spinfull case becomes a $2L \times 2L$ matrix.

On the other hand, considering the BCS Hamiltonian (see Eq.(1.14)), the corresponding BCS wavefunction is given by:

$$|\Psi_{BCS}\rangle = \prod_k (u_k + v_k c^\dagger_{k\uparrow} c^\dagger_{-k\downarrow})|0\rangle \tag{B.13}$$

where $|0\rangle$ is the vacuum, and $u_k$, $v_k$ satisfy the condition:

$$|u_k|^2 + |v_k|^2 = 1$$

The wavefunction defined in (B.13) is a mixed state of various particle numbers, therefore it is not convenient for our Monte Carlo approach, which works with a fixed particle number. In order to overcome this difficulty, in analogy with what is done in Ref. [132], we introduce a simple particle-hole transformation for down spins, namely:

$$d_{i\uparrow} = c_{i\uparrow} \quad d_{i\downarrow} = (-1)^i c^\dagger_{i\downarrow} \tag{B.14}$$

which correspond to the Fourier transformed operators:

$$d_{k\uparrow} = c_{k\uparrow} \quad d_{k+Q\downarrow} = c^\dagger_{-k\downarrow} \tag{B.15}$$

with $Q$ being the $d$-dimensional vector with components $Q = (\pi, \pi, ..)$. In this representation the new vacuum $|\tilde{0}\rangle$ is defined as $|0\rangle = \prod_k d^\dagger_{k+Q}|\tilde{0}\rangle$. In this way we can rewrite the BCS wavefunction as:

$$|\Psi_{BCS}\rangle = \prod_k (u_k d^\dagger_{k+Q\downarrow} + v_k d^\dagger_{k\uparrow}|\tilde{0}\rangle \tag{B.16}$$

where the bands now correspond to mixed states of up and down spins and the total number of particles is now well defined. Notice that, since the BCS quasiparticle have not a defined spin, i.e. each orbital is formed by different contributions coming from both the spin-up and spin-down components, the above discussed $2N \times 2N$ matrices will not be in the block diagonal form as it happens for the simple Fermi sea case. The same holds for the wavefunction corresponding to the ground state of a mean-field Hamiltonian with in-plane magnetization.

## B.4 Ratio among the Jastrow factors

Let us now consider how to efficiently calculate the ratio among the Jastrow factors associated to two different configurations:

$$\mathcal{R}_J = \frac{\mathcal{P}_J(x')}{\mathcal{P}_J(x)} = \frac{\exp\left[\frac{1}{2}\sum_{ij} v_{ij} n'_i n'_j\right]}{\exp\left[\frac{1}{2}\sum_{ij} v_{ij} n_i n_j\right]} = \exp\left[\frac{1}{2}\sum_{ij} v_{ij}(n'_i n'_j - n_i n_j)\right] \tag{B.17}$$

where the two configurations $|x\rangle$ and $|x'\rangle$ differ by the displacement of one electron from the $k$-th site to the $l$-th site. This corresponds to:

$$n'_i = n_i + \delta_{il} - \delta_{ik} \tag{B.18}$$

Substituting (B.18) in (B.17) and considering the translational invariance of the Jastrow parameters (i.e. $v_{ij} = vji$) we find:

$$\mathcal{R}_J = \exp\left[\sum_i v_{il}n_i - v_{ik}n_i\right] \exp\left[v_{ll} - v_{lk}\right] = \frac{T_l}{T_k} V_{lk} \tag{B.19}$$

where in the last equality we have defined:

$$T_i = \exp\left[\sum_j v_{ij}n_j\right] \quad \text{and} \quad V_{ij} = \exp\left[v_{ii} - v_{ij}\right] \tag{B.20}$$

This allows us to perform $O(L)$ operations instead of $O(L^2)$. The matrix $V$ does not depend on the configuration and is calculated only once at the beginning of the simulation. The vectors $T$ are calculated once the configuration $|x\rangle$ is defined, and then updated as we show in the following.

Given the configuration $|x'\rangle$ described above where one electron has been displaced from the $k$-th position to the $l$-th position with respect to $|x\rangle$, the new vector $T_i'$ is given by:

$$T_i' = \exp[\sum_j v_{ij}n_j'] = \exp[\sum_j v_{ij}(n_j + \delta_{jl} - \delta_{jk})] = T_i \exp[v_{il} - v_{ik}] \tag{B.21}$$

which, once we have stored the exponentials $\exp[v_{ij}]$, allows us to make three operation instead of $L$.

# Bibliography


[1] N.F. Mott. *Proc. Phys. Soc. (London)*, **62**:416, (1949).

[2] M. Imada, A.Fujimori, and Y. Tokura. *Rev. Mod. Phys.*, **70**:1039, (1998).

[3] E. Dagotto. *Rev. Mod. Phys.*, **66**:763, (1994).

[4] P.A. Lee, N. Nagaosa, and X-G. Wen. *Rev. Mod. Phys.*, **78**:17, (2006).

[5] J. Hubbard. *Proc. Roy. Soc. London A*, **276**:238, (1963).

[6] E.H. Lieb and F.Y. Wu. *Phys. Rev. Lett.*, **20**:1445, (1968).

[7] A. Georges, G. Kotliar, W. Krauth, and M.J. Rozenberg. *Rev. Mod. Phys.*, **68**:13, (1996).

[8] P.W. Anderson. *Science*, **235**:1196, (1987).

[9] F.C. Zhang, C. Gros, T.M. Rice, and H. Shiba. *Supercond. Sci. Technol.*, **1**:36, (1988).

[10] C. Gros. *Phys. Rev. B*, **38**:931, (1988).

[11] M.C. Gutzwiller. *Phys. Rev. Lett.*, **10** (5):159, (1963).

[12] T.A. Kaplan, P. Horsch, and P. Fulde. *Phys. Rev. Lett.*, **49**:889, (1982).

[13] H. Yokoyama and H. Shiba. *J. Phys. Soc. Japan*, **59**:3669, (1990).

[14] R. Jastrow. *Phys. Rev.*, **98**:1479, (1955).

[15] W.L. McMillan. *Phys. Rev.*, **138**:A442, (1965).

[16] L. Reatto and G.V. Chester. *Phys. Rev.*, **155**:88, (1967).

[17] S. Sorella. *Phys. Rev. B*, **64**:024512, (2001).

[18] G. Misguich and C. Lhuillier. *Frustrated spin models*. H. T. Diep, World Scientific, New Jersey, 2004.

[19] S. Liang, B. Douchot, and P.W. Anderson. *Phys. Rev. Lett.*, **61**:365, (1988).

[20] L. Capriotti, F. Becca, A. Parola, and S. Sorella. *Phys. Rev. Lett.*, **87**:097201, (2001).

[21] N. Read and S. Sachdev. *Phys. Rev. Lett.*, **66**:1773, (1991).

[22] A. Fujimori. *J. Phys. Chem. Solids*, **53**:1595, (1992).

[23] D.B. McWhan, A. Menth, J.P. Remeika, W.F. Brinkman, and T.M. Rice. *Phys. Rev. B*, **7**:1920, (1973).

[24] M. Foex. *C. R. Hebd. Sean. Acad. Sci. B*, **223**:1126, (1946).

[25] D.B. McWhan and J.P. Remeika. *Phys. Rev. B*, **2**:3734, (1970).

[26] J.G. Bednorz and K.A. Muller. *Z. Phys. B*, **64**:189, (1986).

[27] Y. Shimizu, K. Miyagawa, K. Kanoda, M. Maesato, and G. Saito. *Phys. Rev. Lett.*, **91**:107001, (2003).

[28] Y. Kurosaki, Y. Shimizu, K. Miyagawa, K. Kanoda, and G. Saito. *Phys. Rev. Lett.*, **95**:177001, (2005).

[29] F. Kagawa, T. Itou, K. Miyagawa, and K. Kanoda. *Phys. Rev. B*, **69**:064511, (2004).

[30] M. Greiner, O. Mandel, T. Esslinger, T. W. Hansch, and I. Bloch. *Nature*, **415**:39, (2002).

[31] J. Kanamori. *Progr. Theor. Phys.*, **30**:275, (1963).

[32] H.J. Shulz. *Phys. Rev. Lett.*, **64**:1445, (1990).

[33] T.A. Maier, M. Jarrell, T.C. Schulthess, P.R.C. Kent, and J.B. White. *Phys. Rev. Lett.*, **95**:237001, (2005).

[34] F.C. Zhang and T.M. Rice. *Phys. Rev. B*, **37**:3759, (1988).

[35] J.R. Schrieffer and P.A. Wolff. *Phys. Rev.*, **149**:491, (1966).

[36] I. Affleck. *J. Phys. A: Math. Gen.*, **31**:4573, (1998).

[37] J.D. Reger and A.P. Young. *Phys. Rev. B*, **37**:5978, (1988).

[38] A.W. Sandvik. *Phys. Rev. B*, **56**:11678, (1997).

[39] M. Calandra Buonaura and S. Sorella. *Phys. Rev. B*, **57**:11446, (1998).

[40] J.E. Hirsch. *Phys. Rev. B*, **31**:4403, (1985).

[41] W.F. Brinkman and T.M. Rice. *Phys. Rev. B*, **2**:4302, (1970).

[42] H. Yokoyama and H. Shiba. *J. Phys. Soc. Japan*, **56**:1490, (1987).

[43] W. Metzner and D. Vollhardt. *Phys. Rev. Lett.*, **59**:121, (1987).

[44] P. Fazekas and K. Penc. *Int. J. Mod. Phys. B*, **1**:1021, (1988).

[45] H. Yokoyama, Y. Tanaka, M. Ogata, and H. Tsuchiura. *J. Phys. Soc. Japan*, **73**:1119, (2004).

[46] P. Limelette, A. Georges, D. Jerome, P. Wzietek, P. Metcalf, and J.M. Honig. *Science*, **302**:89, (2003).

[47] A. Georges and G. Kotliar. *Phys. Rev. B*, **45**:6479, (1992).

[48] X.Y. Zhang, M.J. Rozenberg, and G. Kotliar. *Phys. Rev. Lett.*, **70**:1666, (1993).

[49] T. Maier, M. Jarrel, T. Pruschke, and M.H. Hettler. *Rev. Mod. Phys.*, **77**:1027, (2005).

[50] B. Sutherland. *Phys. Rev. A*, **4**:2019, (1971).

[51] F.D.M. Haldane. *Phys. Rev. Lett.*, **60**:635, (1988).

[52] B.S. Shastry. *Phys. Rev. Lett.*, **60**:639, (1988).

[53] G. Gaglione, G.L. Masserini, and L. Reatto. *Phys. Rev. B*, **22**:1237, (1980).

[54] P.A. Whitlock, D.M. Ceperley, G.V. Chester, and M.H. Kalos. *Phys. Rev. B*, 19:5598, 1979.

[55] T. MacFarland, S.A. Vitiello, L. Reatto, G.V. Chester, and M.H. Kalos. *Phys. Rev. B*, **50**:13577, (1994).

[56] R.B. Laughlin. *Phys. Rev. Lett.*, **50**:1395, (1983).

[57] G. Fano, F. Ortolani, and E. Colombo. *Phys. Rev. B*, **34**:2670, (1986).

[58] W.M.C. Foulkes, L. Mitas, R.J. Needs, and G. Rajagopal. *Rev. Mod. Phys.*, **73**:33, (2001).

[59] S. Fahy, X.W. Wang, and S.G. Louie. *Phys. Rev. B*, **42**:3503, (1990).

[60] C.S. Hellberg and E.J. Mele. *Phys. Rev. Lett.*, **67**:2080, (1991).

[61] E. Manousakis. *Rev. Mod. Phys.*, **63**:1, (1991).

[62] Z. Liu and E. Manousakis. *Phys. Rev. B*, **40**:11437, (1989).

[63] F. Franjic and S. Sorella. *Progr. Theor. Phys.*, **97**:399, (1997).

[64] A. Paramekanti, M. Randeria, and N. Trivedi. *Phys. Rev. B*, **70**:054504, (2004).

[65] T. Gaskell. *Proc. Phys. Soc.*, **77**:1182, (1961).

[66] L. Pitaevskii and S. Stringari. *Phys. Rev. B*, **47**:10915, (1993).

[67] W. Kohn. *Phys. Rev.*, **133**:A171, (1964).

[68] R.P. Feynman. *Phys. Rev.*, **94**:262, (1954).

[69] R.P. Feynman and M. Cohen. *Phys. Rev.*, **102**:1189, (1956).

[70] S.M. Girvin, A.H. Mac Donald, and P.M. Platzman. *Phys. Rev. B*, **33**:2481, (1986).

[71] A. W. Overhauser. *Phys. Rev. B*, **3**:1888, (1971).

[72] R. Resta and S. Sorella. *Phys. Rev. Lett.*, **82**:370, (1999).

[73] R.B. Laughlin. cond-mat/0209269, (2002).

[74] C.L. Kane, P.A. Lee, and N. Read. *Phys. Rev. B*, **39**:6880, (1989).

[75] D. Poilblanc and E. Dagotto. *Phys. Rev. B*, **42**:4861, (1990).

[76] S. Sorella. *Phys. Rev. B*, **46**:11670, (1992).

[77] J. Friedel. *Nuovo Cimento Suppl.*, **7**:287, (1958).

[78] N. Metropolis, A. Rosenbluth, M. Rosenbluth, A. Teller, and E. Teller. *J. Chem. Phys.*, **21**:1087, (1953).

[79] A.O. Gogolin, A.A. Nersesyan, and A.M. Tsvelik. *Bosonization and Strongly Correlated Systems*. Cambridge Univ. Press, Cambridge, 1999.

[80] M. Ogata and H. Shiba. *Phys. Rev. B*, **41**:2326, (1990).

[81] C. Gros. *Annals of Physics*, **189**:53, (1989).

[82] P. Horsch and T.A. Kaplan. *J. Phys. C*, **16**:L1203, (1983).

[83] M. Fabrizio. *Phys. Rev. B*, **54**:10054, (1996).

[84] K. Nomura and K. Okamoto. *J. Phys. A*, **27**:5773, (1994).

[85] C.K. Majumdar. *J. Phys. C*, **3**:1911, (1970).

[86] B.S. Shastry and B. Sutherland. *Phys. Rev. Lett.*, **47**:964, (1981).

[87] R. Arita, K. Kuroki, H. Aoki, and M. Fabrizio. *Phys. Rev. B*, **57**:10324, (1998).

[88] S. Daul and R.M. Noack. *Phys. Rev. B*, **61**:1646, (2000).

[89] S.R. White and I. Affleck. *Phys. Rev. B*, **54**:9862, (1996).

[90] S. Sorella, L. Capriotti, F. Becca, and A. Parola. *Phys. Rev. Lett.*, **91**:257005, (2003).

[91] M. Holzmann, D.M. Ceperley, C. Piereoni, and K. Esler. *Phys. Rev. B*, **68**:046707, (2003).

[92] P. Nozieres and D. Pines. *Theory of Quantum liquids*. Perseus, Cambridge, 1999.

[93] F.D.M. Haldane. *J. Phys. C*, **14**:2585, (1981).

[94] F.D.M. Haldane. *Phys. Rev. Lett.*, **45**:1358, (1980).

[95] F.D.M. Haldane. *Phys. Rev. Lett.*, **47**:1840, (1981).

[96] N. Kawakami and P. Horsch. *Phys. Rev. Lett.*, **68**:3110, (1992).

[97] H.J. Schulz. *Int. J. Mod. Phys. B*, **5**:57, (1991).

[98] S. Sorella and A. Parola. *Phys. Rev. B*, **57**:6444, (1998).

[99] H. Yokoyama and H. Shiba. *J. Phys. Soc. Japan*, **56**:3570, (1987).

[100] P. Minnhagen. *Rev. Mod. Phys.*, **59**:1001, (1987).

[101] P. Gumpta and S. Teitel. *Phys. Rev. B*, **55**:2756, (1997).

[102] P.A. Bares and X.-G. Wen. *Phys. Rev. B*, **48**:8636, (1993).

[103] R. Valenti and C. Gros. *Phys. Rev. Lett.*, **68**:2402, (1992).

[104] E. Plekhanov, F. Becca, and S. Sorella. *Phys. Rev. B*, **71**:064511, (2005).

[105] S.R. White, D.J. Scalapino, R.L. Sugar, E.Y. Loh, J.E. Gubernatis, and R.T. Scalettar. *Phys. Rev. B*, **40**:506, (1989).

[106] N. Bulut, D.R. Scalapino, and S.R. White. *Phys. Rev. B*, **47**:14599, (1993).

[107] M. Lugas, L. Spanu, F. Becca, and S. Sorella. *Phys. Rev. B*, (in press), (2006).

[108] J. P. Bouchaud, A. Georges, and C. Lhuillier. *J. Phys. (Paris)*, **49**:553, (1988).

[109] N. Trivedi and D.M. Ceperley. *Phys. Rev. B*, **41**:4552, (1990).

[110] M.P.A. Fisher, P.B. Weichman, G. Grinstein, and D. Fisher. *Phys. Rev. B*, **40**:546, (1989).

[111] W. Krauth and N. Trivedi. *Europhys. Lett.*, **14**:627, (1991).

[112] G.G. Batrouni, R.T. Scalettar, and G.T. Zimanyi. *Phys. Rev. Lett.*, **65**:1765, (1990).

[113] G.G. Batrouni and R.T. Scalettar. *Phys. Rev. B*, **46**:9051, (1992).

[114] T.D. Kuhner and H. Monien. *Phys. Rev. B*, **58**:R14741, (1998).

[115] T.D. Kuhner, S.R. White, and H. Monien. *Phys. Rev. B*, **61**:12474, (2000).

[116] D.S. Rokhsar and B.G. Kotliar. *Phys. Rev. B*, **44**:10328, (1991).

[117] W. Krauth, M. Caffarel, and J. Bouchaud. *Phys. Rev. B*, **45**:3137, (1992).

[118] S. Sorella and L. Capriotti. *Phys. Rev. B*, **61**:2599, (2000).

[119] A. Lenard. *J. of Math. Phys.*, **2**:682, (1961).

[120] N. Laflorencie, S. Capponi, and E.S. Sorensen. *Eur. Phys. J. B*, **24**:77, (2001).

[121] E.L. Pollock and D.M. Ceperley. *Phys. Rev. B*, **36**:8343, (1987).

[122] M. Wallin, E.S. Sorensen, S.M. Girvin, and A.P. Young. *Phys. Rev. B*, **49**:12115, (1994).

[123] W.R. Magro and D.M. Ceperley. *Phys. Rev. B*, **48**:411, (1993).

[124] W.R. Magro and D.M. Ceperley. *Phys. Rev. Lett.*, **73**:826, (1994).

[125] H. Nordborg and G. Blatter. *Phys. Rev. Lett.*, **79**:1925, (1997).

[126] S. De Palo, S. Conti, and S. Moroni. *Phys. Rev. B*, **69**:035109, (2004).

[127] V. Apaja, J. Halinen, V. Halonen, E. Krotscheck, and M. Saarela. *Phys. Rev. B*, **55**:12925, (1997).

[128] M. Capello, F. Becca, M. Fabrizio, S. Sorella, and E. Tosatti. *Phys. Rev. Lett.*, **94**:026406, (2005).

[129] M. Capello, F. Becca, S. Yunoki, M. Fabrizio, and S. Sorella. *Phys. Rev. B*, **72**:085121, (2005).

[130] M. Capello, F. Becca, S. Yunoki, and S. Sorella. *Phys. Rev. B*, **73**:245116, (2006).

[131] M. Capello, F. Becca, M. Fabrizio, and S. Sorella. (in preparation).

[132] H. Yokoyama and H. Shiba. *J. Phys. Soc. Japan*, **56**:3582, (1987).

# Publications

## Publications related to this work

- *Variational description of Mott insulators*. M. Capello, F. Becca, M. Fabrizio, S. Sorella and E. Tosatti, Phys. Rev. Lett., **94**, 026406, (2005).
- *From Luttinger liquid to Mott insulator: the correct low-energy description of the one-dimensional Hubbard model by an unbiased variational approach*. M. Capello, F. Becca, S. Yunoki, M. Fabrizio and S. Sorella, Phys. Rev. B, **72**, 085121, (2005).
- *Unconventional metal-insulator transition in two dimensions*. M. Capello, F. Becca, S. Yunoki and S. Sorella, Phys. Rev. B, **73**, 245116, (2006).
- *The superfluid-insulator transition in one- and two-dimensional bosonic systems: Insight from the variational approach*. M. Capello, F. Becca, M. Fabrizio and S. Sorella, (in preparation)

## Other publications

- *A new class of solutions of the DMPK equation*. M. Capello, M. Caselle. J. Phys. Cond. Matt. 15, 6845 (2004)

# Acknowledgments

First of all I would like to acknowledge my supervisors for having thought me so many things during these years and for giving me the opportunity to study these interesting subjects. Thanks to Sandro Sorella, for his enlightening support and for the passion that he transmits to his students. Thanks to Federico Becca, for the precious and constant help in understanding the codes and the physical problems, and to Michele Fabrizio, for his useful advises and his interest in this work.

I would like to thank Seiji Yunoki, for the fruitful collaboration. Thanks to Erio Tosatti and Alberto Parola, for the interesting discussions.

Moreover, I would like to acknowledge Prof. Didier Poilblanc, for the warm hospitality in Toulouse and for reading this thesis, and Profs. A. Sandvik, X-G. Wen and P.A. Lee for the hospitality at Boston University and MIT.

I am grateful to all the members of the Condensed Matter Theory group, for the beautiful work atmosphere that they create, and to the people of the Computer Staff, for their precious support. I remember with pleasure all the SISSA members, the people of the SISSA bar for the friendly atmosphere they provide, my present office mates, Massimo, Paola, Tatjana and those who are now around the world Claudio, Lorenzo, Michele and Stefano.

Finally, I would like to thank my lovely flatmates Claudia and Stefano and all the friends that I have met during these four years in Trieste, which have been a wonderful human experience.